IMPROVING GEOTECHNICAL PROPERTIES OF HIGH PLASTICITY CLAY SUBJECTED TO ENVIRONMENTAL EFFECTS BY USING DIFFERENT TREATMENT TECHNIQUES

Talal TALEB

T.C.
BURSA ULUDAĞ ÜNİVERSİTESİ
FEN BİLİMLERİ ENSTİTÜSÜ

**Improving Geotechnical Properties of High Plasticity Clay Subjected to
Environmental Effects by Using Different Treatment Techniques**

Talal TALEB
0000-0002-2681-8586

Asst. Prof. Dr. Yesim S. UNSEVER
(Supervisor)

DOCTORATE THESIS
ENGİNEERİNG FACULTY CİVİL ENGİNEERİNG DEPARTMENT

BURSA – 2023

T.C.
BURSA ULUDAĞ ÜNİVERSİTESİ
FEN BİLİMLERİ ENSTİTÜSÜ

Çevresel Etkilere Maruz Kalan Yüksek Plastisiteli Kilin Geoteknik Özelliklerinin

Farklı Teknikler Kullanılarak İyileştirilmesi

Talal TALEB
0000-0002-2681-8586

Dr. Öğr. Üyesi Yeşim S. Ünsever
(Danışman)

DOKTORA TEZİ
MÜHENDİSLİK FAKÜLTE İNŞAAT MÜHENDİSLİK ANABİLİM DALI

BURSA – 2023
Her Hakkı Saklıdır

THESIS APPROVAL

This thesis titled "IMPROVING GEOTECHNICAL PROPERTIES OF HIGH PLASTICITY CLAY SUBJECTED TO ENVIRONMENTAL EFFECTS BY USING DIFFERENT TREATMENT TECHNIQUES" and prepared by Talal TALEB has been accepted as a **Ph.D. THESIS** in Bursa Uludağ University Graduate School of Natural and Applied Sciences, Department of Civil Engineering following a unanimous vote of the jury below.

Supervisor   : Asst. Prof. Dr. Yeşim Sema ÜNSEVER

Head :   Prof. Dr. Özgür Lütfi ERTUĞRUL   Signature
             0000-0002-1270-3649
             Mersin University,
             Faculty of Engineering,
             Department of Civil Engineering

Member: Assoc. Prof. Dr. Mustafa Abdullah   Signature
             SANDIKKAYA
             0000-0001-5071-0121
             Hacettepe University,
             Faculty of Engineering,
             Department of Civil Engineering

Member: Assoc. Prof. Dr. Ali MARDANİ   Signature
             0000-0003-0326-5015
             Bursa Uludağ University,
             Faculty of Engineering,
             Department of Civil Engineering

Member: Asst. Prof. Dr. Yeşim Sema ÜNSEVER   Signature
             0000-0003-3735-9554
             Bursa Uludağ University,
             Faculty of Engineering,
             Department of Civil Engineering

Member: Asst. Prof. Dr. Ahmet Talha GEZGİN   Signature
             0000-0002-9725-6015
             Bursa Uludağ University,
             Faculty of Engineering,
             Department of Civil Engineering

I approve the above result

Prof. Dr. Hüseyin Aksel EREN
Institute Director
……./…../….

I declare that this thesis has been written in accordance with the following thesis writing rules of the U.U Graduate School of Natural and Applied Sciences;

- All the information and documents in the thesis are based on academic rules,
- Audio, visual and written information and results are in accordance with the scientific code of ethics,
- In the case that the works of others are used, I have provided attribution in accordance with the scientific norms,
- I have included all attributed sources as references,
- I have not tampered with the data used,
- And that I do not present any part of this thesis as another thesis work at this university or any other university.

.../.../.........

Talal TALEB

TEZ YAYINLANMA
FİKRİ MÜLKİYET HAKLARI BEYANI

Enstitü tarafından onaylanan lisansüstü tezin/raporun tamamını veya herhangi bir kısmını, basılı (kâğıt) ve elektronik formatta arşivleme ve aşağıda verilen koşullarla kullanıma açma izni Bursa Uludağ Üniversitesi'ne aittir. Bu izinle Üniversiteye verilen kullanım hakları dışındaki tüm fikri mülkiyet hakları ile tezin tamamının ya da bir bölümünün gelecekteki çalışmalarda (makale, kitap, lisans ve patent vb.) kullanım hakları tarafımıza ait olacaktır. Tezde yer alan telif hakkı bulunan ve sahiplerinden yazılı izin alınarak kullanılması zorunlu metinlerin yazılı izin alınarak kullandığını ve istenildiğinde suretlerini Üniversiteye teslim etmeyi taahhüt ederiz.

Yükseköğretim Kurulu tarafından yayınlanan "**Lisansüstü Tezlerin Elektronik Ortamda Toplanması, Düzenlenmesi ve Erişime Açılmasına İlişkin Yönerge**" kapsamında, yönerge tarafından belirtilen kısıtlamalar olmadığı takdirde tezin YÖK Ulusal Tez Merkezi / B.U.Ü. Kütüphanesi Açık Erişim Sistemi ve üye olunan diğer veri tabanlarının (Proquest veri tabanı gibi) erişimine açılması uygundur.

Danışman Adı-Soyadı	Öğrencinin Adı-Soyadı
Tarih	Tarih
Dr. Öğr. Üyesi Yeşim S. Ünsever	Talal TALEB
25 Ocak 2023	25 Ocak 2023

İmza	İmza
Bu bölüme kişinin kendi el yazısı ile okudum anladım yazmalı ve imzalanmalıdır.	Bu bölüme kişinin kendi el yazısı ile okudum anladım yazmalı ve imzalanmalıdır.

ÖZET

Doktora Tezi

ÇEVRESEL ETKİLERE MARUZ KALAN YÜKSEK PLASTİSİTELİ KİLİN GEOTEKNİK ÖZELLİKLERİNİN FARKLI TEKNİKLER KULLANILARAK İYİLEŞTİRİLMESİ

Talal TALEB

Bursa Uludağ Üniversitesi
Fen Bilimleri Enstitüsü
Mühendislik Fakülte Inşaat Mühendislik Anabilim Dalı

Danışman: Dr. Öğr. Üyesi Yeşim S. ÜNSEVER

Killi zeminler dünyanın geniş bölgelerine yayılmıştır. Bu zemin tipi, düşük mukavemeti, yüksek sıkıştırılabilirliği ve yüksek hacimsel değişimleri nedeniyle birçok probleme sahiptir. Bu zorlukların üstesinden gelmek için birçok araştırmacı çalışmalarını zemin iyileştirme teknikleri üzerine yoğunlaştırmıştır. Bu araştırma, yüksek plastisiteli kil için düşük maliyetli ve çevre dostu bir takviye malzemesi olarak polipropilen elyafın (PP) kullanımının fizibilitesini araştırmayı ve optimumu belirlemek için elyaf içeriği ile fiziksel, mukavemet, şişme, sıkıştırılabilirlik ve dayanıklılık davranış değişikliğini değerlendirmeyi amaçlamaktadır. Etkili iyileştirme oranını karşılayan lif içeriği. Standart proktor testleri, Atterberg Limit testleri, direkt kesme testleri, serbest basınç dayanımı (SBD) testleri, drenajsız konsolide edilmemiş (UU) üç eksenli testler, şişme testleri, konsolidasyon testleri, kurutma testleri, kuru/ıslak çevrim testleri, donma/çözülme testleri gibi bir dizi laboratuvar deneyi (D-Ç) testleri, kompozit kilin (lif ile karıştırılmış kil) fiziksel, mukavemet, sıkıştırılabilirlik, çatlama direnci, hacimsel değişiklikler ve davranışın dayanıklılığı üzerindeki etkisini değerlendirmek için yapılır. Lif içeriği %0 ila %1.5 arasında değişir (toprağın kuru ağırlığına göre). Sonuçlar, fiberin dahil edilmesinin mekanik davranışı (kesme, SBD ve UU üç eksenli mukavemet) ve ayrıca sıkıştırılabilirlik davranışını (şişme ve konsolidasyon) geliştirdiğini göstermektedir. Ayrıca, kurutma işlemi sırasında oluşan kuruma çatlaklarına ve ıslak/kuru çevrimler sırasında oluşabilecek hacim değişikliklerine direnç göstermek için piyasada bulunan katkı maddeleri kullanılarak en uygun zemin iyileştirme tekniği araştırılmıştır. Sonuçlar, elyaf takviyeli numunelerin, çimento ve kireç stabilize numunelere kıyasla en düşük hacimsel deformasyona sahip olduğunu göstermektedir. Çatlama direnci ile ilgili olarak, lif içeriğine bağlı olduğu ve lif içeriğinin artmasıyla arttığı gözlemlenmiştir. Ayrıca, numuneler 10 döngü (D-Ç) 'ye tabi tutulduktan sonra UU üç eksenli mukavemet araştırıldı ve sonuçlar hem mukavemet davranışında hem de hacimsel değişim direncinde bir gelişme olduğunu gösterdiburada mukavemet azalması %0 lifde %51'den %18'e %0 lifde düşürüldü. Son olarak, sonlu elemanlar yöntemi uygulaması ile PLAXIS yazılımı kullanılarak 13 model programlanmış ve temel altında PP kullanımının fizibilitesi araştırılmıştır. Sonuç analizi, fiber eklenmesiyle taşıma kapasitesinin arttığını göstermektedir.

Anahtar Kelimeler: Lif-killi, mukavemet davranışı, sıkıştırılabilirlik, dayanıklılık.
2023, xviii + 159 sayfa.

ABSTRACT

Ph.D. Thesis

IMPROVING GEOTECHNICAL PROPERTIES OF HIGH PLASTICITY CLAY
SUBJECTED TO ENVIRONMENTAL EFFECTS BY USING DIFFERENT
TREATMENT TECHNIQUES

Talal TALEB

Bursa Uludağ University
Graduate School of Natural and Applied Sciences
Department of Civil Engineering

Supervisor: Asst. Prof. Dr. Yesim S. UNSEVER

Clayey soils are found all over the world. Because of its poor strength, high compressibility, and high amount of volumetric variations, this soil type presents various issues. To tackle these challenges, several researchers have focused their efforts on soil improvement approaches. The purpose of this study is to look into the feasibility of using polypropylene fiber (PP) as a low-cost and eco-friendly reinforcing material for high plasticity clay, as well as to assess the strength, compressibility, swelling, and durability behavioral changes with fiber content in order to find the optimum fiber content that satisfies the effective improvement rate. A set of laboratory tests, such as standard proctor tests, Atterberg Limits tests, direct shear tests (DST), unconfined compressive strength (UCS) tests, undrained unconsolidated triaxial tests, swell tests, consolidation tests, drying tests, dry/wet cycles tests, freeze/thawing (F-T) tests are conducted out to evaluate the effect of PP inclusion on the physical, strength, compressibility, cracking resistance, volumetric changes, and durability behavior of the clay composite (clay mixed with fiber). The inclusion of fiber varies from 0% to 1.5% (by soil dry weight). The results indicate that the addition of fiber improves the mechanical behavior (direct shear strength, UCS, and UU triaxial strength) as well as the compressibility behavior (swell and consolidation). Furthermore, The most appropriate soil improvement methods for resisting the generated desiccation cracks during the drying process, and resisting volume changes that might occur during wet/dry cycles were explored by utilizing the commercially available additives. The results reveal that in comparison to cement and lime-stabilized samples, fiber-reinforced samples had the lowest volumetric deformation. Regarding cracking resistance, it was observed, that it is connected to fiber content and increases as fiber inclusion increases. Moreover, UU triaxial strength was investigated after subjecting the samples to 10 cycles of (F-T) and the results show an improvement in both strength behavior and volumetric changes resistance where the strength reduction was decreased from 51% at 0% of fiber to 18% at 1% of fiber. Finally, through the application of the finite elements method (FEM), 13 models were programmed by using PLAXIS software and the feasibility of PP utilization under the foundation was investigated. The results analysis show the increase of bearing capacity with fiber inclusion.
Key words: Fiber-clayey soil, strength behavior, compressibility, durability.
2023, xviii + 159 pages.

ACKNOWLEDGMENTS

TABLE OF CONTENTS

SYMBOLS and ABBREVIATIONS

Symbols   **Definition**

E   Elasticity modulus
σv Applied vertical stress
$\Delta\sigma$ Deviatoric stress increment
$\Delta\varepsilon$ Deviatoric strain increment
$\sigma_{1\%}$ Deviatoric stress corresponding to an axial strain of 1.0%
$\varepsilon_{1\%}$ Axial strain of 1.0%
σ_0 Initial stress
ε_0 Initial strain
τ Shear strength
ΔL Displacement
e_t void ratio value at t time
V_o Initial void volume
V_s Solid volume
V_v Void volume
V_{ring} Volume of the testing ring
A_{ring} Area of the testing ring
γ_d Dry density
G Specific gravity weight
δh_t Consolidation settlement at time t
A_{sample} Sample's area
A_{crack} Cracking's area
$N_{crack-elements}$ Number of elements that represent the cracks in image matrix
N_t Total number of elements in image matrix
$\rho_{dry-max}$ Maximum dry density
w_{opt} Optimum water content
f fiber content
f_o Zero of fiber content
C_f Cohesion at f of fiber content
C_{fo} Cohesion at zero of fiber content
$\emptyset_f$ Friction angle at f of fiber content
$\emptyset_{fo}$ Friction angle at zero of fiber content
E_{oed} Elasticity modulus resulting from oedometer
$\Delta h/H$ Swelling/consolidation starin
SS_f Swelling stress at f of fiber content
SS_{fo} Swelling stress at zero of fiber content
Cc_f Compression index at f of fiber content
Cc_{fo} Compression index at zero of fiber content
q_u Unconfined compressive strength
q_{ult} Ultimate bearing capacity
D   Layer thickness/depth

Abbreviation Definition

C   Cement
DST   Direct shear test
FEM   Finite elements method
F-T   Freeze- thaw
L   Lime
LL   Liquid limit
MDD   Maximum dry density
OMC   Optimum moisture content
PP   Polypropylene fiber
PI   Plastic index
PL   Plastic limit
UU   Undrained unconsolidated
UCS   Unconfined compressive strength
USCS   Unified soil classification system
SEM   Scanning electron microscope
SL   Shrinkage limit

LIST OF FIGURE

LIST OF TABLES

CHAPTER I: INTRODUCTION

1.1 General Overview

Expansive or swelling soils are those that experience volume changes as a result of changes in their moisture content. Due to climatic and seasonal moisture variations, these soils display significant swelling and contraction movements. Thus, these movements seriously cause extensive damage to the structures built upon them. It is projected that shrinking and swelling soils inflict over 2.3 billion dollars in damage yearly in the United States alone, which is more than double the total annual cost of damages from earthquakes, hurricanes, floods, and tornadoes (Dasog and Mermut, 2013).

A substantial number of research have been undertaken in order to discover various treatment approaches to stabilize expansive soils and limit their detrimental impacts. These treatment techniques comprise surcharge loading, prewetting, replacing expansive soils with non-expansive soils, managing compaction, moisture control, adding chemical additives, and using thermal approaches (Nelson and Miller, 1992; Vessely and Wu, 2002; Sridharan and Gurtug, 2004). All of these techniques might have the drawbacks of being ineffective and costly. As a result, researchers are still looking into novel techniques and methods to improve the strength characteristics and decrease the swelling behaviors of clayey soils by employing various materials and additives (Akbulut et al., 2007; Raddi M. AlZubaidi et al., 2013; Ahmed M. Al-Mahbashi et al., 2015; Mohammed A. M. Al-Bared et al., 2019; Seyhan et al., 2017). Generally, the chemical soil stabilization technique by using conventional materials like cement, lime, and fly-ash (Panchal et al., 2018; Rios et al., 2015; Rios et al., 2016) is considered the most used technique. While, recently, geo-polymerization (soil-polymer mixtures) has been presented as a viable method for improving the properties of problematic soils (Zhang et al., 2012; Kua et al., 2017; Hoy et al., 2017).

Recently, randomly oriented synthetic and natural fiber materials have been mixed with problematic soils to enhance soils' strength behavior. Numerous experimental

investigations have been conducted on fiber-reinforced soils with different types and materials (Akbulut et al., 2007; Kumar et al., 2007; Sivakumar Babu et al., 2008; Viswanadham et al., 2009). These earlier investigations came to the conclusion that the strength characteristics of fiber-reinforced soils comprised of discrete fibers are a function of fiber content and fiber-surface friction along with the soil and fiber strength properties.

Reinforcement techniques are carried out either by adding continuous reinforcement in the form of slides, sheets, bars, mesh, or mat within the soil mass, after determining their location and direction or by mixing separate fibers with the "soil fill" before placing it in the required place at the project site. However, the use of geosynthetic materials has confirmed the effectiveness of enhancing the bearing capacity of shallow foundations and reducing the potential post-construction settlements of the constructions established on embankments on both long-term and short-term (Hoy et al., 2017).

Fibers-reinforcement technique provides an alternative method to chemical stabilization and other techniques for stabilizing clayey soils. Randomly distributed short fibers made of natural, synthetic, and waste materials have demonstrated reasonable promise for soil reinforcing applications, such as the restoration of a slope veneer or in partly failed slopes (Mirzababaei et al., 2017). Yilmaz (2015) demonstrated that combining fly ash and polypropylene fibers successfully improved the unconfined compressive strength of expansive clays. Cai et al. (2006) observed that a decrease in the swelling potential of lime-stabilized clayey soil was caused by an increase in fiber content. However, studies on the utilization of randomly oriented synthetic fibers to study the desiccation cracks behavior and to reduce the volume changes resulting from climatic changes in expansive soils have not been settled yet. The same in reference to the stabilized clayey soils by chemical additives where most of the researches have been focused on the stabilization of soils using various additives such as cement, lime, industrial waste products, fly ash, calcium chloride, potassium nitrate, and phosphoric acid (Aiban et al., 2006; Kalkan, 2006; Guney et al.,2007; Segetin et al., 2007; Degirmenci et al., 2007; Harichane et al., 2011; Sunitsakul et al., 2012; Yilmaz and Ozaydin, 2013). These previous researches were concerned with improving the strength characteristics and behavior, whereas there were very limited researches concerned with cracking resisting and reducing the

volumetric changes due to the climatic conditions. As climatic changes such as long drying periods during summer, drying/wetting cycles, or freezing/thawing cycles due to seasonal changes have a great impact on both strength and compressibility behaviors.

1.2 Research Motivations and objectives

Most recent studies that focused on using various materials as additives to be mixed with weak soils were concerned with improving the strength characteristics and behavior regardless of its environmental impact. Where a number of recent studies have shown that incorporating larger concentrations of coal fly ash into water and soil releases harmful components, resulting in soil and groundwater contamination and serious health, environmental, and land-use issues. (Imran Khan and Rashid Umar, 2018). Therefore, the devastating effects on the environment resulting from the utilization of chemical additives in soil stabilization should be considered, where a substantial amount of greenhouse gases are being released into the airosphere through a strong alkalization phase (as in the lime utilization case), which that will reflect in turns to a high social cost and potential damage to the flora and fauna (Rogers et al., 2009). Alike, large amounts of CO2 are emitted during the production phase of cement and fly ash which prevents plants' growth and pollutes the environment (Caravaca et al., 2017; El-Attar et al., 2017). On the other flip, it is essential as well to consider the effect of environmental changes on soil behavior before adopting any stabilizers or additives to maintain a sustainable solution that can withstand the additional stress resulting from the temperature differences and maintain both strength and compressibility behaviors. Hence, it's crucial to employ sustainable and ecologically friendly alternatives to enhance the soil strength behavior and resist the additional stress resulting from the drying process, drying/wetting cycles, freezing-thawing cycles, or temperature differences. Also, the high resistance of the proposed stabilizers/additives against environmental changes should be considered to maintain the durability and sustainability of the proposed solutions/stabilizers.

Therefore, this research came to assess the viability of using short polypropylene fiber as an affordable and eco-friendly reinforcing material to improve the swelling and strength behavior of clayey soils and track the behavioral changes with the fiber content. Thus, we

aimed to identify the optimum fiber content that should be added to obtain an effective improvement rate for both strength and swell properties and behavior in high-compressibility clayey soil. Additionally, evaluate the effect of polypropylene fiber to reduce the formation of desiccation cracks in clay and reduce the volumetric changes due to dry/wet cycles and freezing/thawing cycles. Furthermore, evaluate the most appropriate stabilization methods by assessing the usage of chemical additives (cement, and lime), and fiber additives and their effectiveness on the cracking and volumetric changes. Thus, determining the optimal fiber content that best fits the effective improvement rate, and highlighting the durability of fiber utilization against the drying process, drying/wetting cycles, and freezing-thawing (F–T) cycles by inspecting the volumetric changes in the fiber-soil mixture with different contents are aimed in this study.

1.3 Research Methodology

This research was done based on the experimental methodology through conducting comprehensive laboratory experiments program performed on clayey soil with high plasticity for studying the influence of polypropylene fibers (FPP) on physical, mechanical, and swell characteristics and behavior. Initially, the studied soil characteristics and index properties were determined and then compared with fiber-reinforced samples (fibrillated polypropylene fiber), where three fiber contents were considered (0.5%, 1%, and 1.5% by soil's dry weight). The fiber content/weight is the studied ratio multiplied by the dry weight of the soil sample for each sample. Therefore, the optimal fiber content was investigated first. Then, drying, drying/wetting cycles, and freezing/thawing cycle conditions were considered to assess the environmental effects on the fiber-clay mixtures. Moreover, the most conventional chemical stabilizers (cement and lime) were considered in the test program to evaluate the most appropriate techniques in terms of environmental changes resistance and related optimum fiber content. Also, for evaluating the feasibility of using the fiber under the foundation, PLAXIS 2D models were programmed in light of the outputs of the experimental findings and the relevant results were presented accordingly.

2. CHAPTER II: THEORETICAL BASICS AND LITERATURE REVIEW

2.1 Soil Reinforcement Technique

The current growth in both construction materials and their implementation technology consider the main reason for the great developments that have taken place in structural engineering recently. Larger structures became possible after using more advanced materials. For instance, using manufactured steel technology enabled engineers to construct longer bridges and taller buildings in comparison with the buildings and bridges that were constructed with wrought iron or other conventional building materials. On the flip side, as it is well known that soil and rock are the prime materials of geotechnical engineering, it is hard to think of similar developments or growth in geotechnical materials in this field. However, in recent years, the soil stabilization technique by using different materials and different techniques could be considered as an example of material and construction application simultaneous development.

Soil reinforcement is defined as a composition of soil and reinforcing material formed by mixing soil with reinforcing material under a pre-identified ratio for realizing the required engineering properties. Reinforcement is carried out either by adding continuous reinforcement in the form of slides, sheets, bars, mesh, or mat within the soil mass, after determining their location and direction or by mixing separate fibers randomly with the "soil fill" before placing it in the required place (stacked at the project site). The advantages of utilizing randomly distributed fibers over planar reinforcement approaches can be mainly summarized as follow (Yetimoglu and Salbas, 2003): absence of potential plane of weakness; Feasibility of application in comparison with the utilize of planar reinforcement such as geotextiles; inert chemical nature, as it does not dissolve in the soil and cannot be absorbed, (does not exhibit any interaction with soil moisture); cost-efficient due to its market availability and cheap.

2.1.1 Types of geosynthetic materials used in reinforcing soils

Geosynthetic has been defined per ASTM as polymeric material utilized in rock, soil, or other geotechnical-related materials as a crucial component of civil engineering projects. A geotextile is a geosynthetic produced from textile materials. Geogrids are mainly utilized for reinforcement; They are made of a symmetrical network of tensile components with openings large enough to connect with the filler material around them. Geomembranes are geosynthetics with very limited permeability utilized as fluid barriers. Geotextile-related products such as grids and nets can be combined or merged with geomembranes and other materials of synthetics to benefit from the advantages of each component. These combinations are called geocomposites, and these can be composites of geotextile geomembranes, geotextile-geonets, geotextile-geogrids, geotextile-polymeric cores, geomembrane-geonets, and even three-dimensional polymeric cell structures (Holtz, 2001). There are almost no limits to the variety of possible and useful geocomposites. The general generic term encompassing all these materials is geosynthetic and generally divided into two main types; Geotextiles and Geofibers.

Recently, due to the great development in manufacturing techniques and high growth in global market demand, geosynthetic materials have been utilized widely. The size estimation of the international geotextile market is approximately in 2019, 4.6$ billion, and the expected compound annual growth rate is to be 11.9%. The Asia-Pacific region, which includes China, India, and other nations, is the biggest market for geotextiles. Due to the high demand for geotextiles in sophisticated and developed countries for infrastructure projects, China made up 45.7% of the geotextile market in the Asia Pacific in 2019. The principal uses of geotextiles, as indicated in Figure 2.1, are road construction, erosion prevention, and drainage systems (Hao Wu et al., 2020).
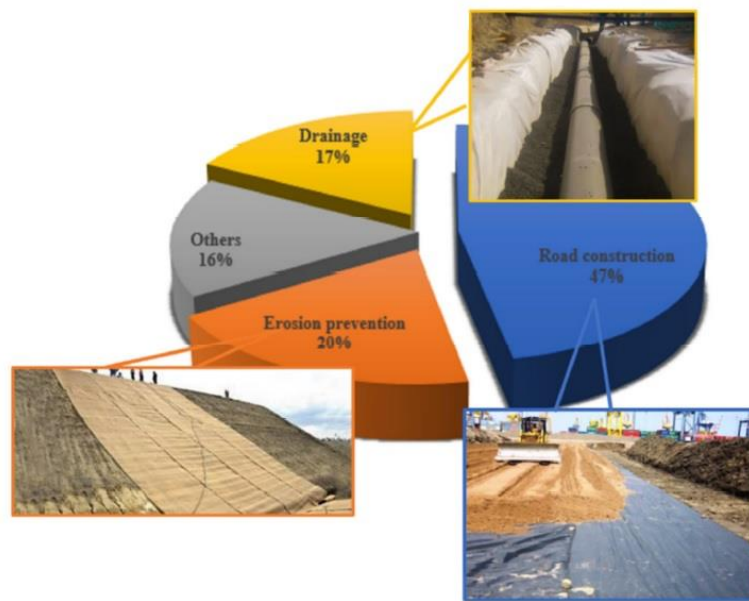
Figure 2.1. Global geotextile market share as of 2019.

2.1.2 Geotextile types and their geotechnical applications

The American Society for Testing and Materials (ASTM) describes geotextiles as permeable fibrous materials bonded to foundations, rocks, soils, or other geotechnical materials as an essential component of man-made projects, structures, or systems. Geotextiles are mainly used for the reinforcement of segregated applications such as unpaved roads, paved roads, and sediment control. Geotextiles are increasingly proving to be an economically viable alternative material in the engineering field. Earlier this decade, the utilization of geotextiles expanded rapidly in the global market. Geotextiles are made primarily of polyolefin, they are lightweight and strong, yet inexpensive. Certain fabrics give high puncture resistance and provide distinct recognition on highway and rail construction projects or where sheeting reliability is required, e.g. in landfills projects.

Referring to the manufacturing process, geotextiles can be classified as woven, non-woven, or knitted. Textiles are made using traditional weaving techniques to create mesh-like or net-like materials with varying mesh opening sizes and weave densities. Woven fabrics exhibit low elongation, high tensile strength, and poor abrasion resistance. On the other hand, non-woven fabrics have high air permeability and high elongation properties.

They are manufactured in different geometric and polymeric compositions to suit different applications. Continuous filament yarns or short staple fibers are used to create nonwoven geotextiles. Fiber bonding is carried out via thermal, chemical, mechanical, or a mix of these methods (Haghi, 2009).

Woven geotextiles generally have higher strength values, while non-woven geotextiles have higher permeability and flow rate. Here's a rundown of the differences in physical attributes: Woven fabrics are plastic-like in feel and appearance, while non-woven fabrics have a fuzzy-like feel and appearance. Figure 2.2 shows the geotextile categories ((a) woven; (b) nonwoven).
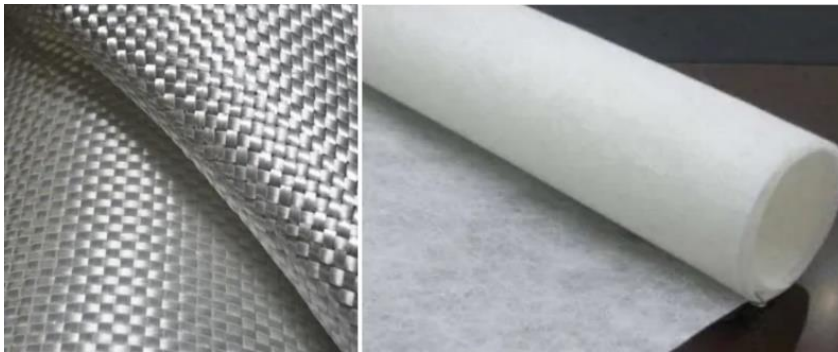
Figure 2.2. Geotextiles categories ((a) woven; (b) nonwoven)

However, the main types of geotextiles that are used in geotechnical applications fall into four main types or categories as follows:

1. Geomembrane: This synthetic sheet is made of materials with limited permeability to control fluid migration in a project as a barrier or liner. The materials may be asphaltic or polymeric or a combination thereof. The term barrier applies when the geomembrane is utilized inside the earth's mass. The term liner applies where the geomembrane is utilized as a surface revetment or an interface (Abdelmawla, 2017). This makes them ideal for forming waterproof or gas-proof barriers between adjacent bodies of soil or soil and fluid. Some of their potential applications include sealing against fluid percolation along the coasts, river banks, reservoirs, and in water storage. A typical thermoplastic geomembrane will have diffusion permeability of the order

of 10-11 to 10-13 cm/s. The main usage of these materials is as a liquid or vapor barrier because of their extraordinarily low permeability (Haghi, 2009).

2. Geogrid: It is a polymeric product made of ribs, which are tensile-resistant intersecting parts that are integrally joined at the joints and have a mesh or net-like regular open network. Geogrids are often made by extruding and stretching high-density polypropylene or polyethylene or by weaving or knitting and coating high-tenacity polyester yarns. The resulting grid structure has large openings (called apertures) that improve interaction with the soil or aggregate. Their physical structure can be divided into the following (see Figure 2.3):

   a) Unidirectional geogrid: The greatest value of tensile strength in one direction (longitudinal or transversal) considers as its main character in comparison with the other directions.
   b) Bidirectional geogrid: It is recognized with identical resistance in the longitudinal and transverse directions.
   c) Extruded geogrid: Created by uniaxial or biaxial stretching, an integral extruded structure.
   d) Bonded geogrid: it is formed by connecting two or more strands at right angles.
   e) Woven geogrid: Made by interlacing, usually at right angles, two or more yarns, filaments, or other elements.
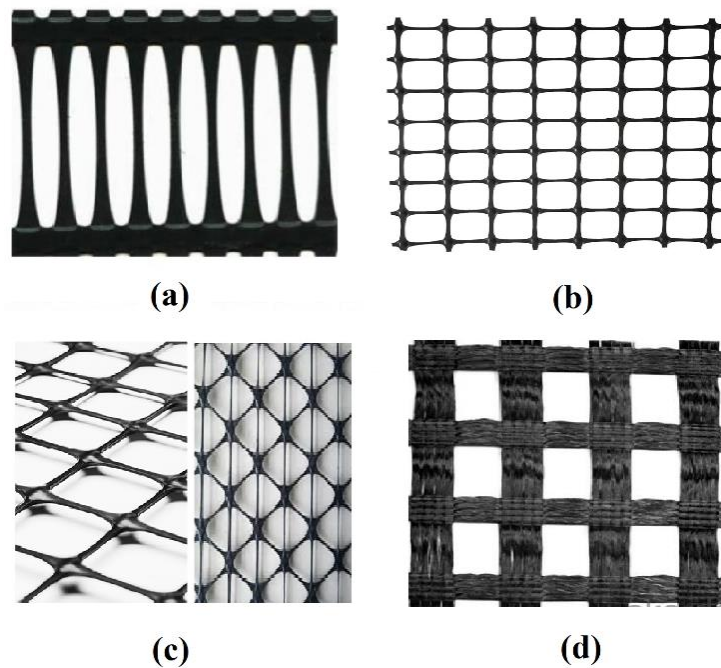
Figure 2.3. Typical geogrids: (a) Unidirectional; (b) Bidirectional; (c) Extruded; (d) woven

3. Geonet: It is a polymeric product made of a symmetrical, dense network of parallel, integrally linked sets of ribs that are layered over one another at varying angles. Geonets appear to be similar to geogrids at first glance; however, geonets differ from geogrids primarily in their roles to accomplish in-plane drainage of liquids or gases, rather than in their material or construction.

4. Geocomposite: This term applies to the product that, when used together, performs a specified function(s) more successfully than when used individually.

2.1.3 Geofibers

They are synthetic fibers, usually 1 to 2 inches in length, and are made in the form of separate filaments or in the form of a strip. Polypropylene fibers are the most commonly used where they are mixed with soil to provide an appropriate reinforcement system for fixing slope failures, strengthening pavement subgrades, stabilizing foundations, and enhancing retaining wall backfill. Geofibers contribute to the creation of a soil

reinforcement system with drastically improved engineering qualities by meshing synergistically with the soil already on site.

Textile fibers are typically divided into two primary categories, natural and man-made fibers. Natural fibers are any fibers that originate from living things (animals, plants, etc.) and do not undergo any kind of processing to become what they are. Natural fibers comprise cellulosic fibers like cotton and linen, as well as protein and mineral fibers like asbestos, silk, and wool. Man-made fibers are those in which the fundamental chemical units have been created by chemical synthesis, followed by the production of the fiber, or in which the polymers from natural sources have been dissolved and then regenerate into fibers after being spun through a spinneret. Synthetic fibers are those created through chemical synthesis, whereas regenerated fibers or natural polymer fibers are those created from natural polymer sources. Polyester, polyolefin, vinyl, acrylic, and elastomeric fibers are examples of man-made synthetic fibers, while cellulose acetates, rayon, regenerated proteins, rubber, and glass fibers are examples of regenerated fibers (Needles, 1980). Figure 2.4 shows the primary fibers' categorization scheme.

Polyolefin fibers are manufactured from polymers created via chain growth polymerization of olefins (alkenes) and comprise at least 85% propylene, ethylene, or other polymerized olefin units. Polypropylene and linear stereoregular high-density polyethylene are the most often utilized materials in textile applications, with polypropylene prevailing because of its greater temperature stability. These fibers offer high strength and toughness, as well as abrasion resistance and a reasonable cost. These fibers are difficult to dye and have low melting temperatures, yet they are useful in a wide range of textile applications (Needles, 1980).
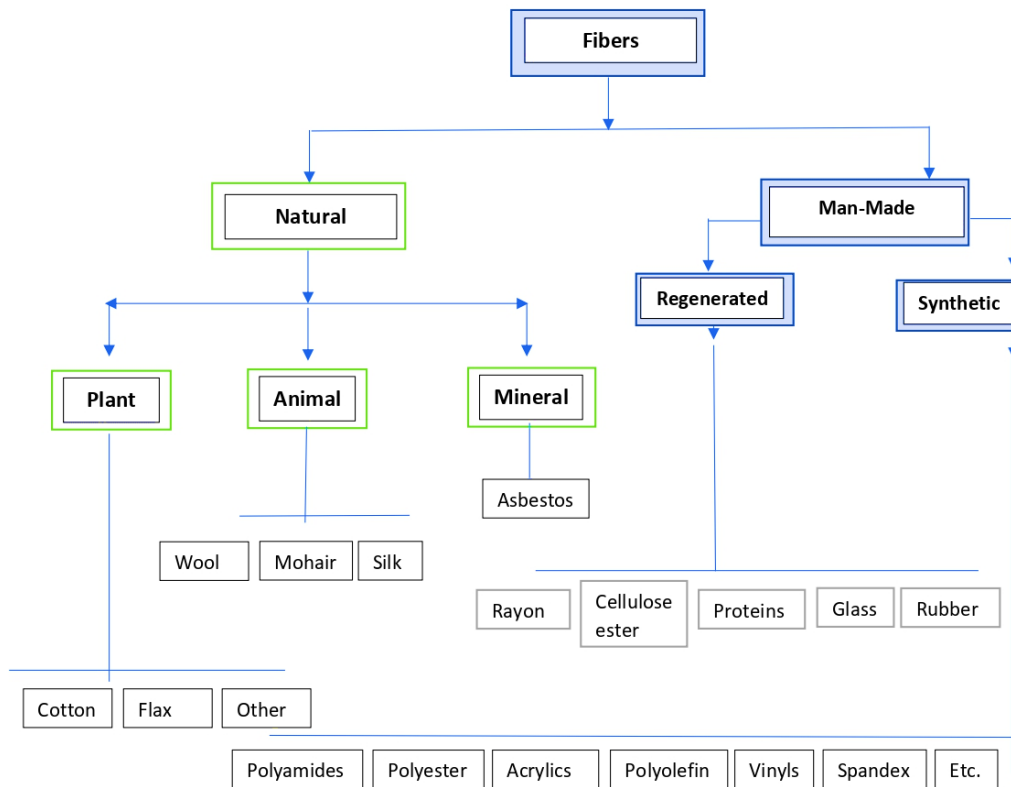
Figure 2.4. Primary fibers' categorization scheme.

Polyolefin fibers are the most used fiber specifically Polypropylene and polyethylene series which are unsaturated hydrocarbons, containing only carbon and hydrogen atoms, they are considered strong fibers with outstanding elongation and recovery characteristics. Figure 2.5 shows hydrocarbon structure and related shapes by using the scanning electron microscope (SEM) technique (Hao et al., 2020). Fibers range in tenacity from 3.5 to 8 g/denier (denier: measurement unit for longitudinal density of the thread its length 9000 m), with an elongation of 0%-30% at break. The fibers stress' recover is 95% recovery at 10% elongation. The fibers are fairly stiff and moderately bending resilient. Also, since polyolefins have no moisture regain and are hydrophobic as well, their moisture does not affect their properties. The specific gravities of polyethylene fibers are varied from 0.95 to 0.96, while it is varied from 0.90 to 0.91 for polypropylene. As a result, these fibers float on water and are the lightest of the major commercial fibers.
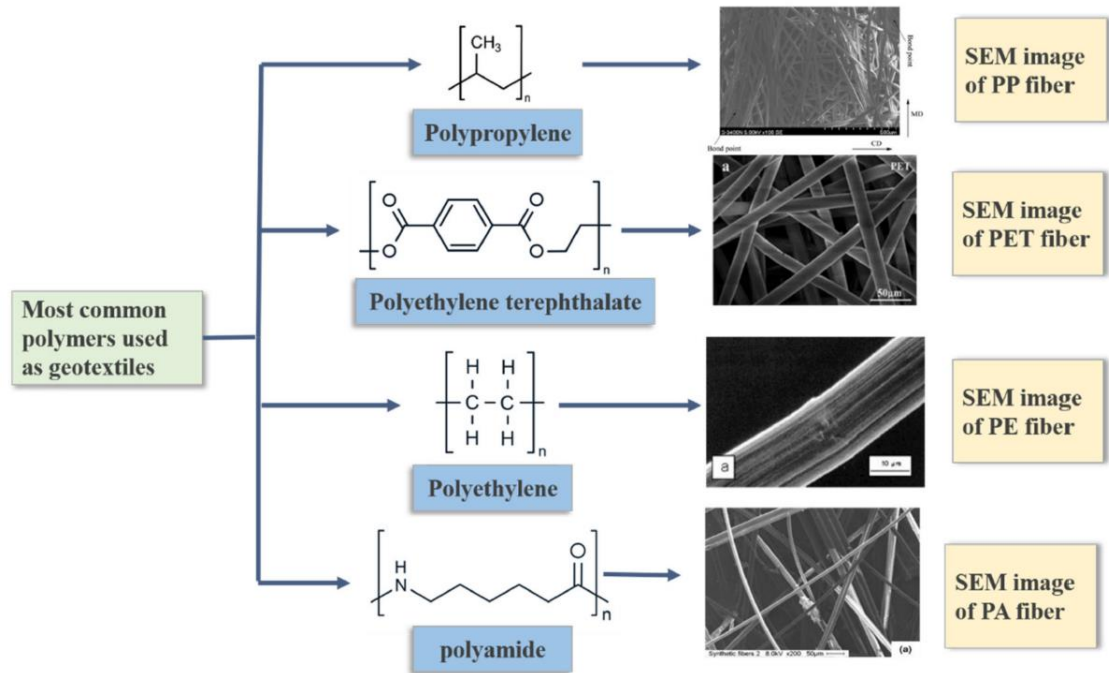
Figure 2.5. Most common fibers are used as geotextiles and SEM images (Hao et al., 2020).

The fibers (polyethylene and polypropylene) are not influenced by solvent substances at room temperature, while at high temperatures, they are affected by hydrocarbons that are aromatic and chlorinated. They manifest excellent heat and electrical insulation characteristics and are extensively employed in these applications. The fibers are heat-sensitive. Polyethylene softens at around 130°C and melts at 150°C, whereas polypropylene softens at around 150°C and melts at around 170°C. Polyolefins are extraordinarily chemically resistant and inert. Under normal circumstances, they are unaffected by biological and chemical agents.

2.1.4 Geosynthetics materials (geotextiles and geofibers) applications

Almost all forms of civil engineering structures may use geosynthetic materials which include but are not limited to geotechnical, geoenvironmental, hydraulic, coastal, sediment and erosion control, and transportation engineering applications, and its main functions are:

- Separation: The separating function of geotextile is mainly used in road construction. The geotextile inhibits the mixing of two adjacent soils. By isolating fine subgrade soil from base course aggregates, for example, the geotextile preserves the aggregate material's drainage and strength capabilities (see Figure 2.6).
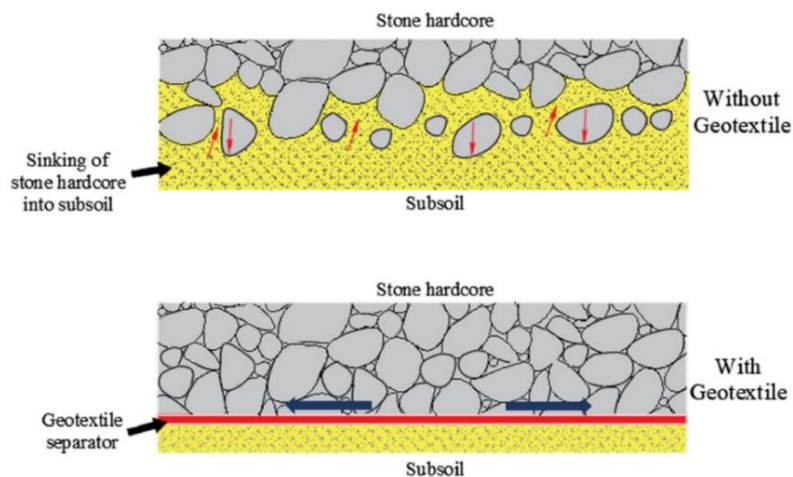
Figure 2.6. Geosynthetics separation function images (Hao et al., 2020).

- Filtration: The balance of the geotextile-to-soil system that allows for appropriate liquid flow while minimizing soil loss across the geotextile plane. The collapse of the soil structure generally is occurred as a result of seepage flow due to the transport of fine particles. Because geotextiles have positive permeability and air permeability (i.e. a geotextile filter allows water to enter drainage medium such as gravel or a geosynthetic while keeping soil particles out), they can be utilized to prevent the loss of soil particles during the liquid flow which allows them to pass, and prevent the fine grains and that contributes to avoiding soil damage (Cao et al., 2020). So thus, the primary features of geotextiles that include infiltration action are porosity and permeability (see Figure 2.7).
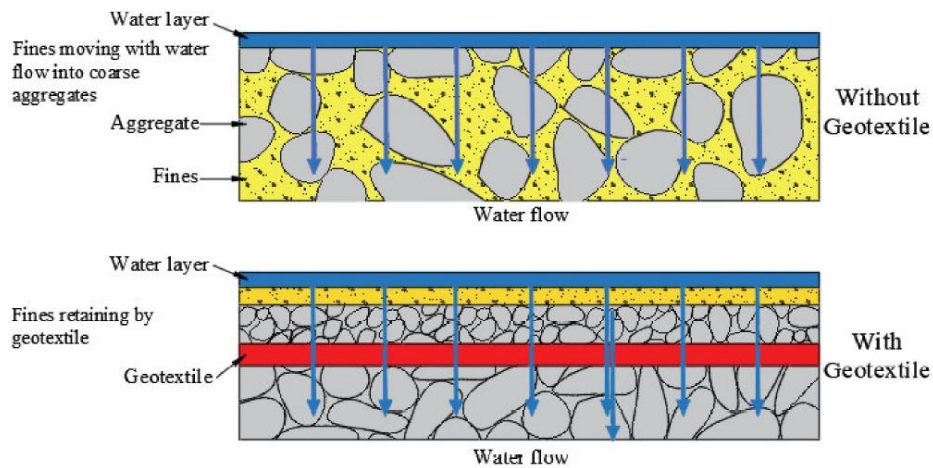
Figure 2.7. Geosynthetics filtration function (Cao et al., 2020).

- Reinforcement: Placing geotextiles in soil improves its tensile strength, as does the equivalent quantity of steel in concrete. The following three mechanisms contribute to soil strength acquisition as a result of geotextile application: Interfacial friction between the geotextile and the soil/aggregate restricts lateral movement; driving the fracture plane of the proposed bearing surface to produce an alternate surface with higher shear strength; support for wheel loads using membranes. Figure 2.8 shows the mechanism of the reinforcement function (Liu et al., 2020).
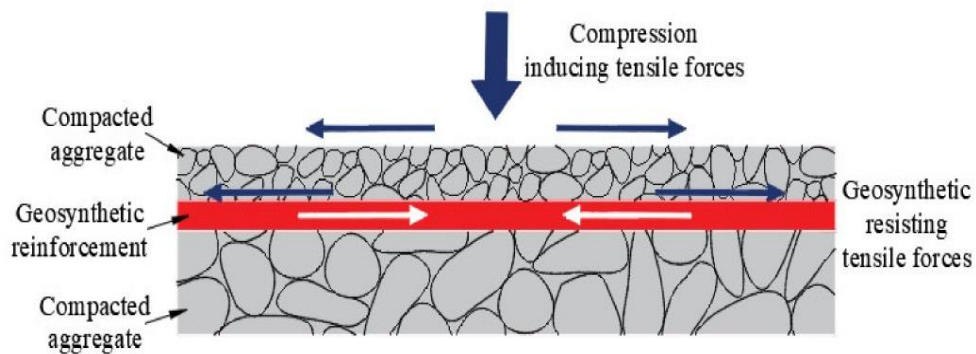
Figure 2.8. Geosynthetics reinforcement mechanism (Liu et al., 2020).

- Sealing: Between the existing and new asphalt layers, a layer of non-woven geotextile is impregnated. The geotextile absorbs asphalt to form a waterproofing barrier, reducing the vertical influx of water into the pavement structure.

15

- Road Work: Geosynthetics (geofibers and geotextiles) are extensively employed in road construction. It strengthens the soil by increasing its tensile strength. It is utilized as a rapid dewatering layer in the road foundation, the geotextiles need to preserve their permeability without losing their separating functions.

- Railway construction: Where the ground is unstable, woven or non-woven fabrics are used to separate the ground from the subsoil without impeding the circulation of groundwater. The wrapping of the individual layers with fabric prevents the material from shifting sideways due to shock and vibration from moving trains.

- Drainage: Recently the utilization of geotextiles as fillers has been considered a viable alternative to conventional systems. Geotextile filters are applied for roads and highways, reservoirs, drainages in earth dams, deep drainage trenches, and behind retaining walls (Chuang Lin and Xiong Zhang, 2018). Figure 2.9 shows the geosynthetic drainage mechanism.
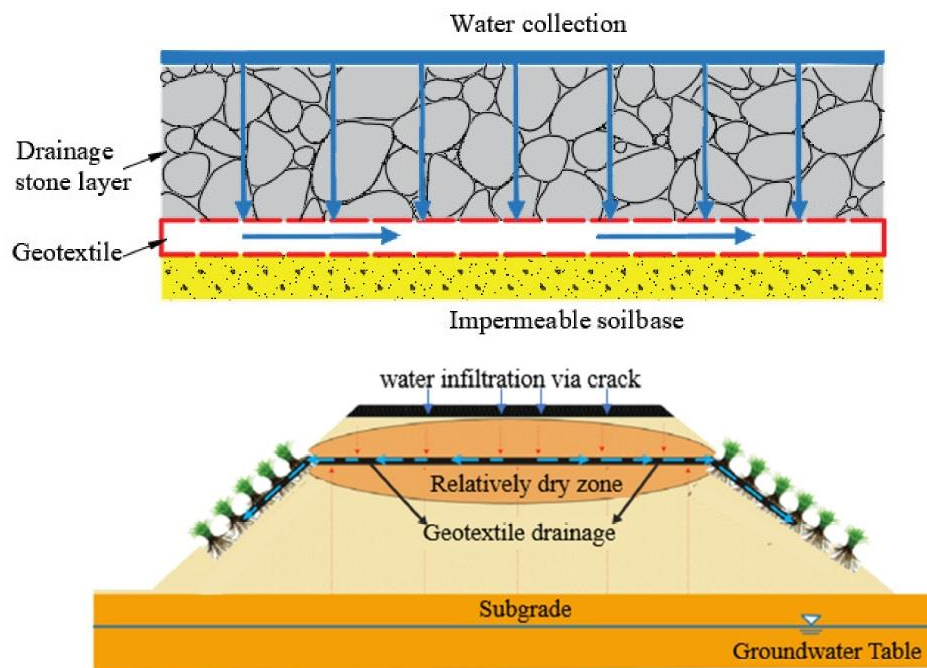
Figure 2.9. Geosynthetics drainage mechanism (Chuang Lin and Xiong Zhang, 2018)

2.2 Soil Stabilization Techniques and Environmental Changes Consideration

2.2.1 General overview

Many earth structures are constructed on clayey soils which tend to shrink and swell when subjected to climatic changes such as long drying periods during summer or drying/wetting cycles due to seasonal changes. During dry times, clay near the slope's surface shrinks, resulting in desiccation cracks. Deep cracks reveal the interior of the soil mass, allowing for more cracking. When the slope is subsequently wetted due mainly to rainfall, the massive network of cracks and fissures formed during clay shrinkage allows for quick percolation of rainwater. Consequently, an extensive network of fissures and cracks is developed. Hereby, and when the water fills the developed cracks, the clay along with the cracks' paths swells, and the strength decreases. Over the time, and due to the exposure to cycles of shrinking and swelling, a failure of the slope may results. Also, extreme dryness and subsequent rainfall might jeopardize dam stability (Chao-Sheng et al., 2011).

In engineering applications, clayey soils, which are prone to drying cracks, are often used in the construction of liners, and slurry walls to contain solid or liquid waste. The existence of cracks often reduces the structural and functional utility of the previously described contamination barriers (Miller et al., 1998). In other cases, cracks generally mean that groundwater recharge can occur faster, a situation that can lead to instability on natural slopes and vertical cuttings (Baker, 1981), and it can reduce the bearing capacity of foundations (Silvestri et al., 1992). Due to the increasing frequency of severe droughts and the continued use of clay in civil engineering, soil desiccation cracking and volume changes due to climatic changes (drying/wetting cycles) receive extra attention in both research and practical aspects. However, the fundamental of desiccation crack initiation and propagation has not been fully understood. Additionally, the geotechnical literature on desiccation cracking is not thorough nor extensive, though notable contributions have been made by many researchers (Corte and Higashi, 1960; Morris et al., 1992; Abu-Hejleh and Znidarcic, 1995; Konrad and Ayad, 1997; Yao et al., 2002; Rodríguez et al., 2007; Péron et al., 2009).

On the other flip, in cold areas, the most serious factor to determine the engineering behavior of expansive soils is freezing-thawing cycles, which can change the engineering properties and behavior of the expansive soils. Due to the existence of clay minerals such as illite and montmorillonite, the clayey soils expose a high level of swell and shrink monuments which results in cracks. The cracks' initiation and propagation in covers and liners structures will lead to the creation of water flow paths that will increase dramatically the hydraulic conductivity and end up in the failure of drainage systems in dams' constructions. During soil freezing, ice crystals of different shapes and sizes cater to partition in soils, resulting in the formation of various structures (Hohmann Porebska, 2002). While during the thawing period, the frozen layer begins to thaw from the top and the bottom simultaneously. As a result, soil behavior is substantially changed, and cracks create pathways for the transfer of fluids. Cracked soils can boost surface water infiltration into the containment system or fluid infiltration into the surrounding soil and groundwater (Benson and Daniel, 1994). The movements and changes caused by the shrinking and swelling of soil particles are frequently large enough to cause damage to highways, sidewalks, and small buildings. The yearly cost of damages to roads, buildings, pipelines, airports, and other structures is around 9$ billion (Jones, 1987).

2.2.2 Cracking Types

From the cracks' formation perspective, cracks can be categorized into two major types as follows:

1. Mechanical cracks: These are developed as a result of deposition or improper construction. Cracking with no good correlation between lifts and inadequate compaction is an example of this kind.
2. Physicochemical cracks: These are classified into three types: cracks generated by freeze-thaw cycles, syneresis cracks, and cracks generated by full-material drying.

2.2.3 Factors affecting cracking

The following factors affect the shrinkage and cracking behavior of soils are:
content of clay, drying process, drying/wetting cycles, freezing/thawing cycles, unit weight, soil particle orientation, compaction conditions, pore fluids, and exchangeable

ions. When the plasticity index is high, the probability of shrinkage and expansion is high. However, by adding coarse particles to clay soils, the risk of shrinkage and cracking can be reduced (Kleppe and Olson, 1985).

Daniel and Wu (1993) showed that the near-optimal water content range with the highest compaction energy measurements was adequate to achieve three objectives: reducing the capacity to shrink and crack when dry, achieving low hydraulic conductivity, and being capable of sustaining shear strength structural stresses.

Albrecht and Benson (2001) studied the effect of desiccation on compacted natural clay. They found out that the volumetric contraction strain that takes place in compacted natural clays during dryness is a direct function of the water volume/soil volume when the soil is saturated. Soils with higher clay content and higher plasticity index generally have higher water volume and are therefore more susceptible to large volumetric shrinkage deformations during drying. In addition, samples that were compacted at higher compaction efforts near the optimal moisture content had less water volume when saturated and fewer volumetric shrinkage changes. The same findings were reported by Puljan (2010) who investigated the expansion strain and shrinkage of compacted soil at the wet side of optimal water content, at optimal water content, and at the dry side of optimal water content.

Eventually, according to results obtained by Omidi (1993), Albrecht and Benson (2001), Osinubi and Eberemu (2010), and others, the shrinkage strain is connected to three main factors: dry density (compaction effort), water content, and soil plasticity index. When the soil's plasticity index increases, so do its water content and shrinkage strain. Furthermore, an increase in compaction effort leads to an increase in dry density and, as a result, a decrease in shrinkage strain. See Figure 2.10 which summarizes the findings resulted by the aforementioned researchers conducted on different types of soils.

(a)   (b)

(c)
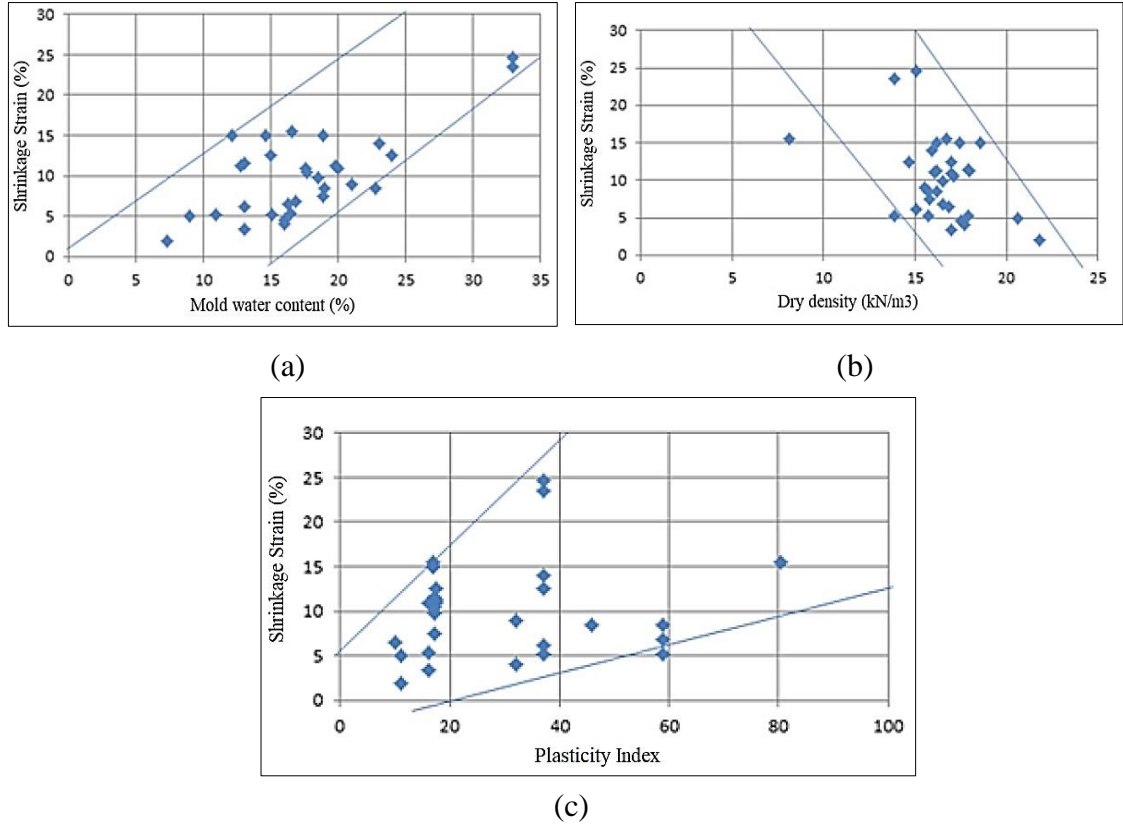
Figure 2.10. Parameters affecting shrinkage strain as presented by (Omidi, 1993); Albrecht and Benson, 2001; Osinubi and Eberemu, 2010): (a) Effect of mold water content (b) Effect of dry density, (c) Effect of plasticity index on the shrinkage strain for different types of soil

2.2.4 Cracking mechanisms

Under the influence of the surrounding environment, the soil shrinks internally, loses water, and develops internal tensile stresses, changing its microstructure. When the tensile stress exceeds the soil's tensile strength itself, the mechanical and physical properties of the soil progressively deteriorate and eventually cracking occurs. Under conditions of drying application and freeze-thaw cycles, interactions induced by water migration in the soil disrupt the soil particulate skeleton, reducing the strength of the soil sample and leading to soil site failure. Jianwei et al. (2022) elucidated that the soil cracking during freeze-thaw and dry-wet conditions is comprised of a combination of micro and macro cracks. Where it was observed that the freeze-thaw cycle mostly creates invisible micro-cracks in soil samples, whereas the dry-wet cycle primarily produces obvious macro cracks. However, it is worth keeping in mind that these changes are connected to the water

content of the soil sample. Shi et al. (2021) figured out that erosion destroys the cementation between soil particles, weakens the mechanical strength of the soil, and changes the arrangement structure between soil particles. Zhao et al. (2021) discovered that moisture content has a significant impact on the microcracking and microstructural composition of clay in the freeze-thaw cycle test, which weakens the soil's mechanical characteristics.

Recently, extensive researches were done to study the mechanism of shrinkage cracking of earthen sites (Leng et al., 2018; Weiss et al., 2018; Bachmann and Van, 2015; Tang et al., 2018; Wang et al., 2018), it was figured out that soil cracks are connected to internal water loss. Throughout the dry shrinking process, the soil's pore size decreases, and compactness increases. With continuous drying, water flow increases (ie. water migration from the interior of the soil to the surface), and the water molecules evaporate when the relative humidity of the surface soil is higher than the relative humidity of the atmosphere. So thus, cracks in the soil occur initially at intergranular pores due to the combined action of capillary pressure and surface tension (Figure 2.11). After the formation of a crack network, the following applies: the smaller the thickness of the soil layer, the lower the water content and the lower the surface resistance.
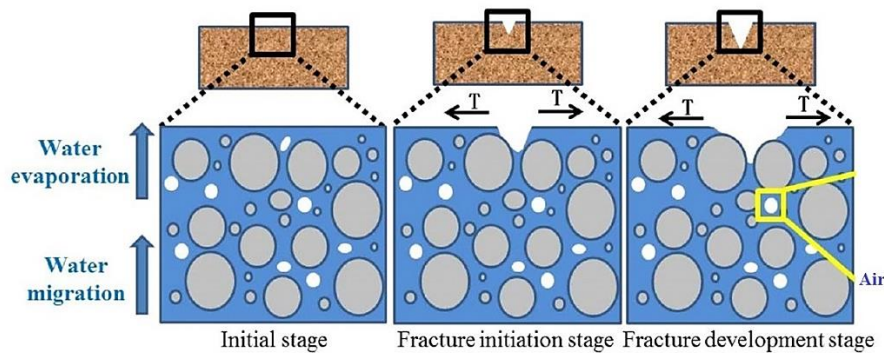
Figure 2.11. Dry shrinkage cracking process schematic diagram (Tang et al., 2018 and Wang et al., 2018)

The cracks or volume changes, that result due to freeze-thaw cycles, take place when the temperature is below 0°C, and the volume of frozen water between the particles of the soil expands, causing these particles to move relative to one another. This process leads to frost-heaving or frost deformation forces in the soil. Xue et al. (2017) have proved

experimentally that the migration of liquid water led to frost heaving in the soil. The schematic diagram of the earthen soil capillary frost heaving model is illustrated in Figure 2.12 and as it was described by Jianwei et al. (2022), which depicts heat, air, and liquid water flow in the soil. Under the influence of the water potential gradient, unfrozen liquid water and steam move along the direction of temperature reduction when a temperature gradient is generated in the soil. Moist air moves toward the freezing front (where the surface temperature is about the freezing point) because it has the same potential energy gradient as liquid water. Also, due to the low temperature, water vapor condenses at the edge of the ice, allowing only liquid water and dry air to be transported into the freezing zone. A thin ice layer is generated on the soil's surface with further migration of liquid water.
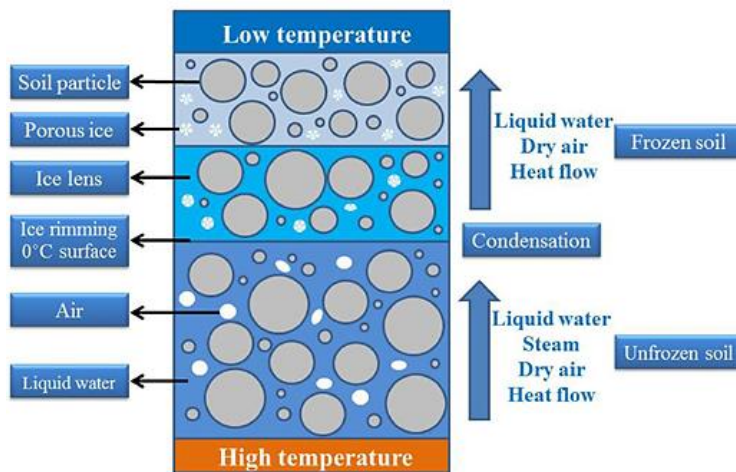
Figure 2.12. Frost heaving process schematic diagram of (Xue et al., 2017).

In the soil melting stage, the opposite movement to the freezing stage is observed (i.e. the movement of liquid water, heat, and air in the earthen soil is opposite to the freezing stage) see Figure 2.13. After the crystalline water, in the pores, in the upper section of the soil melts, a small portion of the water evaporates through the surface while the other portion migrates through the "neck/throat" into the sample, causing water loss and cracking on the surface of the earth (Jianwei et al., 2022).
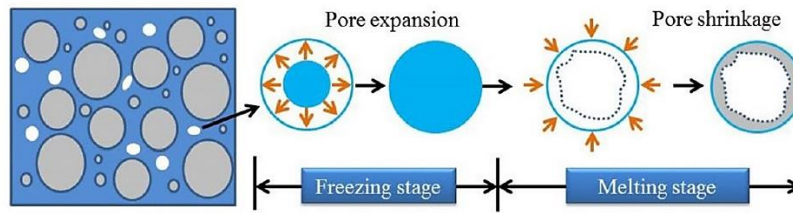
Figure 2.13. Schematic diagram of the freezing-thawing process (Jianwei et al., 2022)

2.2.5 Soil stabilization techniques commonly used

Soil stabilization techniques can be summarized by adding fibers, chemicals, or other materials or additives to the soil to improve its engineering properties and behavior. Chemical soil stabilization is considered the most used technique, and it is likely more cost-effective to treat an in-place soil material with a stabilizing agent or addition, such as soil cement or lime, than to import aggregate for the same base course thickness. The type of additive, the amount used, and the method of mixing play a vital role in the project's success, so in order to apply this technique correctly, the following things must be taken into account:

1) An obvious idea about the required result
2) A thorough understanding of subject soil properties and behavior
3) A thorough understanding of the additive's role, and its interactions with both soil and environmental changes
4) A thorough understanding of additive's incorporating (mixing) way
5) Knowledge of how the resulting engineered soil should be performed

For ensuring the proper mixing of any additives with the soil, as uniform as possible, many mixing techniques are usually used. The most cost-effective and time-efficient technique is to utilize a rotary mixer. This is a big machine that mixes additives into the soil by spinning it in a large mixing chamber with grinding and mixing rotors. The soil can be comminuted into optimally homogenous granules while evenly distributing additives and water. Rotary mixers do all mixing on-site and are unmatched in production compared to other methods. Pugmill is generally used when precision is required for specific applications, which is a big mixing chamber like a cement mixer. its common

utilization is mixing the additives, water, and pre-graded aggregates to perform a uniform thickness in road application. Pugmills generate high-quality stabilization at a higher cost and at a slower rate.

Regarding the most commonly used stabilization agents that have been utilized frequently to act as binders, increase soil density, modify the effects of moisture, enhance the geotechnical properties, or neutralize the detrimental effects of substances in various types of soil, these can be summarized as follows (Huffman,1995):

- Portland cement is a mechanical additive that can be utilized for soil modification (to improve soil quality) or soil stabilization (to transform soil into a cementitious mass). Almost all types of soil can benefit from the strength gained by cement stabilization.

- Quicklime/Hydrated Lime is a chemical that has been utilized for ages as a soil stabilizer. Experiments have proved that lime will react quite well with medium-grained, and fine-grained clay soils. The primary stabilization effect of lime on clay soils is reducing the plasticity of the soil by decreasing the moisture content which consequently leads to hardening the soil structure and increasing both soil strength and soil workability.

- Fly ash is a chemical additive composed primarily of aluminum and silicon compounds and is a by-product of coal combustion. Fly ash can be combined with lime and water to stabilize granular materials with few fines and create a hard cementitious mass. Its primary function in the stabilization process is to eliminate air voids by acting as a filler and/or pozzolana. Applying lime, cement, and fly ash (LCF) to stabilize coarse soils with few or no fine grains is a conventional treatment method.

- Calcium chloride is a chemical additive that can absorb moisture from the air until it liquefies into a solution. The existence of calcium chloride in soil lowers the freezing point of the moisture. This explains why calcium chloride is an effective stabilizer addition for cold-weather applications. There will be less soil movement (i.e., Frost-heaving) and the soil will be considerably more stable if the water in the soil cannot freeze. Calcium chloride is also an excellent binder, enhancing soil compaction and decreasing dust.

- Bitumen is a mechanical additive that are existing naturally or is manufactured through petroleum distillation. It is the black pitch needed to manufacture asphalt. Asphalt emulsions, cutback asphalt, asphalt cement, and tar are all utilized to acquire bituminous soil mass. Weather conditions, type of soil, and construction technologies used are all factors controlling the selection of bitumen type in stabilization. Bitumen strengthens the soil and makes it more resistant to water and frost. The utilization of bitumen makes soil compaction easier and more consistent.

2.3 Evaluating the Feasibility of PP as Reinforcement Material under Foundations

One of the most important issues in the field of foundation engineering and soil mechanics is the performance of the foundation as All structures are eventually placed on the ground. Foundations can be subjected to static, dynamic, or a combination of loads. If the soil under the foundation does not have sufficient resistance to withstand the loads, the methods of replacing suitable soil and compaction instead of loose soils are generally utilized (in conventional treatment, increasing the dimension of the foundation is a widely utilized method to enhance the performance level). In some cases, the thickness of the replaced soil does not meet the required bearing capacity, or in addition, geometric and economic constraints may make the implementation of soil improvement methods inappropriate. In these conditions, the use of reinforcements to increase tensile strength and enhance the bearing capacity of the soil will be a suitable solution (Sitharam and Sireesh, 2006).

The utilization of polymeric materials to increase soil-bearing capacity has been explored by engineers and researchers in the geotechnical field recently (Maheshwari et al., 2011; Mirzababaei et al., 2017; El-Soud and Belal, 2018; Vaibhav Sharma & Arvind Kumar, 2019; Alemyparvin, 2020). Several pieces of research have elucidated that the ultimate bearing capacity and the relevant settlement characteristics of building foundations can be afflicted and improved by the inclusion of reinforcements in the ground (Kolay et al., 2013). The findings of various laboratory tests and numerical models indicated the ultimate bearing capacity of shallow foundations can be modified by the application of geogrids and geofibers under the foundation to stabilize the soils with multiple layers.

Maheshwari et al. (2011) assured outstanding improvement in the bearing capacity of highly compressible clayey soil with polyester fibers inclusion. Mirzababaei et al. (2017) reported that the fiber reinforcement increased the bearing resistance of the slope significantly. Alemyparvin (2020) proved through the series of numerical modeling for both unreinforced and reinforced condition that geogrids has a good ability to improve and stabilize soil conditions. Therefore, it's crucial to assess how much the foundations' bearing capacity has increased at various settlement levels. According to several scientific reports, it can be inferred that the bearing capacity of soil also varied as a result of numerous factors such as the number of reinforcement layers, the type of reinforcing materials, and the ratios of reinforcing materials (Mosallanezhad et al., 2016). The ratio of bearing capacity enhancement may be stated in a non-dimensional form as the bearing capacity ratio, which is the ratio of reinforced soil bearing capacity to unreinforced soil bearing capacity.

3. CHAPTER III: MATERIALS AND METHODS

3.1 Research Materials

3.1.1 Clayey Soil

The investigated soil was extracted from an excavation of a residential foundation project in Gaziantep, Turkey, where the soil appeared fairly uniform. Before the tests program was conducted, a series of index property tests were performed to determine the general characteristics of the studied soil. The index property tests were comprised of gradation analysis, hydrometer analysis, Atterberg limit test, and specific gravity test. The results of laboratory testing are summarized in Table 3.1. Also, it worth mentioning that this type of soil is widely distributed over the world as it is illustrated in the Harmonized World Soil Database (HWSD) in Figure 3.1, and that means improving this type of soil is essential and the results of this research can be applied vastly.

Table 3.1. Characteristics of the studied soil

Soil properties	Value
Specific gravity	2.70
Liquid limit	57.00%
Plastic limit	22.67%
Plasticity index	34.33%
Unified Soil Classification System (USCS)	CH
Optimum moisture content	22.5%
Maximum dry density	1.57 g/cm^3
Sand (4.75-0.075mm)	24%
Silt (0.075-0.002mm)	39%
Clay < 2µm	35%
Shrinkage limit	12.3%
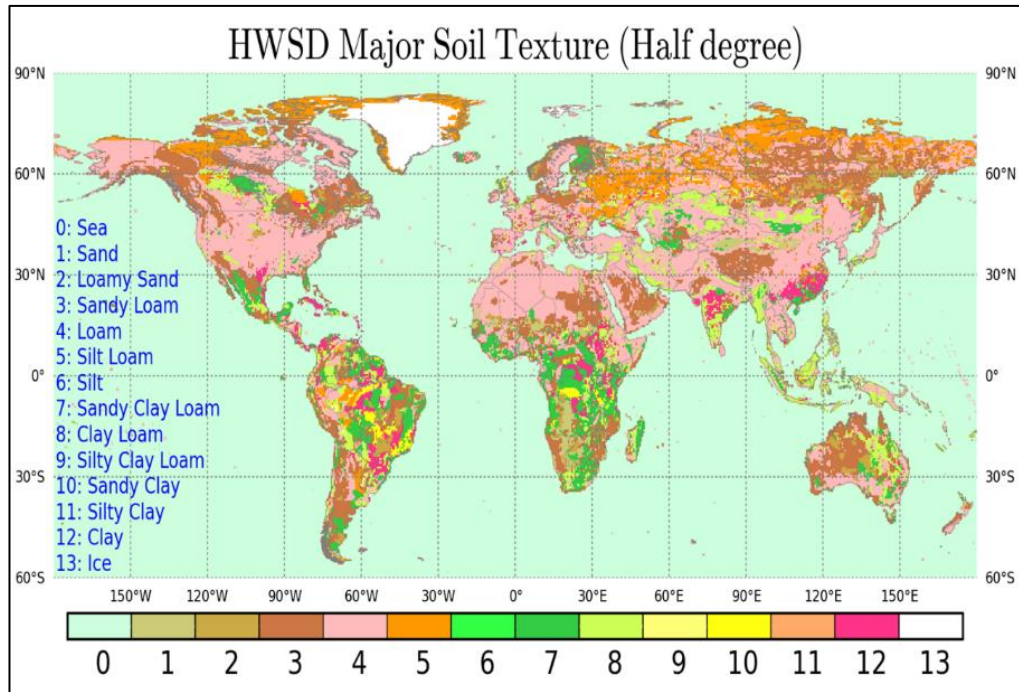
Figure 3.1. Soil types distribution map

3.1.2 Polypropylene Fiber

Polypropylene fiber (PP) is a flexible thermoplastic material produced by polymerizing monomeric units of polypropylene atoms into very long chains of polymers or molecules in the presence of a catalyst at precisely regulated temperatures and pressures. PP is an unsaturated hydrocarbon composed entirely of hydrogen and carbon atoms. There are several types of commercial PP available. One type of PP is a semi-crystalline solid with good mechanical, thermal, and physical characteristics. Another type of PP is produced in considerably smaller quantities as a byproduct of semi-crystalline PP manufacturing and has very poor thermal and mechanical characteristics. The crystallizable form of PP is known as "isotactic," whereas the non-crystallizable form is known as "atactic" (Brown et al., 2002).

PP is also manufactured as continuous cylindrical monofilaments that may be cut to certain lengths or as films and tapes that can be fibrillated to generate rectangular cross-sectional fibrils. Table 3.2 lists the properties of the polypropylene fibers used in this

28

study as shown on its identification card (as provided by the manufacturer). Figure 3.2 shows the shape and type of the used material.

Table 3.2. Properties of the used polypropylene fibers

Behavior parameters	Values
Fiber type	Single fiber
Unit weight	0.91 g/cm^3
Average diameter	0.034 mm
Average length	12 mm
Breaking tensile strength	350 MPa
Modulus of elasticity	3500 MPa
Fusion point	165 °C
Burning point	590 °C
Acid and alkali resistance	Very good
Dispersibility	Excellent

Figure 3.2. Used polypropylene fiber

The main reason for selecting this type of fiber to be considered in this research is the fact that these fibers are more industrial materials commonly used, as well as, because of their low cost (with reference to other traditional additives) and their nature chemical inert where this material cannot be absorbed, and they do not interact with soil moisture. According to Hejazi et al. (2012), the general advantages of fiber composite soils are their availability, ease of work, economical benefits, rapid to perform, and useability in various

weather conditions. However, it is important to refer that obtaining a homogeneous soil–fiber matrix in the field is troublesome as reported by many researchers in comparison with the hand mixing (lab mixing) that allows fibers to merge properly with the soil mass, but this issue can be overcome and mitigated by oscillatory or helical mixing techniques (Hejazi et al., 2012). Also, it is worth mentioning that polypropylene fibers currnetly are produced from recycled materials. The recycling process involves grinding and melting down the used polypropylene into pellets or granules, which can then be used as raw material to produce new polypropylene fibers. This process not only reduces waste, but it can also save resources and energy compared to producing virgin polypropylene fibers from raw materials.

Additionally, using recycled polypropylene in fiber production can also have addtional positive impact on the environment, as it helps to decrease the demand for petroleum, a non-renewable resource used in the production of virgin polypropylene. In recent years, there has been a growing demand for environmentally friendly and sustainable products, and the use of recycled materials in the production of polypropylene fibers is becoming more common as a result.

Last of all, it is worth to mention that during the conduction of the laboratory experiments, many samples with various fiber contents (0.5%, 1%, 1.5%, 2%, and 2.5%) were prepared and it was noticed that it is so important to avoid exposing the samples to large pressures during the preparation and maintaining easy sample formation/preparation, therefore, to mitigate these concerns, it is better to consider the fiber contents to be varied between 0% to 1.5% by dry weight of the studied soil (i.e., fiber content/weight is the studied ratio multiplied by the soil's dry weight for each sample). So, the considered fiber contents in this research are 0%, 0.5%, 1%, and 1.5%.

3.1.3 Hydrated high-calcium lime

Lime (L) is one of the oldest and most widely used chemicals for improving the engineering characteristics of soils. In general, four primary lime-based additions are utilized in geotechnical construction: $Ca(OH)_2$ hydrated high calcium lime, which was

used in the current study, calcitic quick lime CaO, dolomitic quick lime CaO MgO, and monohydrated dolomitic lime $Ca(OH)_2$ MgO. The lime treatment generates a chemical reaction similar to cement and can be employed for both modification and stabilization purposes, where a chemical interaction between soil and lime results in a decrease in water content. Further, lime addition increases the optimum moisture content but decreases the maximum dry density, significant reduction in the plasticity index, and finally, an immediate increase in the strength. Extensive research has been conducted on the application of lime to stabilize clay soils (Bozbey and Garaisayev, 2010; Harichane et al., 2011; Stoltz et al., 2012; Wang et al., 2013; Abass, 2013; Asgari et al., 2013; Ghobadi et al., 2013; Tran et al., 2014; Nguyen, 2015; Kiliç et al., 2016; Ahmad A.F. et al., 2020) confirmed the positive effect of lime addition on the reduction of swelling, plasticity index, and the increase of the strength in clayey soils.

Referring to the considered lime content in this study, as both lime and cement are considered the most widely used in geotechnical engineering specifically for improving the mechanical and physical soil properties, this research focuses on the utilization of these stabilizers to assess their impact against the environmental changes in comparison with the impact of fiber additive that is proposed in this research. In order to determine the relevant optimal contents for both lime and cement, extensive previous studies were reviewed, and all suggestions related to optimal contents were figured out, eventually, the optimal contents were determined before starting the testing stage. Office of Geotechnical Engineering (2008) presented the criteria that are preferred to be considered for chemical selection based on the index properties of the soils as it is shown in Table 3.3. Also, the optimal chemical quantities for both stabilization or modification purposes, for getting the best-required properties were suggested in Table 3.4.

Table 3.3 Chemical selection criteria

Chemical Selection for Stabilization
a.   Lime: If PI > 10 and clay content (2μ) > 10%.
b.   Cement: If PI ≤ 10 and < 20% passing No. 200.
Chemical Selection for Modification
a.   Lime: PI ≥ 5 and > 35 % Passing No. 200
b.   Fly ash and lime fly ash blends: 5 < PI < 20 and > 35 % passing No. 200
c.   Cement and/ or Fly ash: PI < 5 and ≤ 35 % Passing No. 200
Notes:
• Fly ash shall be class C only.
• Lime Kiln Dust (LKD) shall not be used in blends.
• Appropriate tests showing the improvements are essential for the exceptions listed above.

Table 3.4 Optimal chemical contents as per Office of Geotechnical Engineering (2008).

Additive type	Suggested content
Lime or Lime By-Products	4% to 7 %
Cement	4% to 6 %
Fly ash Class C	10% to 16 %

Similarly, Indiana's development of transportation (INDOT, 2020) suggested the optimal contents for lime which were (5% to 7%). Therefore, for the current study, the following content of Lime (6% by dry weight) was considered to evaluate their impact against environmental changes and to be compared with PP additive and eventually, evaluate the most appropriate technique to resist the additional stress resulting due to temperature differences of the weather, which causes moisture differences of the soil.

3.1.4 Portland Cement

Portland cement (C) is a finely fragmented material produced by grinding clinker and gypsum together. Clinker is a pyro-processed hydraulic material composed of four major

oxide phases: dicalcium silicate (C2S), tricalcium silicate (C3S), tricalcium aluminate (C3A), and tetra calcium alumino-ferrite (C4AF) (as per chemical notation for cement, C = Ca, A = Al2O3, S = SiO2, and F = Fe2O3). The two calcium silicate phases are the most crucial for stabilizing soil. Cement is typically utilized extensively in civil engineering projects like road construction, foundation slabs, embankments, and piles foundations. Many studies have confirmed that cement-soil mixture has high stiffness properties for expansive soils (Portelinha et al., 2012; Pakbaz and Alipour, 2012; Aparna, 2014; Ikhlef et al., 2015; Sharo et al., 2022). Accounting for the mineral compositions of both soil and cement, many chemical reactions can take place between the cement and the silica and alumina in the clay, and the calcium hydroxide. These reactions, in the short term, cause a change in the soil structure, while in the long term, a formation f cementitious compounds binding soil particles which leads to the hardening of the soil (Pakbaz and Alipour, 2012; Ikhlef et al., 2015).

Referring to the considered cement content in this study, and with reference to Office of Geotechnical Engineering (2008) and INDOT (2020) recommendations, the following content of cement (5% by dry weight) was considered to evaluate their impact against environmental changes and to be compared with PP additive and eventually, evaluate the most appropriate technique to resist the additional stress resulting due to temperature differences.

3.2 Research Methods

In order to satisfy the research aims, a full set of tests was conducted on clayey soil with high plasticity after mixing the research reinforcing material ((fibrillated polypropylene fiber PP) with different fiber contents (0%, 0.5%, 1%, 1.5%), and all findings and test results were compared with the unreinforced sample to infer the impact of fiber on the studied soil behavior. However, the below-listed aims were fulfilled through the relevant tests or investigations as follows:

1. Standard Proctor tests and Atterberg limits tests were carried out to assess the effect of PP on physical properties and inspect the classification change as per the unified soil classification system (USCS).

2. Direct shear test, unconfined compressive strength test, and conventional undrained unconsolidated triaxial strength test were carried out to assess the effect of PP on strength behavior and strength properties.

3. Free swelling tests and Consolidation tests were carried out to assess the effect of PP on swelling and compressibility behavior and properties.

4. Drying tests were conducted to evaluate the desiccation cracks resistance of fiber-reinforced soil and assess its efficiency in comparison with cement-stabilized soil and lime-stabilized soil.

5. Dry/wet cycles tests were conducted to evaluate the cracks and volume changes' resistance of fiber-reinforced soil and assess its efficiency in comparison with cement-stabilized soil and lime-stabilized soil.

6. Freeze/thaw cycles tests were conducted to inspect the effect of frost heave and thawing–settlement on the UU strength and assess the PP durability against the resulting volumetric changes and their impact on the strength behavior and properties

Furthermore, to assess the feasibility of using PP as reinforcing material under foundations, the finite elements method (FEM) was used by PLAXIS software through modeling a typical footing placed on fiber reinforced layer with different thicknesses and different fiber contents (13 models) to provide the appropriate assessment of PP effect on the bearing capacity of shallow foundation and settlement conditions.

3.2.1 Standard proctor test

At the outset, 4.5 kg of the studied soil was dried, then, polypropylene fibers were added according to the pre-identified ratios (0%, 0.5%, 1%, 1.5%), and for each ratio/fiber content, the specimens were formed in the Proctor mold (10.1 cm in diameter, 944 cm^3 in volume) in compliance with the ASTM D 698 standards [98]. The specimens were formed in the proctor mold through a three-layer and each layer was compacted by a hammer with a weight of 2.5 kg, and a falling height of 30 cm with 25 beats for each layer. The standard Proctor experiments were carried out on the fiber-reinforced soil with different contents of the dry weight of the studied soil (0.5%, 1%, 1.5%) and compared with the unreinforced situation.

3.2.2 Atterberg Limits Test

After drying the soil, it was sieved on sieve No.40 and then mixed with the pre-identified fiber contents. The tests were carried out in compliance with ASTM D4318 (2017) standards. Therefore, the plastic limit, liquid limit, and shrinkage limit were investigated for each fiber content.

3.2.3 Inspecting the change in Soil classification as per USCS

For inspecting the effect of PP on the soil classification as per (ASTM D2487-17, 2018) the unified soil classification system (USCS), the values of plasticity index (PI), and liquid limit (LL) for each fiber content were depicted on the Casagrande chart which is shown in Figure 3.3. Considering that the plasticity index (PI) can be identified by subtracting the value of the plasticity limit from the liquid limit.
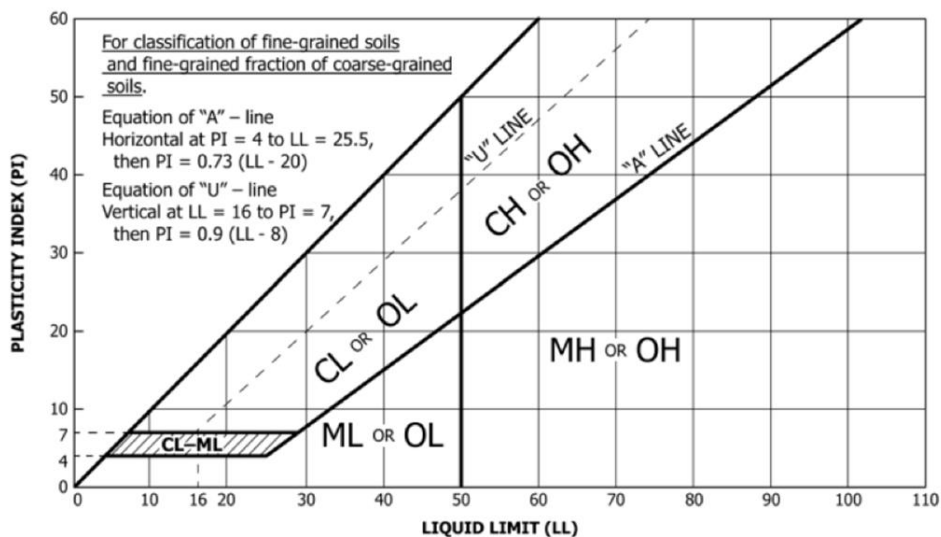
Figure 3.3. Soil classification as per four fiber contents (0%, 0.5%, 1%, and 1.5%) as per (ASTM D2487-17, 2018)

3.2.4 Direct shear tests (DST)

For sample preparation, it was differentiated four kinds of samples according to the fiber content value (0%, 0.5%, 1%, 1.5%). The samples were prepared at the optimum moisture content (OMC) and maximum dry density that were determined for the untreated soil

35

(i.e., the sample's dry density corresponds with maximum dry density (MDD) which is 1.57 g/cm^3, and with the optimum moisture content (OMC) which is 22.5%). To achieve the desired maximum dry density, soil-fiber mixtures were poured progressively into the sample mold and then static compacted by a jack. There were two steps involved in the soil and fiber mixing. First, fibers (with the considered contents) were manually mixed into the soil with approximately 10% of water (approximately half of the OMC value) until a random distribution of fibers is attained by eye inspection. A water content of 10% was considered in this step to prevent fiber segregation from the soil. Second, to achieve the optimum moisture content, a particular amount of water (the second half of the OMC value) was added to the combination of fibers and soil formed in the first step.

The mixtures were placed in plastic bags and sealed for 72 hours to ensure an even distribution of water content within the mixtures. Before the formation of the specimens, the water content was double-checked (i.e. before compacting the mixtures of soil-fiber in the steel mold). After the static compaction was completed, all of the samples were ready for testing.

As an example of sample preparations and calculation, the needed quantities (with respect to the direct shear box ring's properties, with an area of 32 cm^2 and a volume of 80 cm^3) of dry soil, water, and fiber to prepare six samples for each fiber content were summarized in Table 3.5. After that, the soil samples were extracted from the Proctor apparatus. Then, the samples were placed in the testing machine (Shear box machine, unconfined compressive machine, and triaxial machine accordingly).

Table 3.5 Quantities calculations for shear test's samples preparation

Fiber Content PP (%)	Dry Weight of Soil (g)	PP Weight (g)	Water Weight (g)	No. of Samples
0%	125.6	0	28.26	6
0.5%	125.6	0.63	28.26	6
1%	125.6	1.26	28.26	6
1.5%	125.6	1.89	28.26	6

The prepared samples were placed in the direct shear box apparatus (as shown in Figure 3.4) and subjected to different vertical loads (25; 50; 100; 150 kPa) for each fiber content. Next, the tests were conducted in accordance with ASTM D3080 standards [100]. The test results were presented and compared with the unreinforced samples. Also, shear parameters (friction angle and cohesion) were determined by considering the shear stresses at the failure stage for each applied vertical load, where the Coulomb failure envelopes were depicted for each fiber content and therefore the values of both friction angle and cohesion were determined and then compared to each other. Furthermore, a function-based fiber was provided to predict the friction angle and cohesion values at each fiber content that should not exceed 1.5%.

Figure 3.4. Direct shear apparatus

3.2.5 Unconfined compressive strength tests (UCS)

Referring to the aforementioned sample preparation method (as in DST) and after considering the mold size of the UCS apparatus, the prepared samples were placed in the electronic unconfined compressive strength apparatus (as shown in Figure 3.5), and then the tests were carried out in accordance with ASTM D2166 (2016) standards. Please note that for each fiber content, three samples were tested to assuring the accuracy of the results. Also, the elastic modulus for each reinforcement ratio was determined by taking the slope (inclination) of the straight part of the test resulting in stress-strain curves, therefore, the resulted elastic modulus and unconfined compressive strength at the failure

stage were represented with the fiber content to infer the impact of fiber content inclusion. Furthermore, a function-based fiber was provided to predict the UCS value at each fiber content that should not exceed 1.5%.

3.2.6 Conventional undrained unconsolidated triaxial tests

Conventional undrained unconsolidated (UU) triaxial tests were performed by using a strain-controlled apparatus as per (ASTM D2850–15, 2007). Each of the four kinds of samples (0%, 0.5%, 1%, 1.5%), was tested at one confining pressure of 200 kPa at a strain rate of 0.8 mm/min. As per most of the previous researchers' findings (Shukla, 2017; Khiav et al., 2022) have confirmed the similar strength behavior of the treated and untreated soil for different confining pressures (similarity of the stress-strain behavior under different confining pressures). The UU triaxial compression strength tests were conducted for all samples and each test was repeated at least three times to assure its accuracy. So thus, the stress-strain curves were depicted and the strength values at the failure stage were represented with the variation of fiber content. Furthermore, the test results can be used for determining the resilient modulus which is considered as a decisive key to characterizing the deformation type under traffic loading for pavement materials. The resilient modulus is calculated by dividing the deviatoric stress increment at 1% axial strain by the deviatoric strain increment, which can be stated by Eq. 3.1 below:

$$E = {\Delta\sigma}/{\Delta\varepsilon} = \frac{\sigma_{1\%} - \sigma_0}{\varepsilon_{1\%} - \varepsilon_0} \tag{3.1}$$

where $\Delta\sigma$ is the deviatoric stress increment, $\Delta\varepsilon$ is the deviatoric strain increment; $\sigma_{1\%}$ (1%) is the deviatoric stress corresponding to an axial strain of 1.0% ($\varepsilon_{1\%}$); σ_0 and ε_0 are the initial stress and strain respectively (Wang et al., 2007). Therefore, the effect of PP can be observed and presented by representing the calculated resilient modulus with the variation of fiber. Figure 3.6 shows the used machine and samples before and after testing.
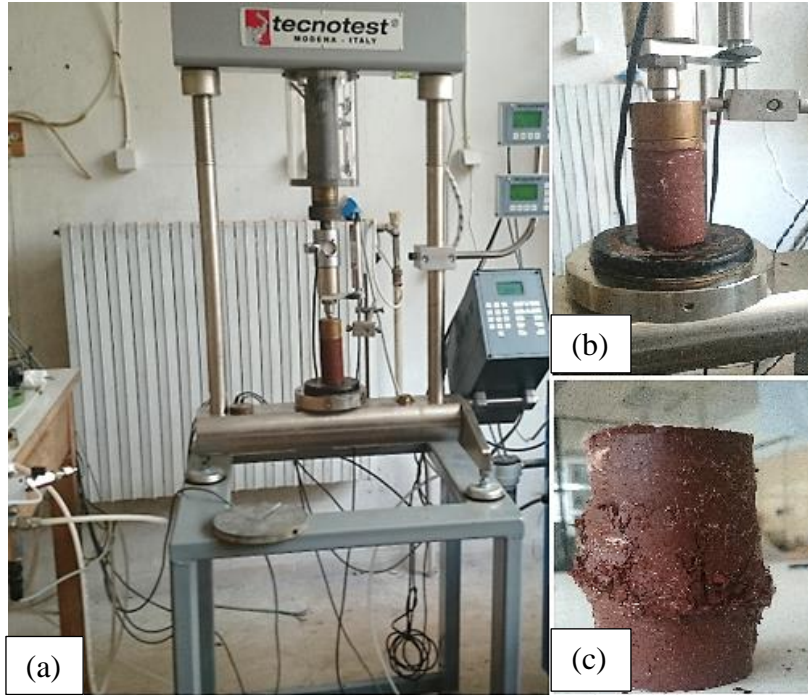
Figure 3.5. Unconfined compressive strength testing: (a) Unconfined compressive strength machine used, (b) Specimen before testing, (c) Specimen after testing.

Figure 3.6. Undrained unconsolidated triaxial testing: (a) Unconfined unconsolidated triaxial machine used, (b) Specimen preparation for testing, (c) Specimens before testing.

3.2.7 Free swelling tests

The soil samples were extracted from the proctor apparatus. After that, the samples were placed in the odometer which is shown in Figure 3.7, then they were loaded with a small

vertical load of 7 kPa to achieve the leveling of the sample's surface. Then, the samples were submerged, and swelling reads were measured and recorded (as per ASTM D4546 standards, 2021). The free-swelling test was performed on three samples for each reinforcing ratio and the final swelling values for each case were determined. After getting the final swelling value, the samples were loaded gradually for 24 hours for each load, and by this, the calculation for identifying the swell stress for each fiber content was performed and the impact of fiber inclusion on the swell stress was presented. Furthermore, a function-based fiber was provided to predict the swell stress value at each fiber content that should not exceed 1.5%.

Figure 3.7. Oedometer apparatus (swelling and consolidation test apparatus)

3.2.8 Consolidation test

The soil samples were extracted from the proctor apparatus. After that, the samples were placed in the odometer which is shown in Figure 3.7. Then, the samples were subjected to vertical loads that were increased gradually under distill water submerging conditions, and the application of these tests was as per (ASTM D2435 standards, 2020). The load application period is 24 hours for each load value and during these periods the consolidation settlements were measured with respect to time. The consolidation tests were performed on three samples for each reinforcing ratio (0%, 0.5%, 1%, 1.5%), then, the average of these three readings was represented and considered for further evaluation.

Also, for tracking the changes in the void ratio for each sample type during the test implementation, the following equation (Eq. (3.2)) is applied to find the void ratio value that meets every settlement, and therefore the representation of void ratio changes during the testing application was presented with respect to both time and vertical loads applied.

$$e_t = \frac{V_v}{V_s} = \frac{V_o - V_t}{V_s} = \frac{\left(V_{ring} - \gamma_d * \frac{V_{ring}}{G}\right) - (A_{ring} * \delta h_t)}{\gamma_d * V_{ring}/G} \qquad (3.2)$$

where e_t is the void ratio value at the time, t; V_v is the void volume; V_s is the solid volume; V_o is the initial void volume (i.e., 0.72); V_{ring} is the volume of the odometer ring which is the same as the soil sample volume (i.e., 80 cm^3); γ_d is the dry density (i.e., 1.57 g/cm^3); G is the specific gravity weight (i.e., 2.7); A_{ring} is the ring area (i.e., 40 cm^2); δh_t is the consolidation settlement at the time, t.

Furthermore, the elasticity modulus (E$_{oed}$) for each situation/fiber content was found by calculating the inclination of each stress-strain curve. Also, the compression index (C$_c$) was calculated based on the resulting outputs by finding the inclination of the represented curves of void ratio- applied load and therefore a function-based fiber was provided to predict the Cc value concerning fiber content which should not exceed 1.5%.

3.2.9 Desiccation/Drying tests

For inspecting the impact of the drying process on fiber-reinforced soil and to evaluate the effect of fiber in comparison with conventional chemical additives (lime and cement), the desiccation/drying tests were carried out on the prepared samples; six kinds of samples were differentiated according to the fiber content (0%, 0.5%, 1%, 1.5%), cement content (5%), and lime content (6%). Firstly, the samples were dried (air-dried by oven at 100° C) and then they were sieved by using a sieve size 2 mm diameter to remove the large particles, and then samples were submerged with distilled water under approximate moisture content of 170% (i.e. mixture content is 170%). After that, they were poured into circular cans with a diameter of 70 mm and placed (for 5 minutes) on a vibrator

41

apparatus to eliminate the air bubbles in the soil. Then, the specimens were covered and left for 72 hours to allow soil deposition (precipitation). The thickness of the samples was measured, which was about 8mm, and its moisture after precipitation was about 90%.

Before submerging stage, the mixture of soil-fibers was done manually by adding the fiber to the dried soil and then mixing them with distilled water. In order to form a slurry, the amount of water was maintained above the liquid limit (LL). The exact amount of water was calculated and gradually added to the mixture of soil-fiber. The slurry was mixed by hand steer for about one hour until a smooth liquid was achieved to ensure the uniformity of the fiber distribution in the mixture by visual examination. This procedure also was done for cement and lime-stabilized samples after considering the optimum content of 6% and 5% respectively. After that, the four kinds of samples (untreated samples, reinforced samples, lime stabilized samples, and cement stabilized samples) were submerged as mentioned above. For cement and lime stabilized samples, the curing period was ignored as the thickness of these samples was very thin and the deposition period of three days ensured a good uniformity and interaction between the added material and the slurry (soil and water).

For each situation, four samples were prepared for the drying test at a room temperature of ($25 \pm 1°$ C). The samples were then heated in an oven at a constant temperature of ($50°C$). Throughout the drying process, the missed amount of water was measured (with 0.01 gr accuracy) and the corresponding humidity at each time was calculated. The surface of these samples was also monitored/photographed during the same periods by using a digital camera (with a focal length of 35 mm) to track the progression of the cracks and to determine the engineering specifications of the cracks (length, width). This mechanism is called visual analysis. Therefore, at the end of these tests, two outputs have been found as follows:

1. Representation of water content changes with time (evaporation rate) for each situation by depicting the experimental results (changes of the water content to the time).
2. Photographic database by photographing the samples' surfaces for different periods for all situations, and this database was analyzed by using MATLAB program for

determining the crack's properties (length, width, area) and the outputs were compared for each situation to evaluate the impact of fiber inclusion, cement content, and lime content on the cracking resistance.

To identify the area of generated cracks in each sample for all cases, the digital processing (through MATLAB program) method was applied. The digital processing method can be summarized by capturing high-resolution images of the samples' surface at various stages of the drying process. To calculate the area of the developed cracks, the captured image at the final stages of the drying process was inserted into the MATLAB program for analysis. MATLAB Analyzing procedure depends on dividing the image into an array of elements, and the number of lines and columns (number of elements) in this matrix, which depends on the resolution of the used camera which affects the calculation accuracy/analysis. After dividing the image into an array of elements, each element takes specific values for each color (Red, Green, Blue) as shown in Figure 3.8. So thus, by identifying the range of color that cracks are located in (through applying a set of programming commands), the number of elements that meet specific values of each color (color ranges) can be found, therefore, the area of the generated cracks in each image and for each studied case can be determined by using the equation Eq. (3.3) which was derived from the aforementioned image analysis method (Abhishek, 2015). However, it was noticed that by using this method, the areas of shrinkage/contraction were considered as cracks.

$$A_{cracks}(cm^2) = A_{sample} \times \frac{N_{cracks-elements}}{N_t}$$
(3.3)

Where $N_{crack-elements}$ is the number of elements that represent the cracks, N_t is the total number of image elements, A_{sample} is the area of the pictured sample (38.48 cm^2), and A_{cracks} is the cracks' area.
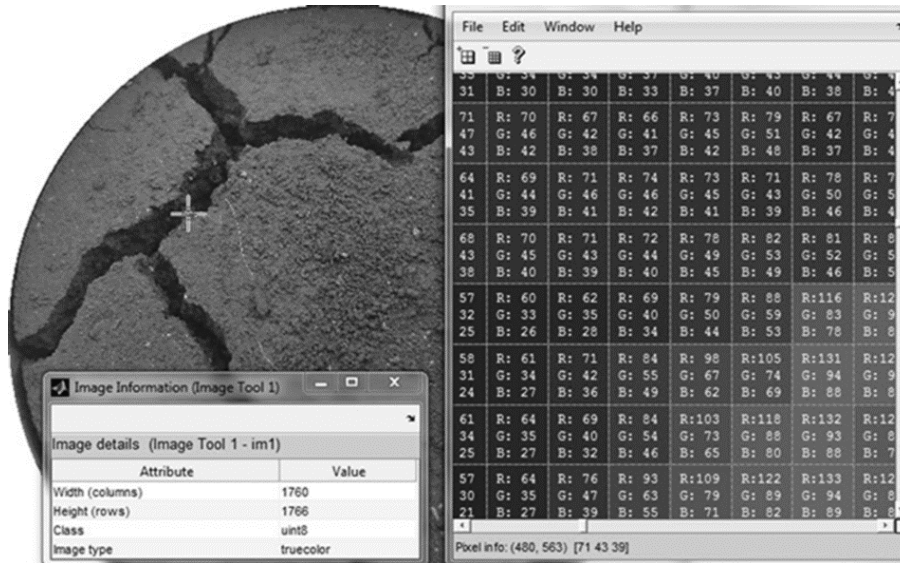
Figure 3.8. Digital processing by using MATLAB

3.2.10 Dry/wet cycles tests

For inspecting the impact of dry/wet cycles on fiber-reinforced soil, and to assess the effect of fiber in comparison with conventional chemical additives (lime and cement), the dry/wet cycles tests were carried out to evaluate the influence of PP, lime, and cement on the volumetric changes resulting from the drying/wetting process. Six kinds of samples were differentiated according to the fiber content value (0%, 0.5%, 1%, 1.5%), cement content (5%), and lime content (6%) as explained above.

Samples were prepared at the optimum moisture content (OMC) and maximum dry density (MDD) that was determined for the untreated case. To attain the required maximum dry density, the studied soil and fibers were poured progressively into the Proctor mold and then subjected to static compaction by a jack. The mixture of soil and fibers was done in the same way as the DST sample preparation way to prevent fiber balling. After the static compaction was completed, all samples were extracted by using a metal cylinder (10 cm in height and 11.7 cm in diameter). The same technique was performed to prepare compacted homogeneous samples for both the lime-soil mixture and the cement-soil mixture as well. After the static compaction was completed, all the specimens were transferred to a curing room of (24 $\mp$ 1° C) in which they were cured for 21 days (this was for both lime and cement-stabilized samples).

44

After that, all samples were undergone to the drying/wetting cycles, where all samples were initially exposed to the drying process for 24 hours in the oven at (50° C). Then, after 24 hours of drying, the samples were submerged in distilled water for another 24 hours at room temperature, and this was repeated for four cycles. Figure 3.9 shows a schematic diagram for the volume change (dry/wet cycles) test.

As it is shown in Figure 3.9, volumetric changes and the developed cracks of each sample were measured at the end of each drying cycle, where the approximate length and width of the developed cracks on the peripheral surface were measured, then the total area of cracks can be calculated and multiplied by four (the number of samples for each situation) to obtain the total area of cracks generated on the peripheral surface of the sample. Cracking is estimated relatively by using the digital processing method (Abhishek T. [108]), as the area of generated cracks on the peripheral surface (perimeter surface) is attributed to the area of the cylinder face. Regarding the volumetric changes, they are connected to the initial cylinder volume (sample cylinder's volume) as well.

After conducting the measurements during the testing phase, the final volume change for each studied case can be obtained by subtracting the final measured volume (at the last drying cycle) from the initial volume (cylindrical can volume) and dividing the result by the initial volume. Therefore, the volumetric changes for all situations (untreated sample, fiber-reinforced sample, cement stabilized samples, and lime stabilized samples) were determined and compared together to assess the most appropriate additives to resist both cracking and volumetric changes resulting from the drying/wetting cycles.
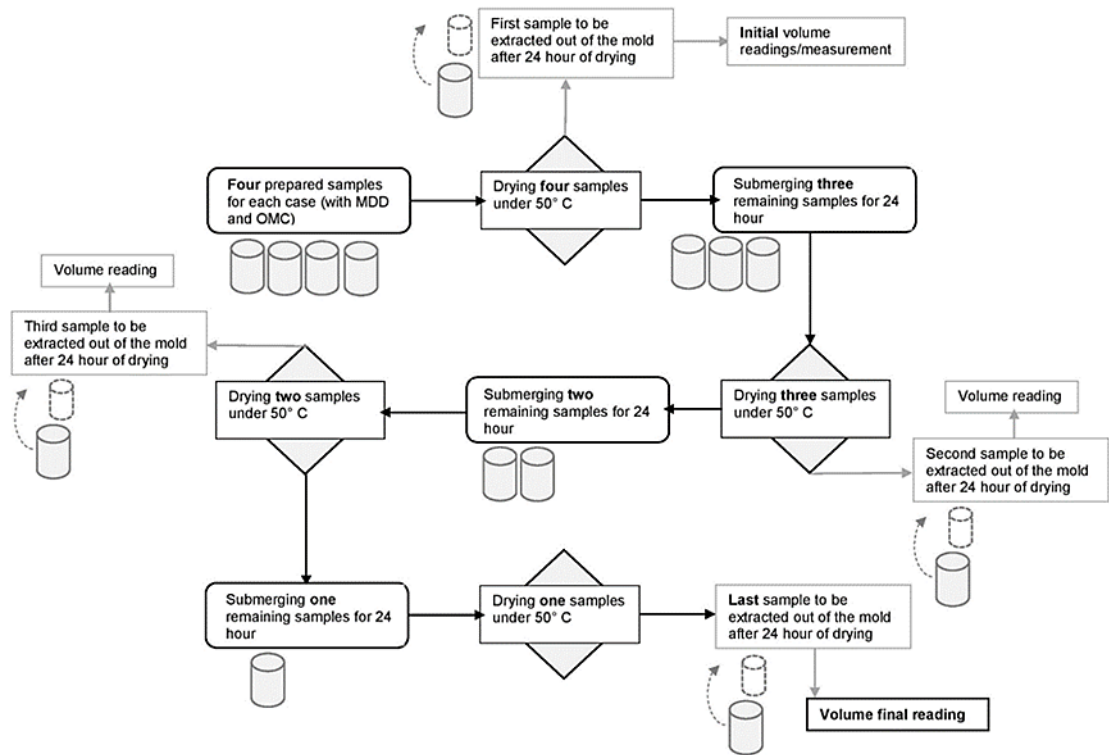
Figure 3.9. The schematic diagram for the volume change (dry/wet cycles) test.

3.2.11 Freeze-thaw (F-T) cycles

Laboratory experimental program was performed on the studied clayey soil with high plasticity for studying the feasibility and effectivity of PP on the durability behavior (environmental changes resistance in terms of strength behavior change) due to freeze-thaw (F-T) cycles. For investigating the durability behavior, a series of conventional UU triaxial tests were carried out (under the same conditions that were mentioned in section 3.2.6) on fiber-reinforced samples subjected to a maximum of 10 closed-system of (F–T) cycles, and the behavioral change of UU compressive strength was inspected and compared with the unreinforced situation. Additionally, volume changes and F–T strength reduction were also calculated after (F–T) cycles, and the volume changes were measured and presented as indicators for evaluating durability behavior.

For conducting the tests, four kinds of samples were considered according to the fiber content value (0%, 0.5%, 1%, 1.5%). Cylindrical samples of 38 mm in diameter and 80 mm in height were prepared at maximum dry density (MDD) and optimum moisture

content (OMC) that was determined for untreated soil (i.e., the dry density of the sample corresponds to a maximum dry density (MDD) of 1.57 g/cm^3 and an optimum moisture content (OMC) of 22.5%.). In order to attain the required maximum dry density, soil-fiber mixtures were poured progressively into the sample mold (steel tube) with 38 mm in diameter and 100 mm in height and compacted by a jack statically.

The fiber-soil mixtures were done by using the same way mentioned before to prevent fiber segregation from the soil. After that, to ensure water content uniformity within the mixtures, the mixtures were covered by plastic bags and blocked for 72 hours. For making sure of the final moisture content, water content was checked before the specimens' formation (the compaction of mixtures in the steel mold). After the static compaction was completed, all the specimens became ready for UU triaxial tests (for zero (F–T) cycles cases) see Figure (3.10 a,b).

For assessing the impact of (F–T) cycles, the prepared specimens were undergone to 0, 3, 6, and 10 (F–T) cycles before performing UU triaxial testing. The specimens were placed in a digital and humidity-controlled cabinet (refrigerator) at a constant temperature of -20 °C for 12 hours and ~20 °C for the next 12 h to allow for the thawing period (Figure 3.11). The whole period of 24 hours was considered one cycle. Following that, tests were conducted on the samples at a temperature of around 20°C. Cycles were kept up to 10 closed cycles. The number of (F–T) cycles was selected based on previous research findings where it was confirmed that the maximum decline in soil strength can occur in the first few cycles, and new dynamic stability prevails in the samples after 5–7 of (F–T) cycles (Ghazavi and Roustaie, 2013).

Eventually, once the (F-T) cycle application is completed, changes in physical properties and strength behavior (UU) strength and resilient modulus variation with fiber inclusion and (F–T) cycles) for unreinforced and fiber-reinforced samples were inspected and calculated. Throughout the application of (F–T) cycles, the samples' heights and diameters are measured several times to inspect the volumetric changes.
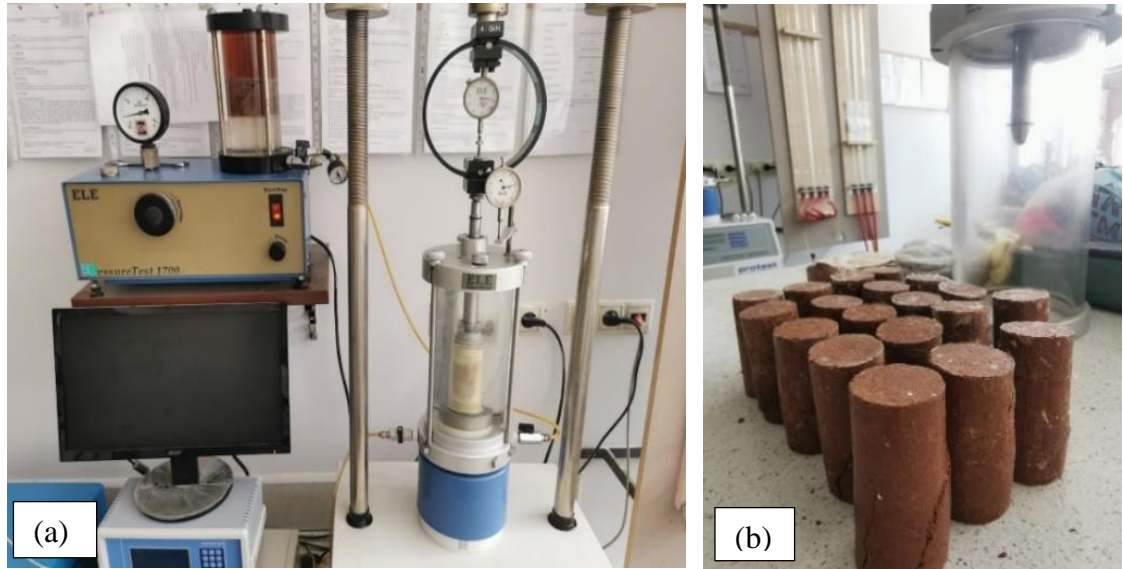
Figure 3.10. Soil specimens' preparation for triaxial testing: (a) The triaxial machine used, (b) Specimens after testing.

Figure 3.11. Soil specimens' preparation in the freeze-thaw cabinet before triaxial testing.

3.2.12 Evaluating The Feasibility Of PP Utilization As Reinforcement Material Under Foundations

In this part of the study, the finite elements method (FEM) was used by Plaxis 2D software to provide the appropriate analysis of the bearing capacity of shallow foundations and settlement conditions. Figure 3.12 presented the studied foundation geometrical status where numerical procedures are conducted.
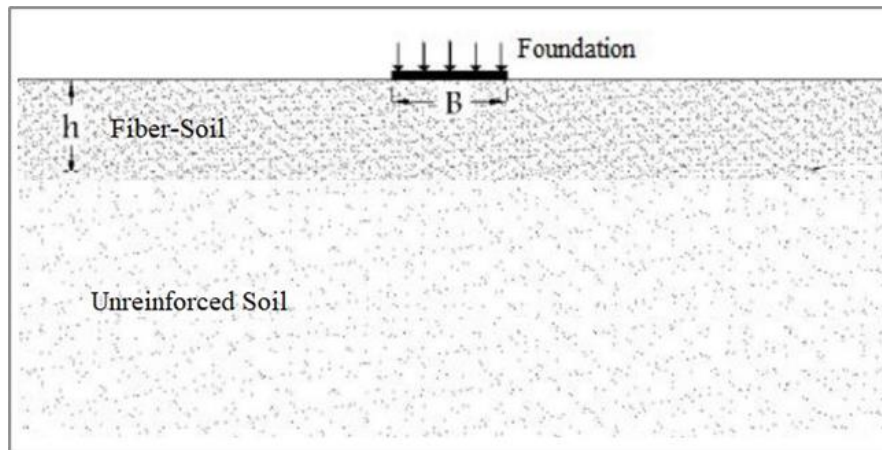
Figure 3.12. Geometrical status of shallow foundation with fiber-reinforced soil.

In order to determine the behavioral characteristics of the studied clay under the shallow foundation model, the choice of footing materials under the vertical load on the studied clayey soil is considered. In the present modeling, a concrete surface foundation of footing is placed on a clayey soil mass and different thicknesses of fiber-reinforced clayey soils are considered. Therefore, thirteen models were analyzed, one for the unreinforced case and twelve for reinforced cases by considering the pre-identified fiber contents (0.5%, 1%, 1.5%) for four different depths (layer thickness (h)) that are connected to the width of the footing and the considered depths were B/4, B/2, 3B/4, and B; where B is the width of the footing.

The modeled concrete footing size was considered as typical size with a square shape (B=1 m in two dimensions) and the length of the model (i.e. effective soil section that will be observed) was more than three times the size of the footing from each side (i.e., B+ 6B) so that it should not include any boundary effects. The foundation material, which is concrete, and its related specifications are shown in Table 3.6. The second material is

related to the parameters in the bed soil for the unreinforced cases (as it is shown in Table 3.1, section 3.1.1), and the third material is related to the geotechnical properties of the fiber-reinforced soil. Table 3.7 lists the input parameters for the modeling, and Figure 3.13 shows the modeling where the extensive elements division in the depth of 2B for increasing the accuracy of the calculation in the effective zone. The behavioral model used in this study is the Mohr-Coulomb elastoplastic model.

Table 3.6. Concrete footing materials specification

Material properties	Parameter	Value	Unite
Unsaturated unit weight	γ_{unsat}	24	kN/m^3
Elasticity modulus	E_{ref}	500000	kN/m^2
Poisson ratio	v	0.25	NA

Table 3.7. Reinforced soil properties

Fiber content (%)	Dry density (g/cm^3)	Friction angle (degree)	Cohesion (kN/m^2)	Elasticity modulus, E_{oed} (kN/m^2)
0	1.57	17.58	31.86	16 000
0.5	1.57	30.4	49.68	20250
1	1.57	33.52	67.26	19630
1.5	1.57	28.54	113.62	12700
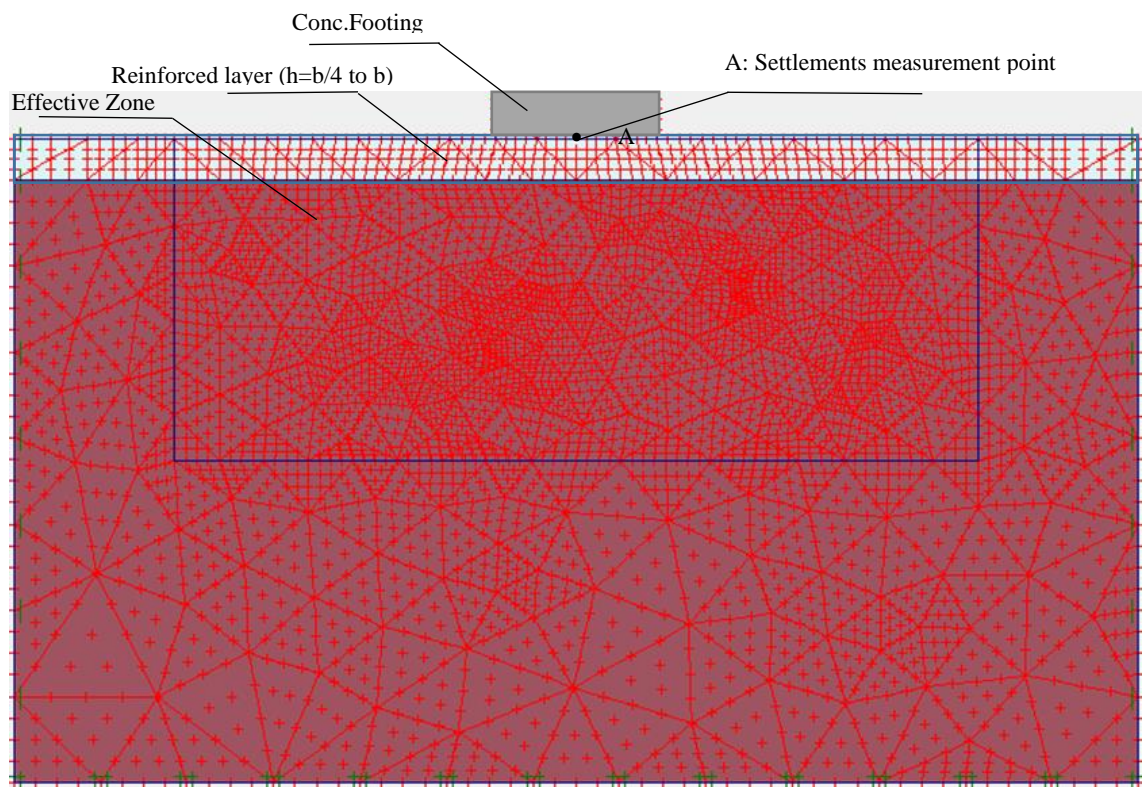
Figure. 3.13. Geometrical modeling of shallow foundation placed on a layer of reinforced clayey soil.

4. CHAPTER IV: RESULTS AND DISCUSSIONS

4.1 Evaluate the Effect of PP on Physical Properties

4.1.1 Evaluate the effect of PP on MDD and OMC

Referring to standard proctor tests, Figure 4.1 demonstrate the results, and by identifying the maximum value of the dry density and its corresponding water content, the MDD and OMC for each fiber content can be easily determined as shown in Table 4.1.
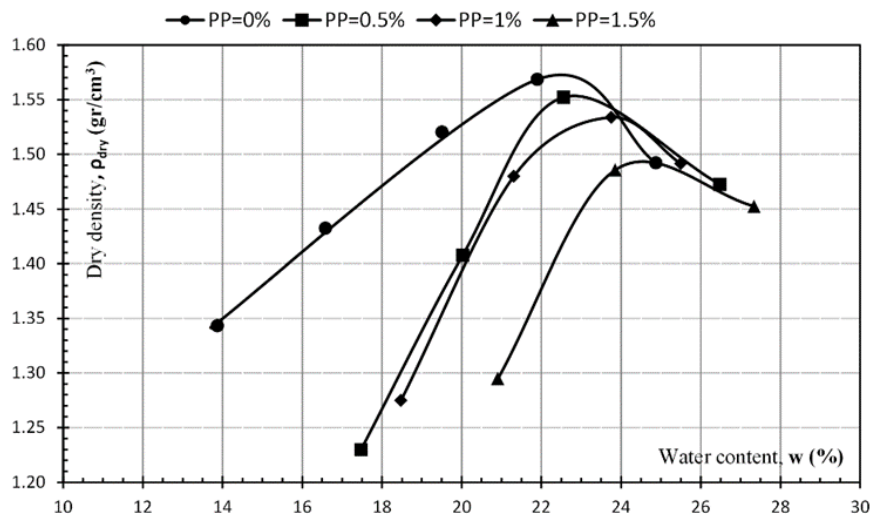
Figure 4.1. Dry density against water content for four polypropylene fiber contents (PP).

Table 4.1. Maximum dry density and optimum water content for each fiber content

Fiber content, PP (%)	$\rho_{dry-max}$ (g/cm^3)	Optimum water content, w_{opt} (%)
0	1.570	22.5
0.5	1.552	22.9
1	1.535	23.8
1.5	1.493	24.3

From the table above, it can be noted easily that the MDD has decreased by increasing the fiber content and that can be contributed to the effect of fibers that play to connect the soil particle and enhance the interlock between them and therefore, reduce the voids ratio which helps to reach to a maximum density at lower soil content. In addition to the interlocking effect, the light unit weight of the added fiber in comparison with its value

for the studied soil also led to reducing the MDD due to reducing the soil content in the mixture (soil-fiber). With reference to the w_{opt}, it was noticed that the change can be ignorable.

4.1.2 Evaluate the effect of PP on Atterberg limits

The outputs of Atterberg Limits tests, the plastic limit, shrinkage limit, and liquid limit were investigated for each fiber content as it is shown in Figure 4.2.
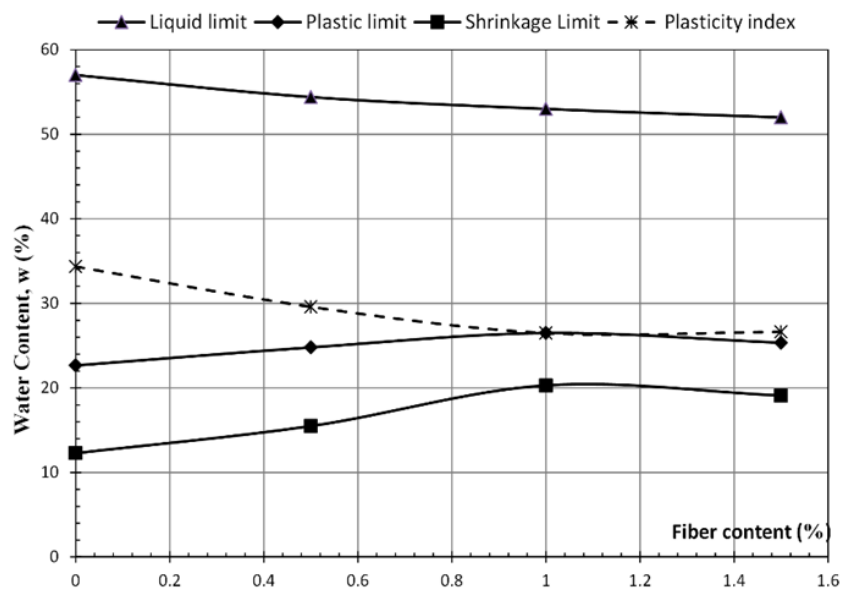
Figure 4.2. Atterberg limits for four polypropylene fiber contents (PP)

From the figure above, it can be easily noticed that the liquid limit decreases by increasing the fiber content (i.e. it varies from 57% to 52%) and this is corresponding to the experiment findings where it was noticed that, for the reinforced samples cases, after spreading the sample in the brass cup by a groove in the liquid limit apparatus and dividing it using a grooving tool, both of the soil portion along the groove has been acted as a separate mass which that expedites its movement to close the groove and reduce the required water that should be added compared with the unreinforced samples, which means the existence of fiber enhances the soil particles' connection.

Regarding the plastic limit, from Figure 4.2 and from the observations of the experiments, the plastic limit has increased by increasing the fiber content (i.e. it varies from 22.6% to 25.3%) where it was a need for more water for ensuring the homogeneous mixing and fiber distribution and therefore, achieving the rolling a soil sample into a thread until it reaches a point where it crumbles.

Regarding the shrinkage limit, from Figure 4.2 and with reference to experiments observations, the shrinkage limit has increased by increasing the fiber content (i.e. it varies from 12.3% to 19.1%), where the volume changes have been decreased by the increase of fiber content and that can be explained due to the fiber that increases the soil particle's connection and interlocking which that led to increasing the volume change resistance. Additionally, the fiber bonding effect has the same impact on the development of the crack during the drying process where it was noticed that cracks were initiated in the unreinforced samples, whereas, in the reinforced samples no cracks were visible or notable. Figure 4.3 shows the changes in shrinkage limit with respect to the fiber content.
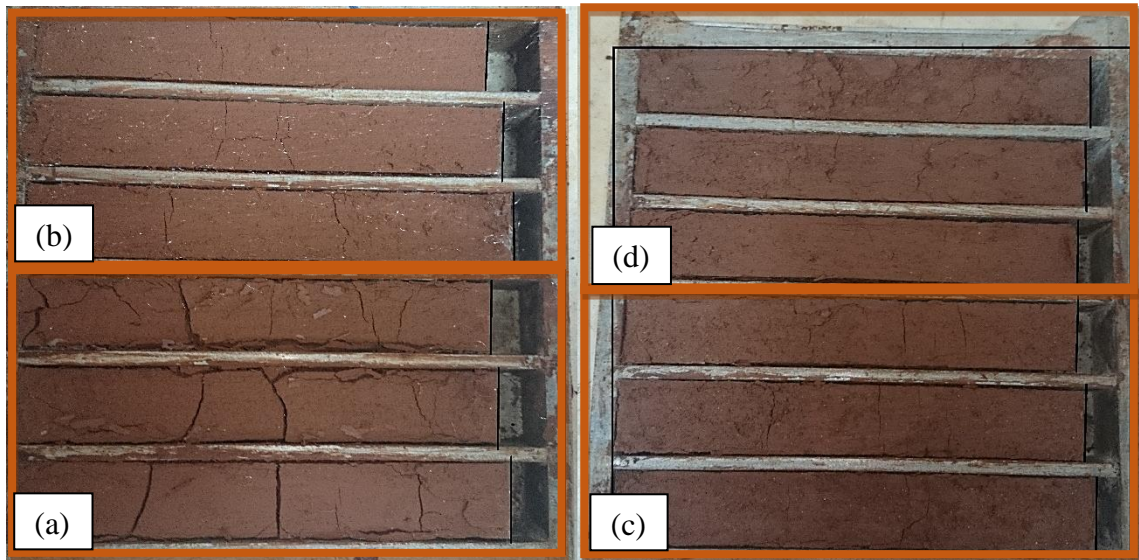
Figure 4.3. Changes in shrinkage limit: (a) Zero PP content; (b) 0.5% PP content; (c) 1% PP content; 1.5% PP content.

4.1.3 Evaluate the effect of PP on soil classification

In light of the resulting liquid, and plastic limits for each fiber content, the plastic index can be calculated. And by depicting the calculated plastic index and liquid limit to the Casagrande chart (see Figure 4.4), we can investigate the effect of PP on soil classification as per USCS, where it was found that for the pre-identified fiber content, the soil classification has been the same (CH) comparing with the unreinforced situation, with a possibility to be changed to (CL) for fiber content higher than 1.5% where the fiber can play a vital role on reducing the plasticity features.
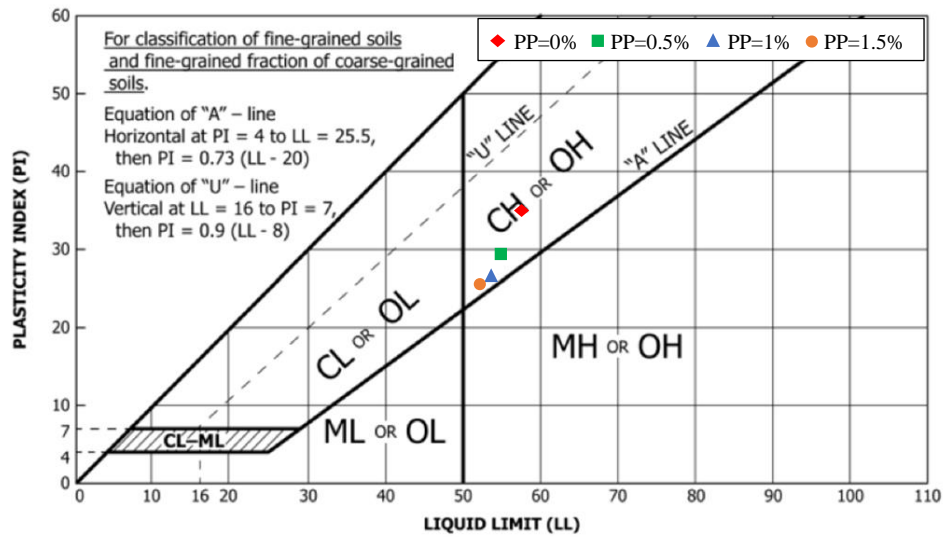
Figure 4.4. Soil classification as per four fiber contents (0%, 0.5%, 1%, and 1.5%).

4.2 Evaluate the Effect of PP on Strength Properties and Behavior

4.2.1 Evaluate the effect of PP on Shear strength properties and behavior

Referring to direct shear tests (DST), Figure 4.5 shows the shear stress values (τ kPa) with the corresponding horizontal displacement (ΔL mm) for each reinforcing ratio (fiber content) and vertical load (S_v) applied. The increase of shear strength by increasing the fiber content can be noticed in Figure 4.5.
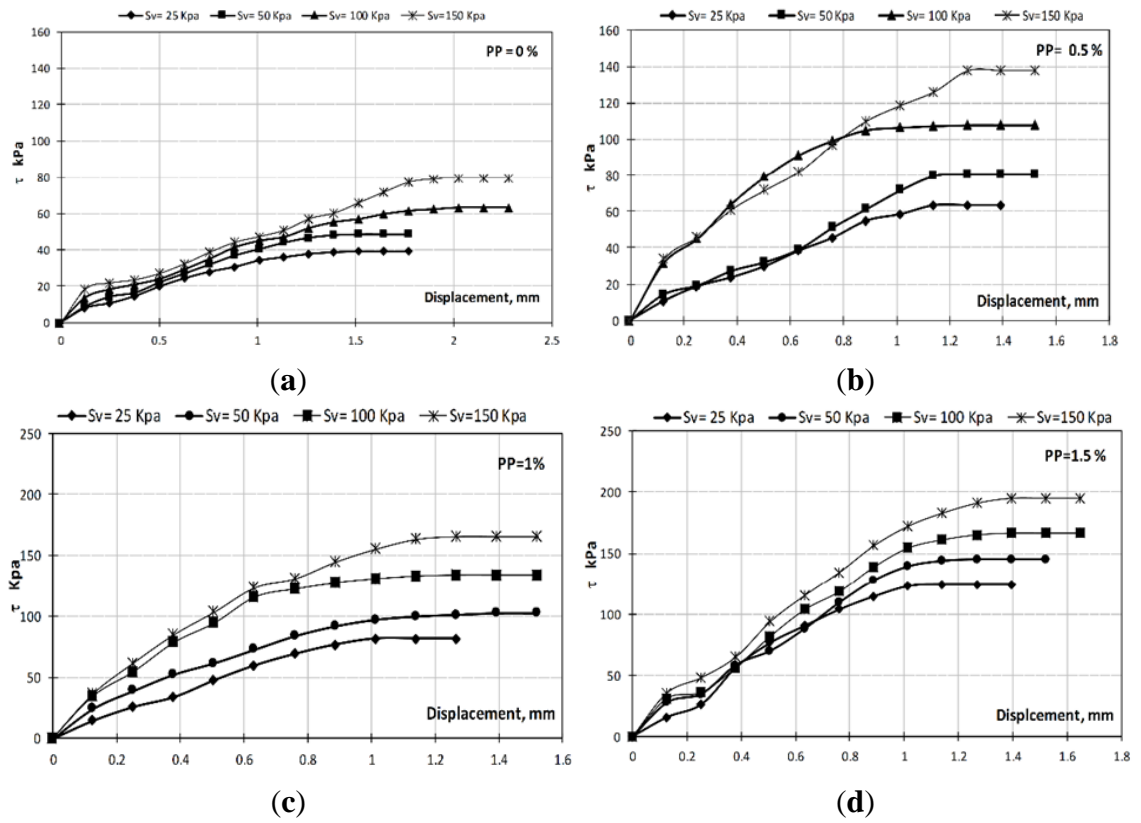
Figure 4.5. Shear stresses against displacements for four polypropylene fiber contents (PP): (a) PP = 0%. (b) PP = 0.5%. (c) PP = 1%. (d) PP = 1.5%.

In order to explore the influence of polypropylene fiber content on the shear strength, a representation of shear stress–displacement under one of the vertically applied loads (for all fiber contents used) is shown in Figure 4.6. It can be easily noticed that the gradient of the stress–displacement curves increases with the increase in fiber content, and this means that increasing the fiber content leads to an increase in the soil stiffness, which can be mainly attributed to the bonding effect that increases the connection between the soil particles through the fibers, which play the role of creating an additional link or additional friction and cohesion among the particles. The relation between the shear strength and the resulting horizontal strain for all reinforcing ratios can be represented in Figure 4.7, which shows the values of shear stresses at the collapse situation (i.e., at the maximum shear stress values) and the corresponding applied load for each fiber content (PP). It can be easily noticed that shear strength is increased with the increase of fiber content and the average increase is 184% at 1.5% of fiber, regardless of the vertical applied load value.
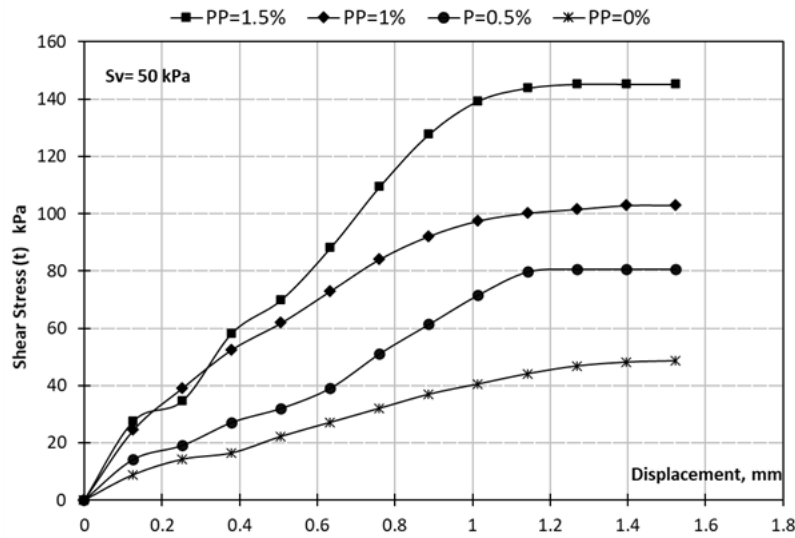
Figure 4.6. Stress–displacement curves under 50 kPa vertical load for different fiber contents.
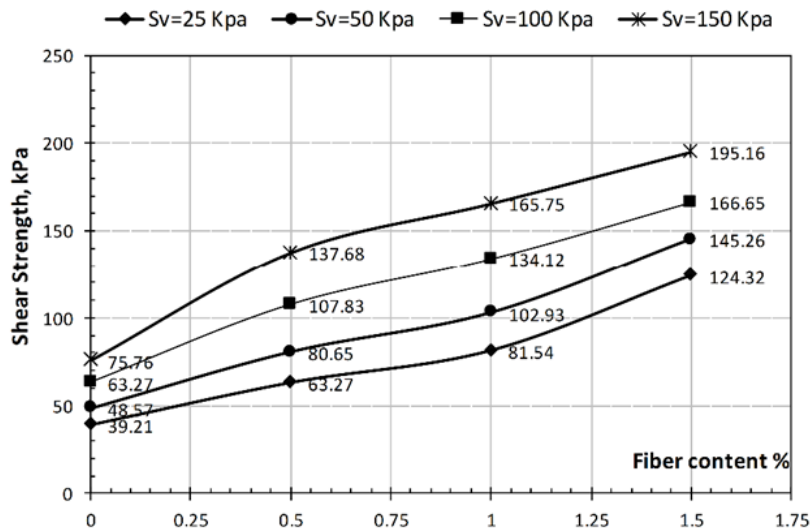
Figure 4.7. Shear strength against fiber content for four vertical applied loads

Referring to Figures 4.5 and 4.7, and by representing the relationship between both friction angle and cohesion with the fiber content as illustrated in Figure 4.8, a gradual increase in cohesion with the increase of the fiber content can be noticed. In addition, there was an increase in the angle of friction for each value of the reinforcing ratio, while the increasing rate decreased with the increase of the fiber content (for a reinforcing ratio bigger than 0.5%). Nevertheless, the friction angle is still greater than the unreinforced situation. These results are consistent with the results of some of the previous studies that

were conducted by other researchers for the same soil classification with minor differences (Mirzababaei et al., 2018; Mali and Singh, 2014; Maheshwari et al., 2013), where their results confirmed the increase of shear properties by increasing the fiber content. Regarding Anagnostopoulos et al. (2014), the reduction of the friction angle for a fiber content greater than 1% was observed. However, the friction angle for this situation was still greater than its initial value (unreinforced situation), and this was consistent with the experimental results. In addition, an increase in the plastic behavior of the reinforced samples in comparison with the unreinforced ones was observed, where it was noticed that the collapsing of reinforced samples took more time than the unreinforced ones, which means that the sample with fiber showed more ductile behavior.

Equations were developed to calculate both the cohesion and friction angles for any value of the reinforcing ratio under the assumption that the maximum ratio should not exceed 1.5% (Equations (4.1) and (4.2)). These equations give the values of the shear parameters for each fiber content that should not exceed 1.5%.

$$C_f(kPa) = 38.69 \times f^3 - 58.52 \times f^2 + 55.22 \times f + C_{f0}$$
(4.1)

$$\phi_f(\deg ree) = 2.133 \times f^3 - 22.6 \times f^2 + 36.4 \times f + \phi_{f0}$$
(4.2)

where, f is the fiber content, and therefore f_0 represents the unreinforced situation.
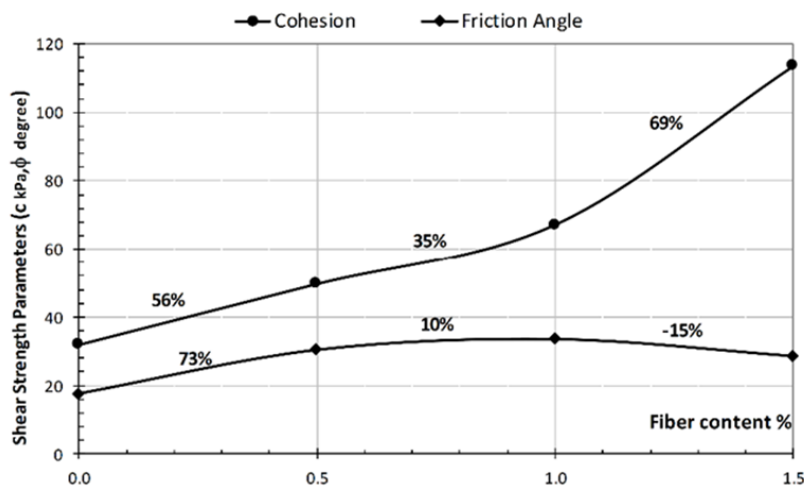
Figure 4.8. Shear strength parameters (c, $\emptyset$) versus fiber content

4.2.3 Evaluate the effect of PP on unconfined compressive strength properties and behavior

Referring to UCS tests, Figure 4.9 shows the values of the UCS for each fiber content.
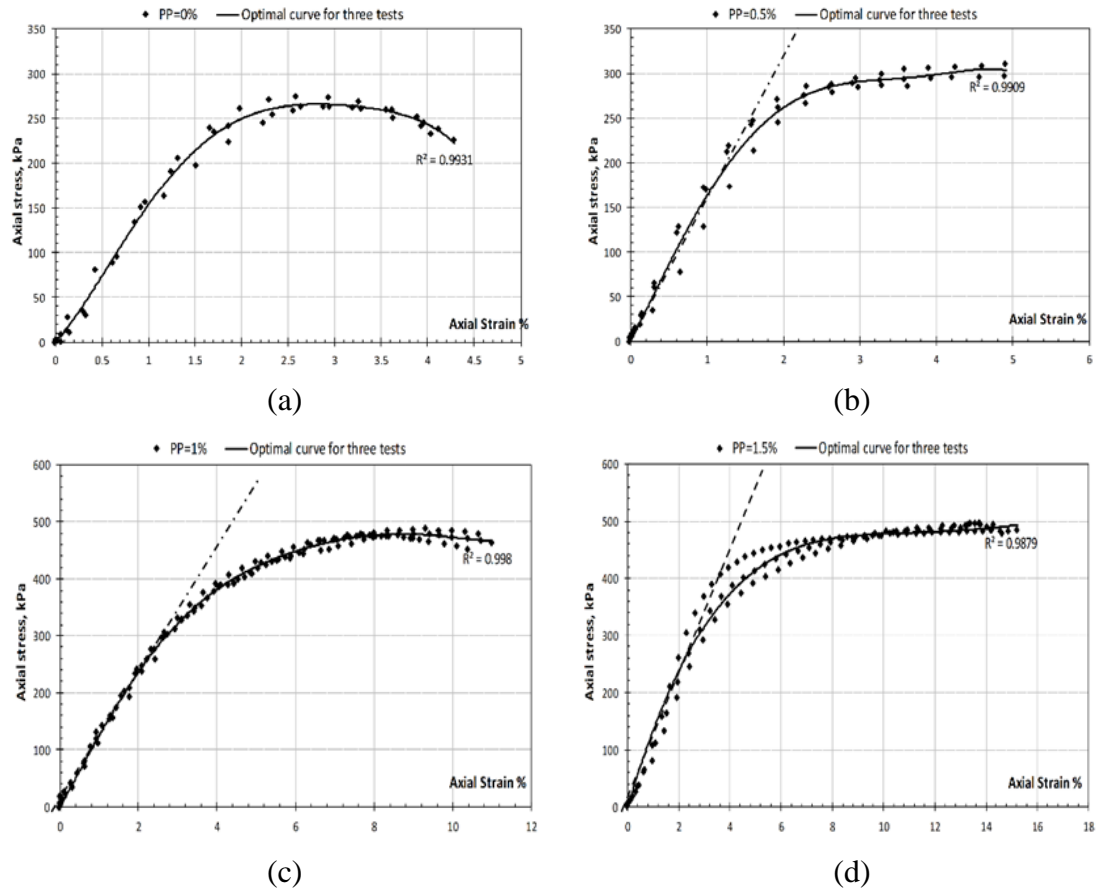
Figure 4.9. Axial stress/axial strain for four polypropylene fiber contents (PP): (a) PP = 0%; (b) PP = 0.5%; (c) PP = 1%; (d) PP = 1.5%.

By taking the slope (inclination) of the straight part of the curve (stress-strain), the elastic modulus for each reinforcement ratio used (PP = 0%, 0.5%, 1%, 1.5%) can be obtained. Table 4.2 shows the values of the elasticity modulus of the studied soil, as well as the values of the unconfined compressive strength at the collapse situation for each value of the fiber content.

Table 4.2. Unconfined Compressive Strength and elasticity modulus values with respect to fiber content

Fiber Content (%)	Unconfined Compressive Strength, q_u (kPa)	Elasticity Modulus, E (kPa)
0%	265	15.00
0.5%	305	15.91
1%	478	13.64
1.5%	493	13.48

Based on the aforementioned tests' outputs, and by representing the values of the unconfined compressive strength and elasticity modulus for all fiber contents used (as it is shown in Figure 4.10), the increase in the unconfined compressive strength by adding 0.5% and 1% of the fiber, respectively, was noticed, and after that, the rate of the increase was reduced by adding 1.5% of the fiber. In other words, the unconfined compressive strength increased by more than 50% when the fiber content increased from 0.5% to 1%. Furthermore, there was an increase in the elasticity modulus by adding 0.5% of fiber, and then the elasticity modulus was decreased for the fiber content of 1% and 1.5%. However, the final value of the elasticity modulus was smaller than its initial value (unreinforced situation) for the fiber content of 1% and 1.5%. This could be attributed due to the fibers' effect that plays a role in developing an additional bonding between the particles when the reinforcing ratio was less than 1%, whereas the bonding effect of the fiber has been decreased after adding more fibers (PP = bigger than 1%), and at this stage, the additional fibers have not had the same bonding effect between the soil particles. This may be due to the behavioral change of the soil samples when adding additional fiber, as when the fiber content increases, the fibers agglomerate in the soil, resulting in loose contact between soil particles and fibers. Consequently, a significant difference in the stiffness of fiber–soil mixture resulted. Similar behavior was reported by (Maheshwari et al., 2013; Yang et al., 2017; and Sharma & Kaushik, 2019).
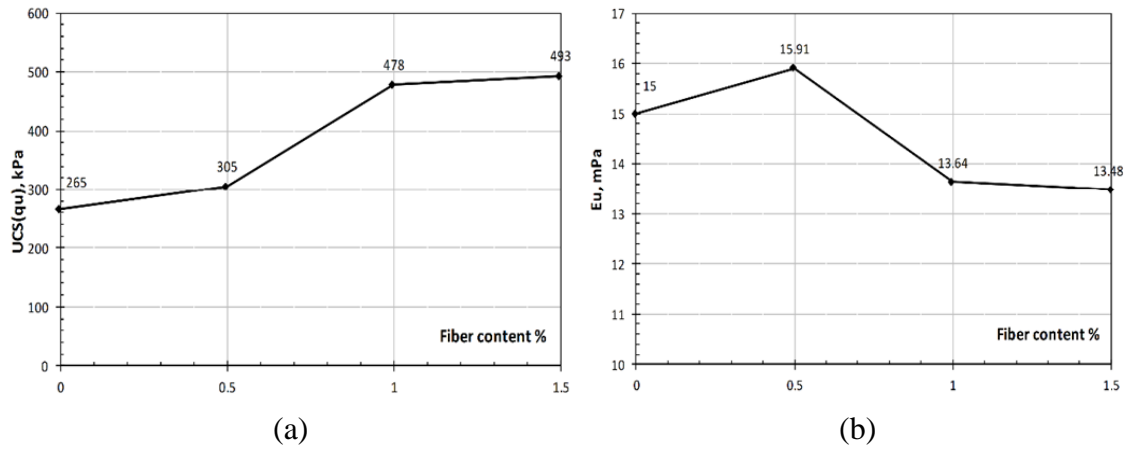
Figure 4.10. Change of unconfined compressive strength parameters (q_u, E_u) with fiber content (PP). (a) q_u; (b) E_u.

According to the experimental findings, increasing the fiber content in each sample increased the necessary time for each sample to reach the failure stage in addition to its influence on the failure pattern. Figure 4.11 shows the failure shapes for samples with fiber contents (0%, 0.5%, 1%, and 1.5%) from left to right, respectively. The failure shape for the unreinforced sample resulted from a straight failure surface (straight fracture plane) spread throughout the sample's height. On the other hand, for the reinforced samples (1% and 1.5%), the center and bottom portions of the specimens eventually extruded, causing the specimen to fail plastically in the shape of a drum. For reinforced samples with fiber content equaling 0.5%, there was no specific failure shape (obvious fracture plane), and it could be considered as a moderate situation (regarding its failure behavior) between the aforementioned failure behaviors.
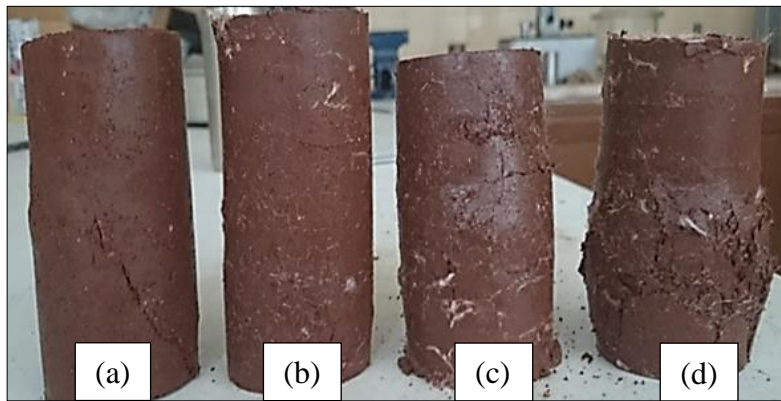
Figure 4.11. Unconfined compressive strength failure shapes concerning the fiber content (a) 0% (b) 0.5% (c) 1.0% (d) 1.5%.

By comparing the obtained results with other studies that have been conducted on soil reinforced with fibers, it can be noticed that the results which were presented by (Sabat, 2012; Maheshwari et al., 2013; Aykut et al., 2014) were compatible with the obtained results, even though the used fibers and/or the studied soil (low plasticity clay) in their studies were different.

Upon the experiments' results, a fiber content-based function was developed to calculate the UCS at any value of the reinforcing ratio under the assumption that the maximum ratio should not exceed 1.5% (Equation (4.3)). The equation provides the values of the UCS for each fiber content that should not exceed 1.5%.

$$UCS_f = q_{uf}(kPa) = -383 \times f^3 + 484 \times f^2 + 247 \times f + q_{uf0} \tag{4.3}$$

where f is the fiber content, and therefore f_0 represents the unreinforced situation. Thus, q_{uf}, and q_{uf} are the UCS values at f and f_0 respectively.

4.2.4 Evaluate the effect of PP on conventional undrained unconsolidated strength behavior

Referring to conventional undrained (UU) triaxial tests, Figure 4.12 shows the results of stress-strain curves of unreinforced and reinforced specimens under 200 kPa confining pressures. Also, Figure 4.13 shows the failure patterns for the fiber-reinforced and unreinforced samples at the end of the testing stage.
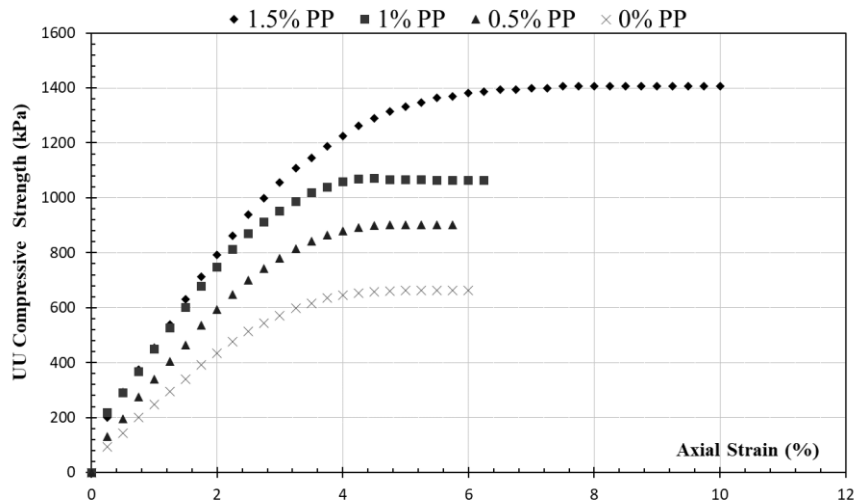
Figure 4.12. Stress-strain relationships of reinforced and unreinforced soil at confining pressures of 200 kPa.
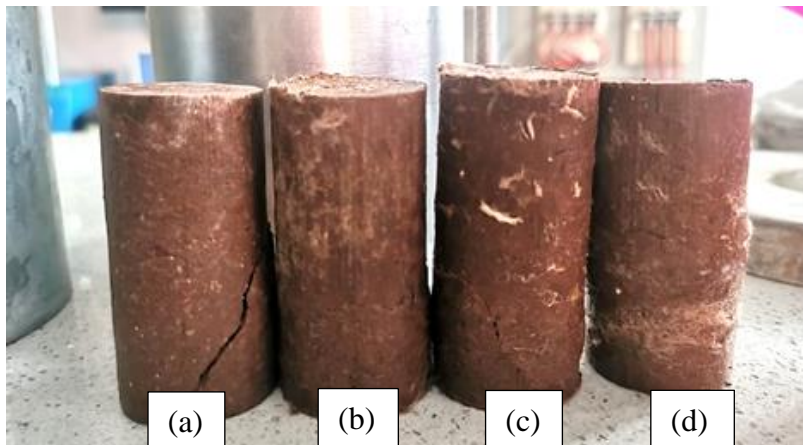
Figure 4.13. Failure patterns respecting the fiber content (a) 0% (b) 0.5% (c) 1.0% (d) 1.5%.

Referring to Figure 4.12, and by representing the failure strength values for all cases (three reinforced samples and one unreinforced sample) as shown in Figure 4.14(a). It can be noticed easily a gradual increase in the UU compressive strength with the increase of fiber content where the increase was 35%, 60%, and 112% after adding 0.5%, 1%, and 1.5% of fiber respectively. This can be attributed to the fibrous effect, which plays an important role in the development of additional bonds between soil grains.

For determining the resilient modulus (E), equation (3.1) was used and resilient modulus values for each fiber content were identified and represented as shown in Figure 4.14,

where it can be noticed that the increase of E with the increase of fiber inclusion, and the maximum value was 40 MPa at 1% and 1.5% fiber content.

(a)   (b)
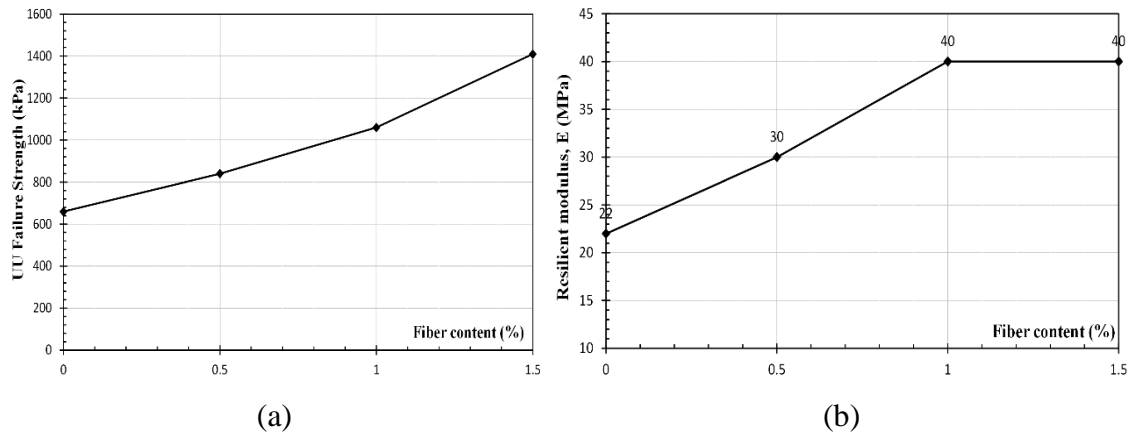
Figure 4.14. UU compressive strength parameters with fiber content (FPP): (a) UU compressive strength, (b) Resilient modulus with fiber content

4.3 Evaluate the effect of PP on the compressibility behavior and properties

4.3.1 Evaluate the effect of PP on the swelling potential and swelling stress

Figure 4.15 shows the results of the free-swelling tests that represent the average of three sample results for each fiber content.
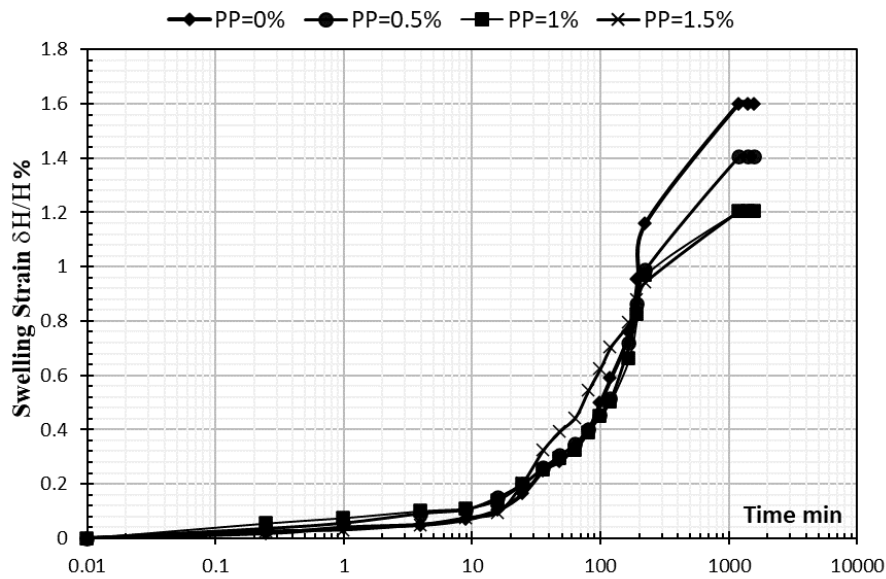
Figure 4.15. Average swelling readings for four fiber contents (PP = 0% to 1.5%).

64

At the end of the free-swelling test (after getting the maximum free swelling values for all tested samples), and in order to find out the value of the swelling stress for each sample, gradual vertical loads (50, 100, 160 kPa) were applied on the samples, and then the total settlement value after 24 h of loading was read. By representing the remaining amount of swelling, during the loading process, the swelling stress could be identified (i.e., at zero swelling value). Table 4.3 shows the maximum swell stress for each reinforcing ratio (fiber content (PP)) and for each applied load. The negative values in the table mean that the settlement at the corresponding load is greater than the final swelling value of each loading case. Therefore, the results of this table are represented to calculate the values of the swelling stress for each case of re-inforcing ratio.

Table 4.3. Swell stress and swell strain values with respect to fiber content

Fiber Content (%)	Swell Stress (kPa)	Maximum Swelling Strain, $\Delta H/H$ (%)
0%	7	1.6
0.5%		1.405
1%		1.205
1.5%		1.205
0%	50	1.275
0.5%		1.03
1%		0.78
1.5%		0.62
0%	100	0.6
0.5%		0.145
1%		−0.245
1.5%		−0.395
0%	160	−0.2
0.5%		−0.1
1%		−0.32
1.5%		−1.045

Figure 4.16 shows the intersection of the curves with the stress axis, which represents the values of the swelling stress of the studied soil for each fiber content. From the figure below, the values of the swelling stress can be found for each rein-forcing ratio that produces zero swelling values, which are summarized in Table 4.4. Based on the aforementioned tests' outputs, and to assess the effect of polypropylene fiber on both swell potential and swell stress (SS), representations of swell stress, and swell potential against fiber contents are shown in Figures 4.17 and 4.18.
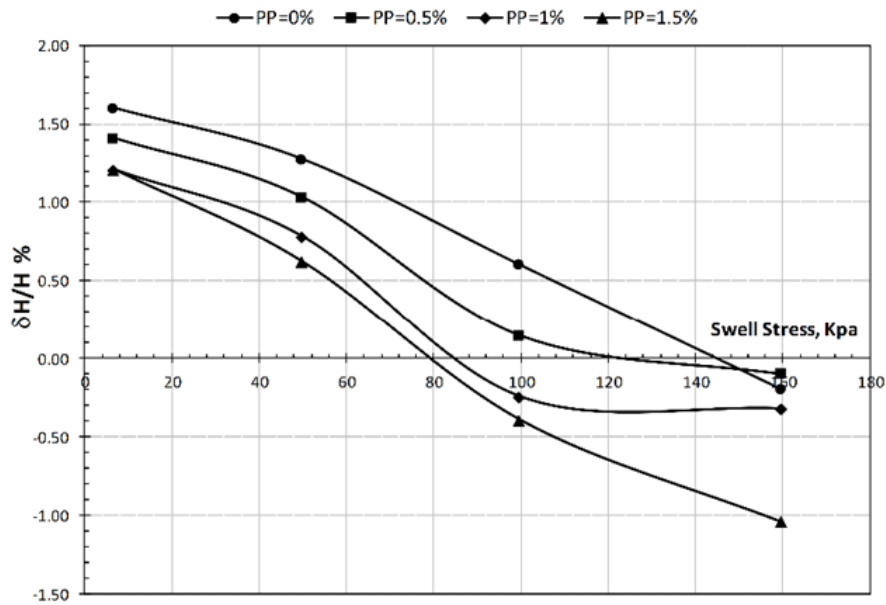
Figure 4.16. Swelling values against swelling stresses for different fiber contents (PP).

Table 4.4. Swelling stress (zero swelling value) respecting fiber content

Fiber Content, PP (%)	Swell Stress, SS (kPa)
0%	145
0.5%	124
1%	85
1.5%	78
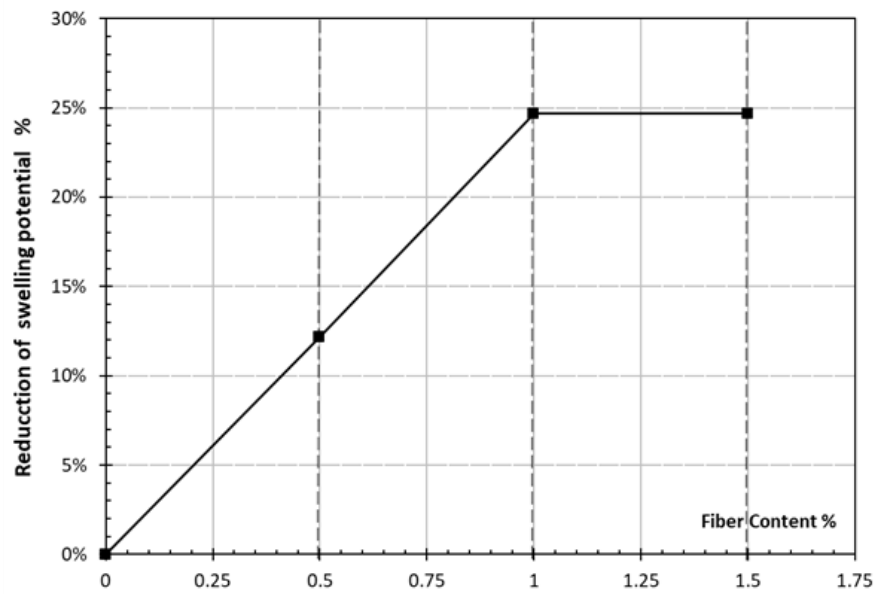
Figure 4.17. Reduction of swelling potential against fiber content.
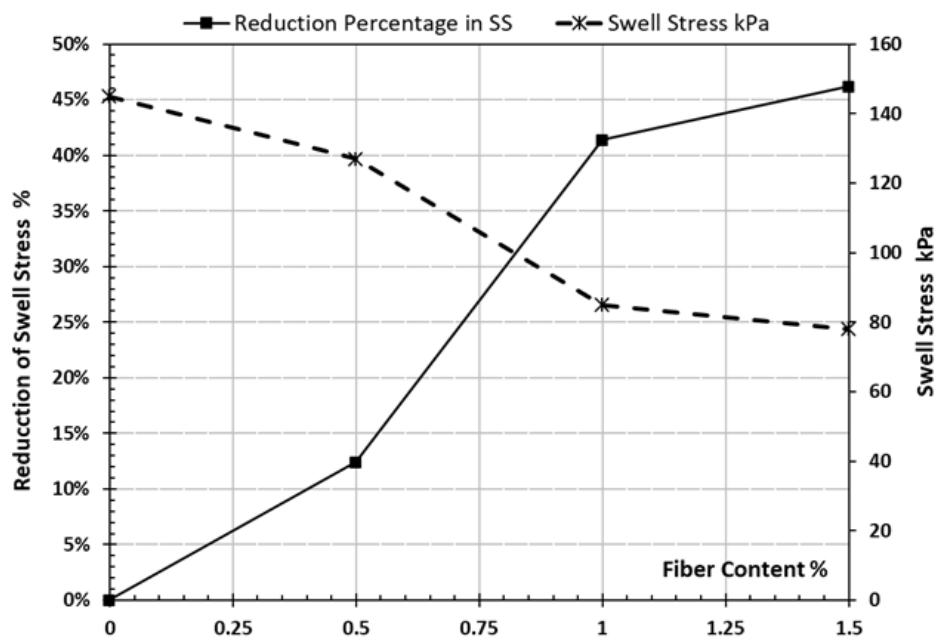
Figure 4.18. Swelling stress value and its reduction percentage against fiber content.

Regarding swell potential, it decreased significantly with increasing fiber content to 1%
and the maximum reduction in the swell potential was 24.6%, as shown in Figure 4.17,
and this could be due to the same behavior that was observed during the conduction of

UCS experiments, where it was observed that the bonding effect of the added fiber was decreased after adding 1% or more of the fiber.

Regarding swell stress, it decreased substantially with increasing fiber content from 0.5% to 1.5%. The maximum reduction was 46.2%, as shown in Figure 4.18. Upon the experiments' results, a fiber content-based function was developed to calculate the swelling stress at any value of the reinforcing ratio, under the assumption that the maximum ratio should not exceed 1.5% (Equation (4.4)). This equation gives the values of the swelling stress for each fiber content that should not exceed 1.5%.

$$SS_f(kPa) = 102.6 \times f^3 - 232 \times f^2 + 76.33 \times f + SS_{f_0} \tag{4.4}$$

where SS_f is the swelling stress respecting f (f is the fiber content), and f_0 represents the unreinforced situation, therefore, SS_{fo} is the swelling stress for the unreinforced situation.

4.3.2 Evaluate the effect of PP on the consolidation properties and behavior

Referring to consolidation tests, Figure 4.19 shows the results of the consolidation tests that represent the average of three sample results for each fiber content. Table 4.6 summarized the final consolidation settlement at each applied load and for each fiber content. Referring to Table 4.5 and Figure 4.19, it can be easily noticed that the consolidation settlements have been decreased with the increase in the fiber content up to 1%, while for the fiber content of 1.5% the final settlements were higher than its intimal value (unreinforced situation).

Table 4.5. Final consolidation settlement respecting fiber content

Vertical applied load, σ_v (kPa)	Consolidation settlement, δh/h (%)			
	PP= 0%	PP= 0.5%	PP= 1%	PP= 1.5%
80	0.675	0.54	0.585	0.755
160	1.425	1.215	1.24	1.795
320	2.425	2.005	2.055	3.055
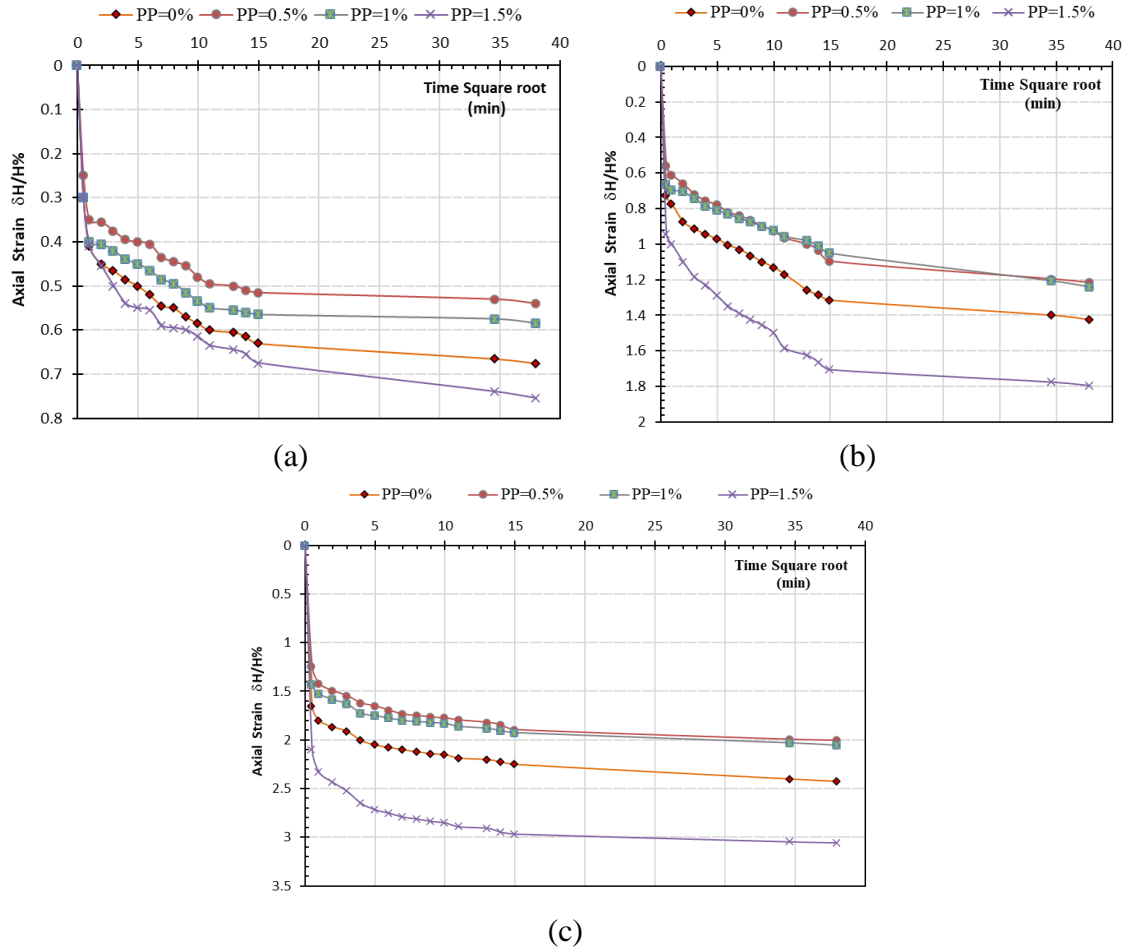
Figure 4.19. Consolidation axial strain with respect to both time and PP content (a) σ_v =80 kPa (b) σ_v =160 kPa (c) σ_v =320.

Also, for tracking the changes in the void ratio for each sample type, the aforementioned equation (Eq (3.2)) is applied to find the void ratio value that meets every settlement, and the representation of void ratio changes during the testing application is shown in Figure 4.20 with respect to both time and vertical loads applied.

By representing the value of settlements and related load applied as it is shown in Figure 4.21, and by determining the inclination of each stress-strain curve, the elasticity modulus for each situation/fiber content can be identified. Table 4.6 presents the elasticity modulus (E_{oed}) resulting from one-dimensional consolidation for each fiber content.
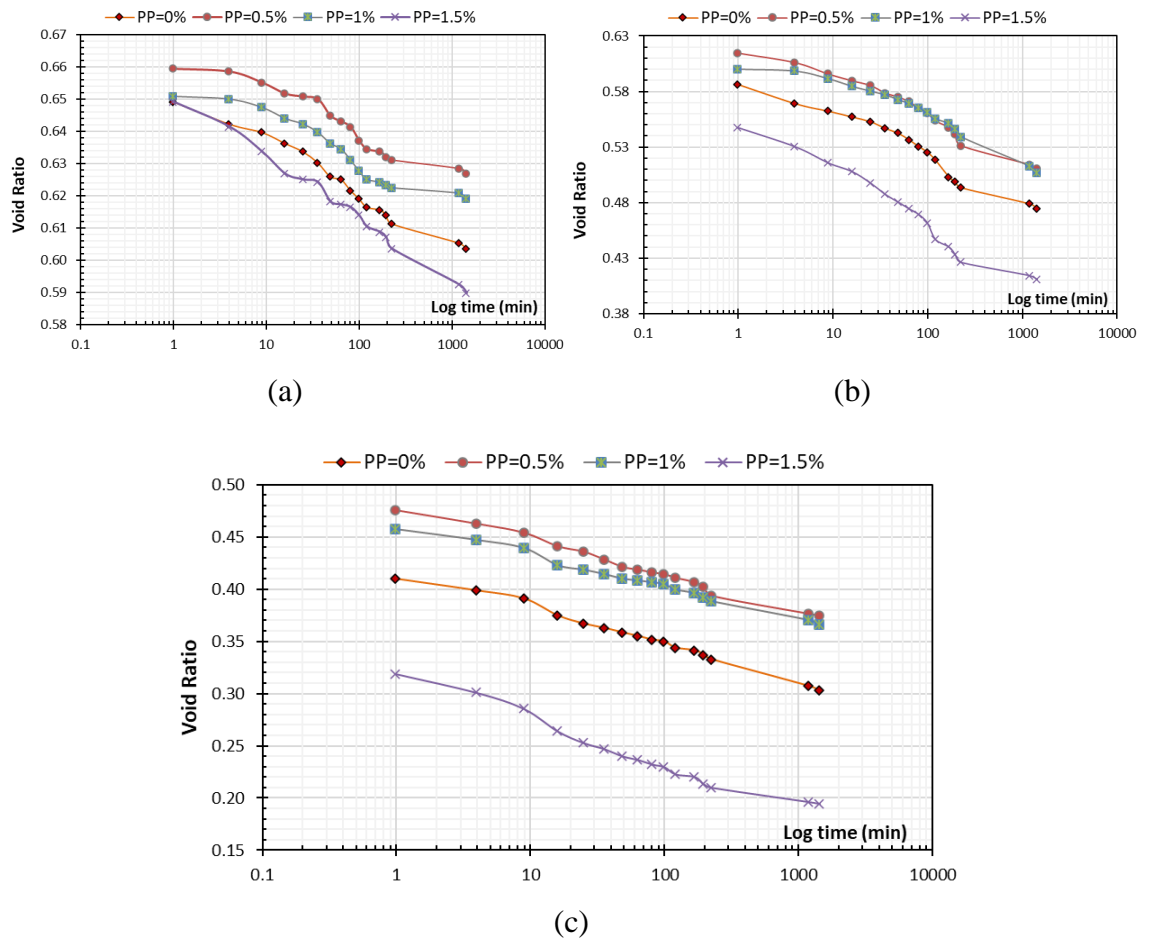
Figure 4.20. Void ratio changes during consolidation test concerning both time and PP content (a) σ_v =80 kPa (b) σ_v =160 kPa (c) σ_v =320 kPa.
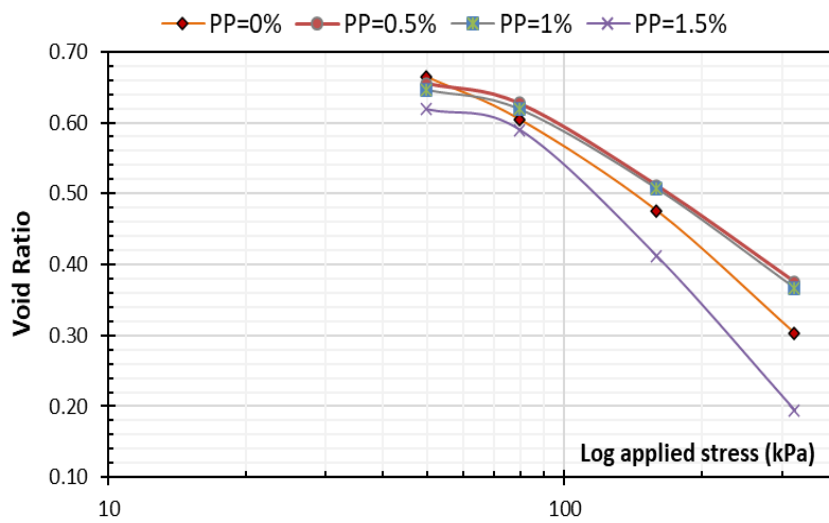
Figure 4.21. Void ratio changes during the consolidation test concerning the applied stresses (80 kPa, 160 kPa, 320 kPa)

Table 4.6. Elasticity modulus resulting from consolidation tests

E_{oed}, MPa			
PP= 0%	PP= 0.5%	PP= 1%	PP= 1.5%
16	20.25	19.63	12.70

From the table above, it can be inferred that the increase of fiber content led to an increase in the elasticity modulus by adding 0.5% and 1% of fiber, and then the elasticity modulus was decreased for the fiber content of 1.5%. However, the final value of the elasticity modulus was smaller than its initial value (unreinforced situation) for the fiber content of 1.5%. This could be attributed due to the fibers' effect that contributed to the development of an extra bonding between the particles when the reinforcing ratio was less than 1%, whereas the bonding effect of the fiber has been decreased after adding more fibers (PP = bigger than 1%), and at this stage, the additional fibers have not had the same bonding effect between the soil particles. This may be due to the behavioral change of the soil samples when adding additional fiber, as when the fiber content increases, the fibers agglomerate in the soil, resulting in loose contact between soil particles and fibers. Consequently, a distinct variation in the fiber–soil mixture stiffness. Similar behavior was reported by (Maheshwari et al., 2013; Yang et al., 2017; and Sharma & Kaushik, 2019).

Referring to Figure 4.21, and by determining the inclination of the void ratio-Log_{10} stress curve for each case the compression index (Cc) can be found as it is shown in Figure 4.22. Where it can be noticed that the compression index decreases with the increase of fiber content up to 1%, and increases when adding fiber of 1.5%. By comparing the obtained results with other studies that have been conducted on soil reinforced with fibers, it can be noticed that the results which were presented by (Malekzadeh and Bilsel, 2012; Rabindra et al., 2012; Maheshwari et al., 2013) were compatible with the obtained results, even though the used fibers and/or the studied soil (low plasticity clay) in their studies were different.

Upon the experiments' results, a fiber content-based function was developed to calculate the compression index at any value of the reinforcing ratio under the assumption that the maximum ratio should not exceed 1.5% (Equation (4.5)). The equation provides the values of the UCS for each fiber content that should not exceed 1.5%.

$$Cc_f = 0.14 f^3 + 0.057 f^2 - 0.303 f^1 + Cc_{fo} \qquad (4.5)$$

where Cc_f is the compression index with respect to f (f is the fiber content); Cc_{fo} is the compression index for an un-reinforcement situation.
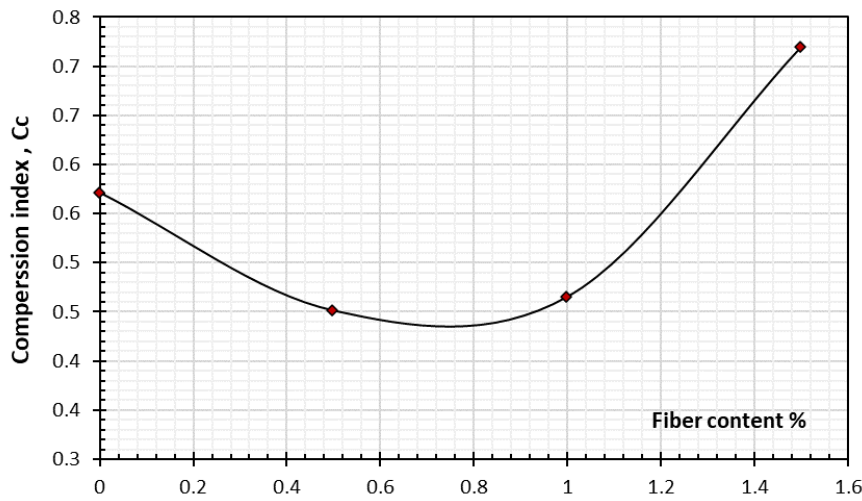
Figure 4.22. Compression index with respect to fiber content.

4.4 Evaluate the Effect of PP and other Chemicals on Cracking and Volumetric Changes due to Environmental Changes

4.4.1 Evaluate the effect of PP and other chemicals on cracking resistance during the drying process
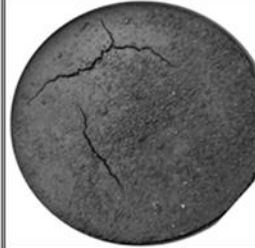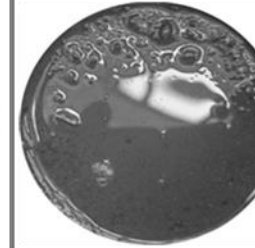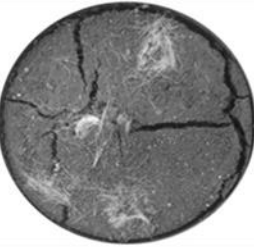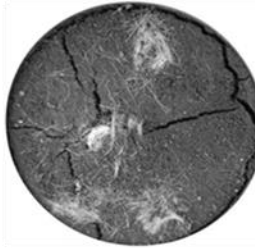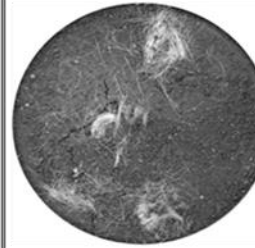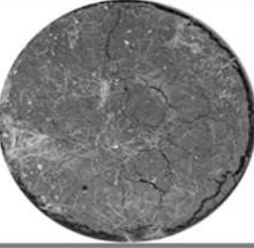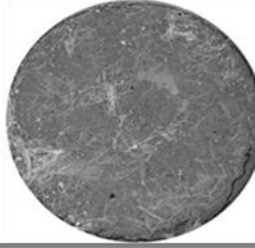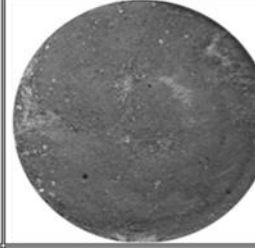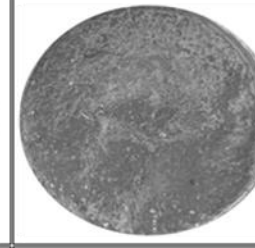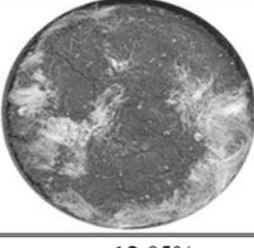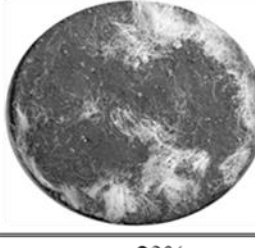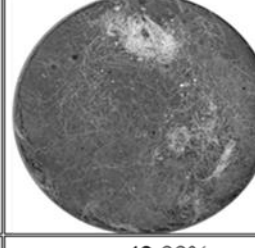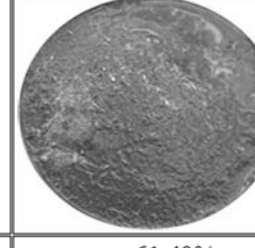
Referring to the desiccation/drying tests, the representation of water content changes with time (evaporation rate) for each situation by depicting the experimental results (changing the water content with respect to the time) is shown in Figure 4.23. Also, the photographic database by photographing the samples' surfaces for different time periods for all situations is shown in Figures 4.24 and 4.25.

Referring to Figure 4.23, it can be noticed easily that the evaporation rate for all studied cases (untreated, reinforced, cement stabilized, lime stabilized) is almost the same, and this indicates that the used treatment method did not affect the rate of evaporation, and therefore the method of treatment did not affect the time required for the appearance of cracks/cracks' development. Even though there were some differences in the values of the evaporation rate at the last stage of drying, this can be attributed to the generated cracks that have affected the evaporation rate.

In order to calculate the area of the generated cracks in each sample for all cases, the digital processing (through the Matlab program) method was applied. Table 4.7 summarizes the results of digital processing in terms of cracks area for each studied case during the drying process.
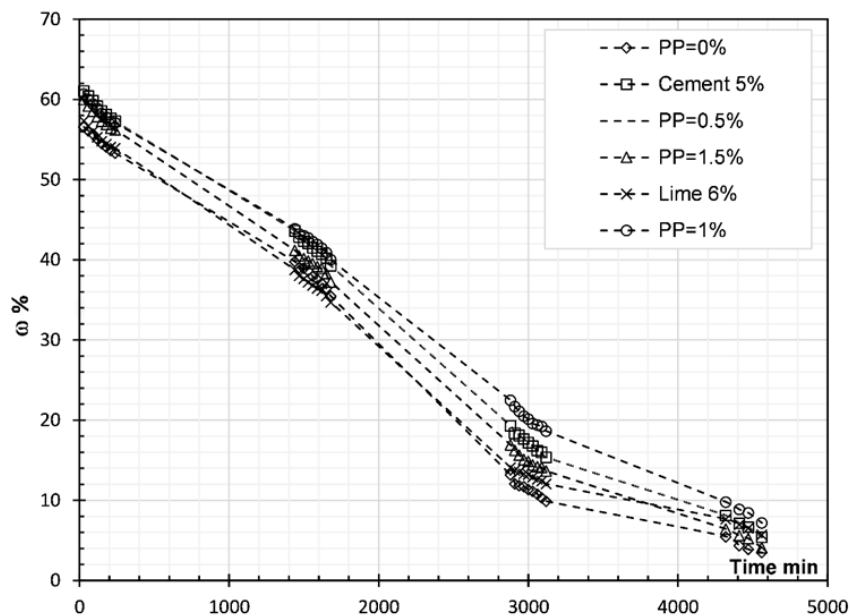
Figure 4.23. Water content changes with time (evaporation rate) for treated and untreated samples

Figure 4.24. Surface samples photos during the drying process for reinforced and untreated samples
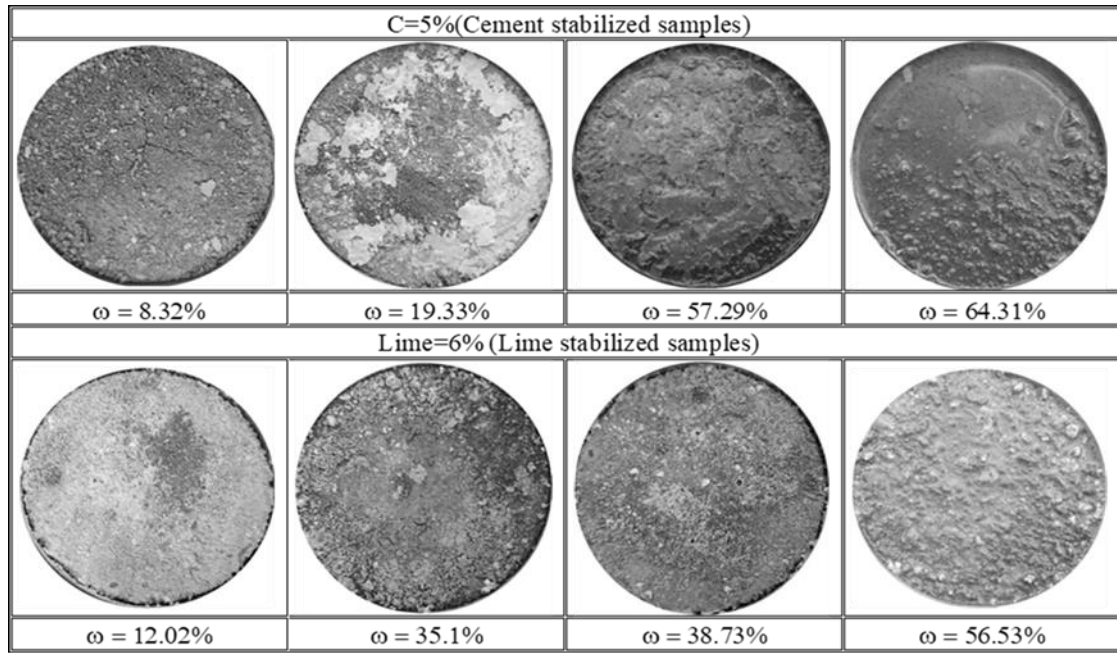
Figure 4.25. Surface samples photos during the drying process for cement and lime-stabilized samples

Table 4.7. Results of digital processing

Additives type	Additives Content	Array size (Pixel)	$N_{cracks-elements}$ (Pixel)	$\dfrac{A_{cracks}}{A_{sample}}$
No Additives	0%	1760 x 1766	310356	12.7% [*1]
Polypropylene fiber	0.5%	1730 x 1735	209626	9.0% [*1]
Polypropylene fiber	1%	1900 x 1880	135879	4.8% [*1]
Polypropylene fiber	1.5%	2160 x 2090	94659	2.8% [*1]
Cement	5%	2066 x 2020	67881	2.0% [*2]
Lime	6%	1960 x 1926	40164	1.4% [*2]

*1 Note: cracks were noticed for reinforced and unreinforced samples during the drying process.
*2 Note: both contraction and cracks have resulted, while for the chemically stabilized samples the effect was limited to contraction.

From the above table, it can be noticed easily that the area of the developed cracks, for reinforced cases, was decreased with the increase of the fiber content, and this can be attributed to the role of the fibers that creates additional bonding between the soil particles, wherein due to the drying, the soil shrinks, and desiccation cracks tend to develop. At this stage, the tensile force starts to be mobilized in the fibers and only adhesion restrains the fibers from the pullout, thus allowing for its tensile resistance to develop and create an additional bonding effect to resist the formation of the cracks.

Regarding the cement and lime stabilized samples, it was noticed that no cracks developed throughout the drying process, and it was limited to the sample contraction only. However, this behavior can be explained due to the cementitious effect/pozzolanic effect that increases the cohesion between the soil particles which led, in turn, to the sample contraction only, and high resistance of cracks development.

From the experimental observations, it was noticed as well that the samples' structure for cement/lime stabilized can be easily broken or crushed at the end of the drying process, while for PP reinforced samples, the structure was more coherent, and this can be attributed to the water role in chemically stabilized samples which plays a vital role in chemical reactions that lead to high cohesion in the soil, and the absence of water affects the chemical-based bonding effect, while for fiber additives the water absence didn't have that effect.

4.4.2 Evaluate the effect of PP and other chemicals on cracking resistance and volumetric changes during the drying/wetting process

Referring to the dry/wet cycle tests, Figure 4.26 shows the generated cracks/volume change at the sample surfaces for each treatment case. Referring to Figure 4.26, it can be noticed (by using the aforementioned image digital analysis method) that no remarkable cracks appeared on the cylindrical surface for all cases. However, small cracks were observed but their width and depth were very small and can be ignored.

After conducting the measurements during the testing phase, the final volume change for each studied case can be obtained by subtracting the final measured volume (at the last drying cycle) from the initial volume (cylindrical can volume) and dividing the result by the initial volume. Figure 4.27 totalize the experimental results of the dry/wet cycles test.
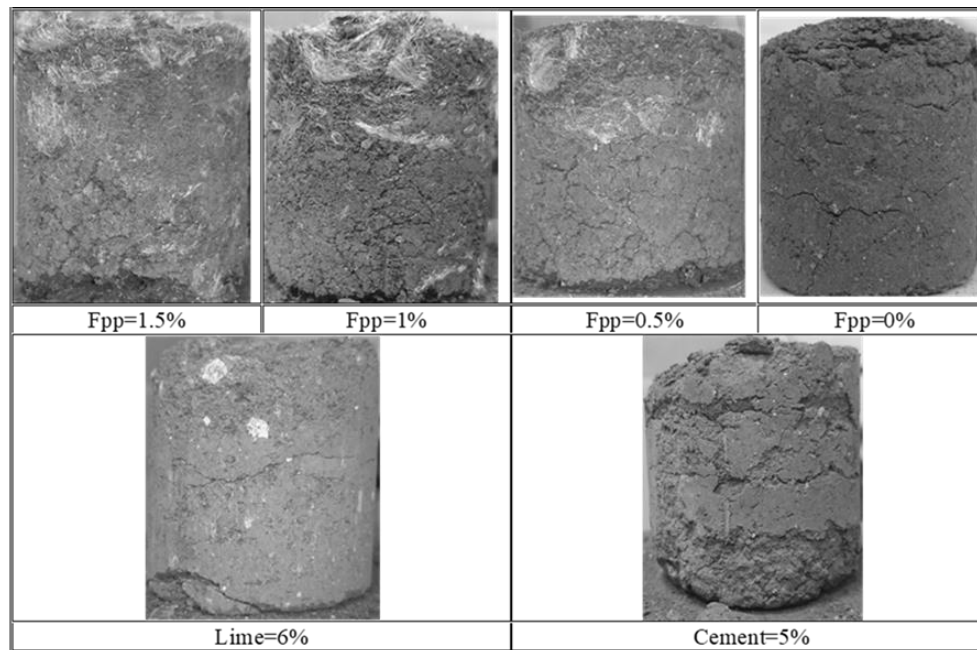
Figure 4.26. Generated cracks/volume change at the fourth drying cycle.
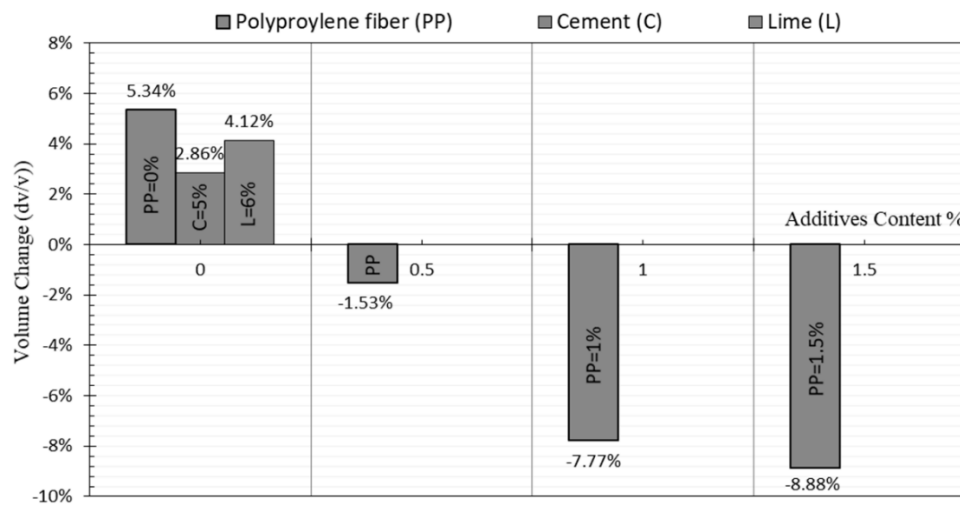
Figure 4.27. Summary of experimental results of the dry/wet cycle test.

Referring to the outputs of the related test which were summarized in Figure 4.27, it was noticed that the volume changes, at the last cycle, for untreated samples and cement/lime stabilized samples were swelling type. In addition, the cement-stabilized samples exhibited lower volume change in comparison with lime-stabilized ones. In contrast, reinforced samples exhibited a volumetric change of contraction/compression type, and the change was increased with the increase of fiber content. However, this behavior can

be attributed to the effect of polypropylene fiber in resisting the swelling pressure during the wetting cycles which was more efficient in comparison with the swelling resistance effect of cement and lime. Likewise, the high crack formation resistance also contributed to reducing the changes during the drying cycles.

In order to find out the optimum fiber inclusion for the reinforced samples in which the volume change was increased with the increase of fiber inclusion, regardless of the change type (contraction or swelling), the volume changes values for all fiber contents (0%, 0.5%, 1%, 1.5%) were represented as shown in Figure 4.28 where it can be found that the optimum fiber inclusion for resisting the volume changes is 0.38%.
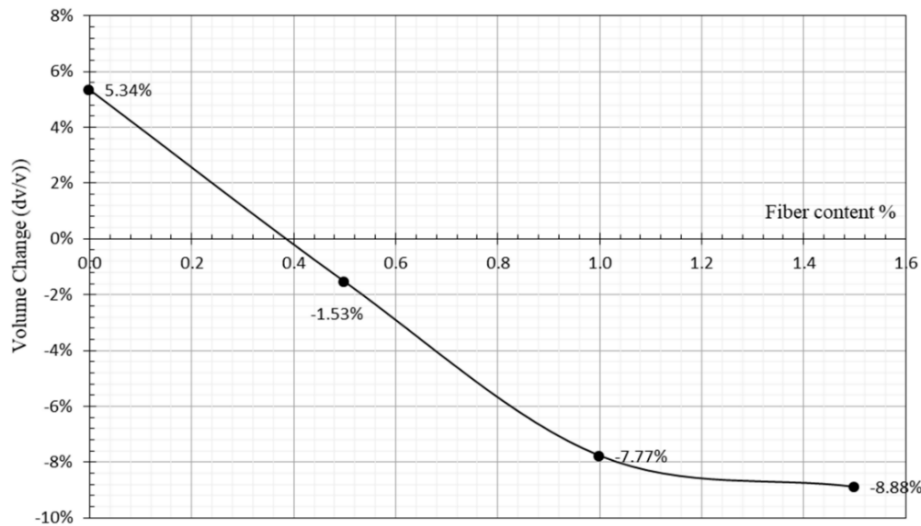
Figure 4.28. The optimal fiber content for resisting volume changes.

4.5 Evaluate the Strength and Durability Behavior of the Fiber–Clay Mixtures Subjected to Freeze–Thaw Cycles

Referring to UU triaxial tests, and after subjecting the samples to 10 closed cycles of freezing and thawing, Figure 4.29 illustrates the stress-strain relations of the fiber-reinforced and unreinforced samples under 200 kPa confining pressures after application of 0, 3, 6, and 10 (F–T) cycles respectively. Also, during the application of (F–T) cycles, the samples' heights and diameters are measured several times. Table 4.8 presents the physical properties (height and diameter) of the studied samples after exposing them to (F–T) cycles and before UU triaxial strength testing.

78
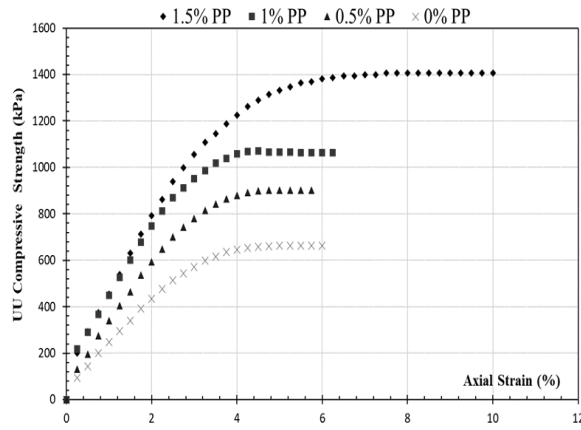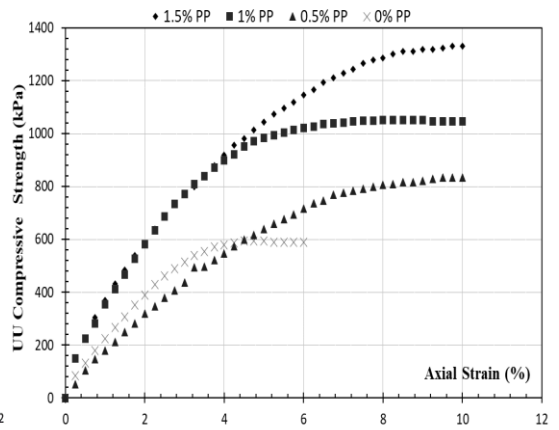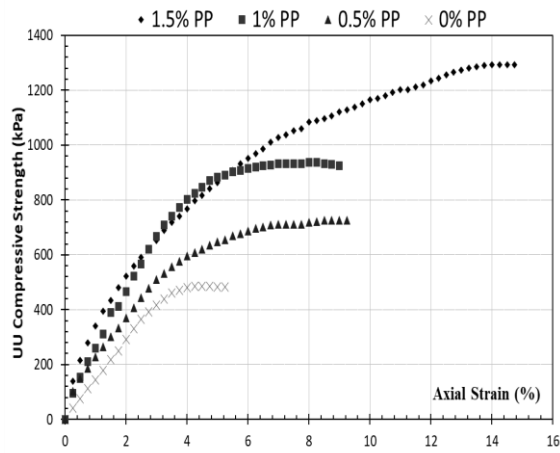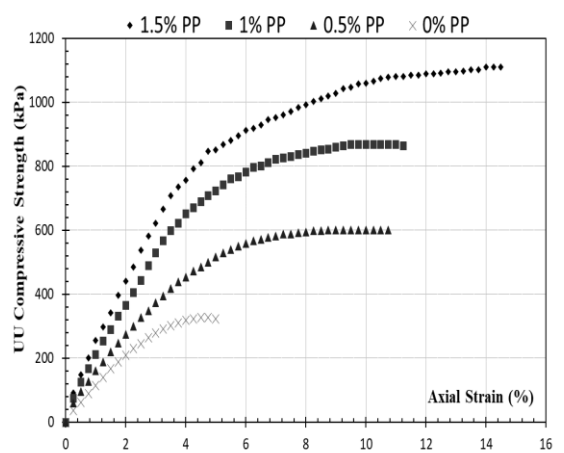
Figure 4.29. Stress-strain relations of unreinforced and reinforced soil under various cycles of (F–T): (a) Zero cycles of (F–T), (b) 3 cycles of (F–T), (c) 6 cycles of (F–T), (d) 10 cycles of (F–T).

Table 4.8. Physical changes after (F–T) cycles application and before UU triaxial strength testing

Number of (F–T)	Sample's diameter (D, mm)	Sample's hight (h, mm)	Fiber content (%PP)
0	38	80	0%
	38	80	0.5%
	38	80	1%
	38	80	1.5%
3	38	84.3	0%
	38	84.1	0.5%
	38	83.7	1%
	38	83.6	1.5%
6	38.3	85	0%
	38.2	84.8	0.5%
	38.3	84	1%
	38.3	84.5	1.5%
10	38.3	85.3	0%
	38.2	84.9	0.5%
	38.3	84.5	1%
	38.3	85	1.5%

Referring to Figure 4.29, and by representing the failure strength for all cases at 0, 3, 6, and 10 freeze-thaw cycles as it is shown in Figure 4.30 (a), it can be noticed clearly that the strength behavior for all unreinforced and reinforced samples is similar, where the strength decreases with the increase of (F–T) cycles, specifically. The UU compressive strength of the unreinforced sample has been reduced up to 51% after subjecting to 10 (F–T) cycles; this decreasing tendency was about 33% for 0.5% of PP content, 18.4% for 1% PP content, and 21.1% for 1.5% of PP content. This phenomenon can be attributed to ice formation and ice thawing causes, wherein in the freezing phase, the pore water in the soil turns into ice. Ice creates a force that separates soil particles, increasing the pore water pressure during this stage. On the other flip, during the thawing phase, excessive pore water pressure can not return to its original or previous state. So thus, (F–T) cycles

generally weaken soil strength (Andersland and Ladanyi, 2004; Wang et al. 2007; Ghazavi and Roustaie, 2013). Despite the fact that several studies have clearly demonstrated that soil strength decreases with an increase in the number of (F-T) cycles for both fiber- and non-fiber-reinforced soil, fiber-reinforced soils exhibited the least amount of strength loss in comparison with the non-reinforced ones, i.e. the greatest strength reduction was 51% for unreinforced samples while it was 18% after adding 1% of FPP which means fiber-reinforced samples reduced the frost heave by about 30% and 1% fiber content can be considered as an optimum content for frost heave resistance. 4.30 (b) shows the increase of the strength reduction by the increase of fiber inclusion.
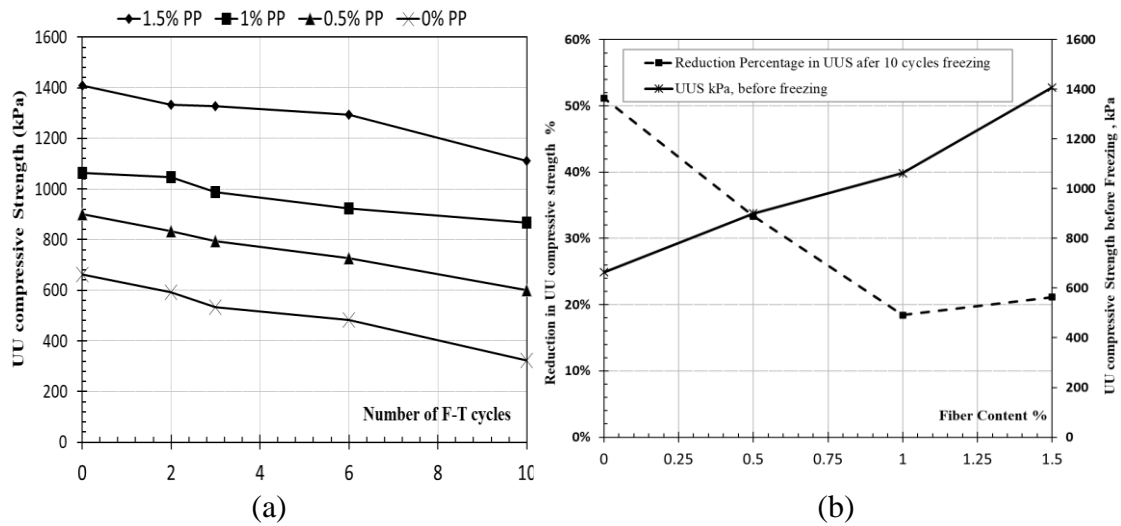
Figure 4.30. UU compressive strength values with fiber content (FPP): (a) UU compressive strength under different cycles of (F–T), (b) UU compressive strength reduction with fiber content.

For evaluating the effect of (F–T) cycles on the resilient modulus (E), the resilient modulus was calculated for both reinforced and unreinforced samples that were exposed to 10 cycles of (F–T). Figure 4.31 shows the reduction of resilient modulus with the increase of (F–T) cycles. However, the reinforced samples exhibited a minimum reduction rate, and this rate decreased with the increase in fiber inclusion.
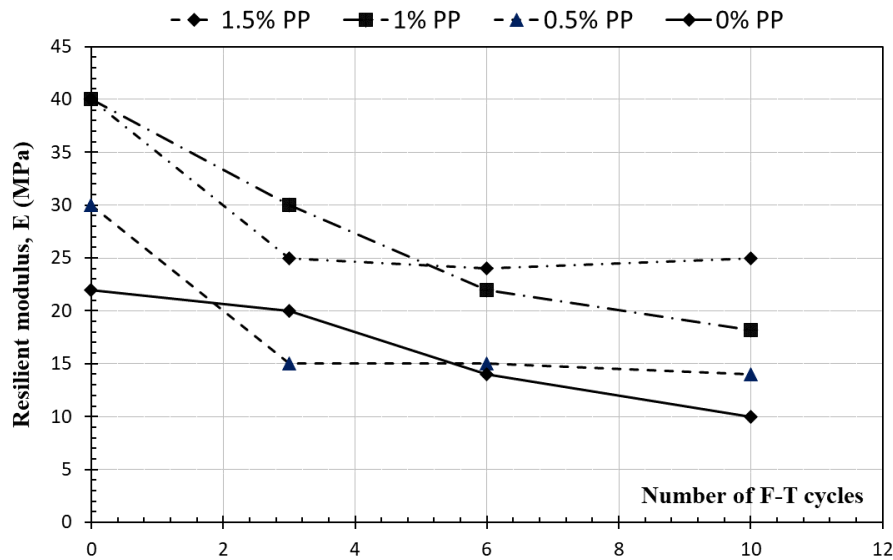
Figure 4.31. Resilient modulus values with fiber content (PP) under different cycles of (F–T)

Regarding the evaluation of the influence of (F–T) cycles on physical properties (volumetric resistance), and with reference to Table 4.9, it can be noticed a clear increase in the sample's dimensions (volume) by the increase of (F–T) cycles for both reinforced and unreinforced cases. However, the reinforced samples experienced minimum volumetric changes in comparison with the unreinforced situation, and that can be attributed to the role of the fiber in creating coupling forces (bounding forces) that connect the soil particles and decrease the volumetric changes in the reinforced ones. However, the height (volume) variation throughout the (F–T) cycles can be explained according to each stage, where during the thawing stage, the ice crystals that were formed during the freezing stage, start to melt and the resulting water moves deeper into the sample due to gravity. This phenomenon contributes to an increase in the sample height (Andersland and Ladanyi, 2004; Wang et al. 2007; Ghazavi and Roustaie, 2013). As shown in Figure 4.32, the changes in the samples' height affect the unit weight. Thus, the unit weight of the sample decreases even in the presence of polypropylene fibers. However, polypropylene fibers have contributed effectively in resisting more changes in the unit weight in comparison with the unreinforced situation. After ten (F–T) cycles, the unit weight of the unreinforced sample decreases by about 0.9% more than PP-reinforced samples. These findings are in true agreement with the findings of Wang et al. (2018).
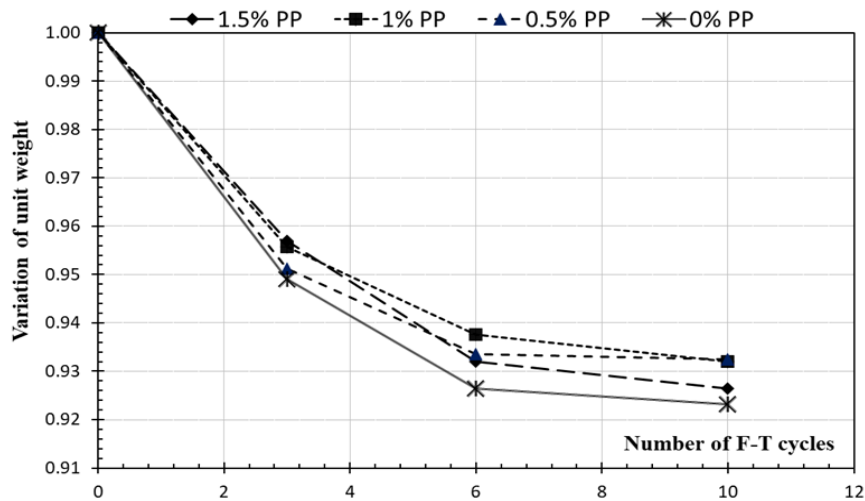
Fig. 4.32. Unit weight variation with fiber content and under different cycles of (F–T).

4.6 Evaluating The Feasibility Of PP Utilization as Reinforcement Material under Shallow Foundations

In this part, geometric modeling for twelve models that represented the fiber-reinforced soil for three fiber contents (0.5%, 1%, 1.5%) and for four depths/layer thicknesses of reinforced layer (b/4, b/2, 3b/4, b) were considered. Additionally, one model for unreinforced soil was considered to be compared with other models. The results of the modeling analysis are illustrated in Figure 4.33, where deformation shape and value, stress distribution, and related settlements are presented.
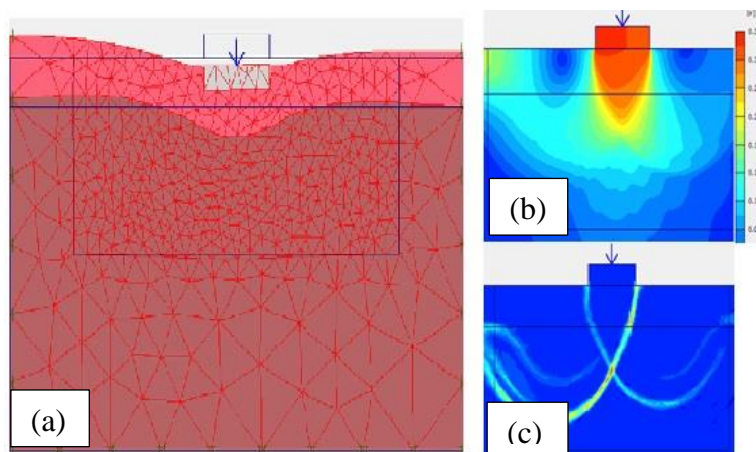
Figure 4.33. Geometrical modeling analysis results forms: (a) deformation shape; (b) settlements distribution; (c) Stress distribution.

For evaluating the influence of PP fiber inclusion on bearing capacity, curves of ultimate bearing capacity (q_{ult}) and relevant displacements/deformations (u) are generated for each fiber content and for different layer thicknesses (i.e., fiber-reinforced layer thickness). Figures 4.34 to 4.37 show (q_{ult} – u) curves for four depths of fiber-reinforced soil (D= b/4, b/2, 3b/4, b) with respect to fiber inclusion for each depth (thickness).
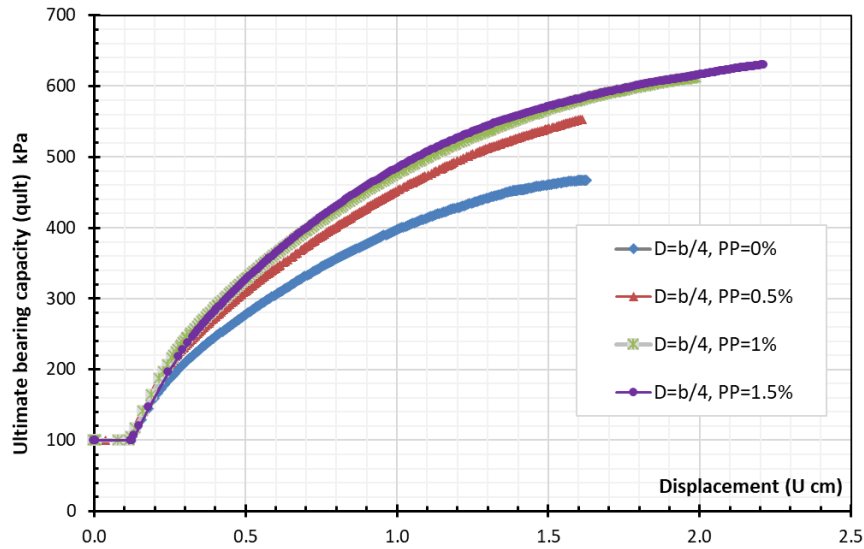
Figure 4.34. Ultimate bearing capacity (q_{ult}) and relevant displacements for (b/4) of fiber-reinforced layer thickness
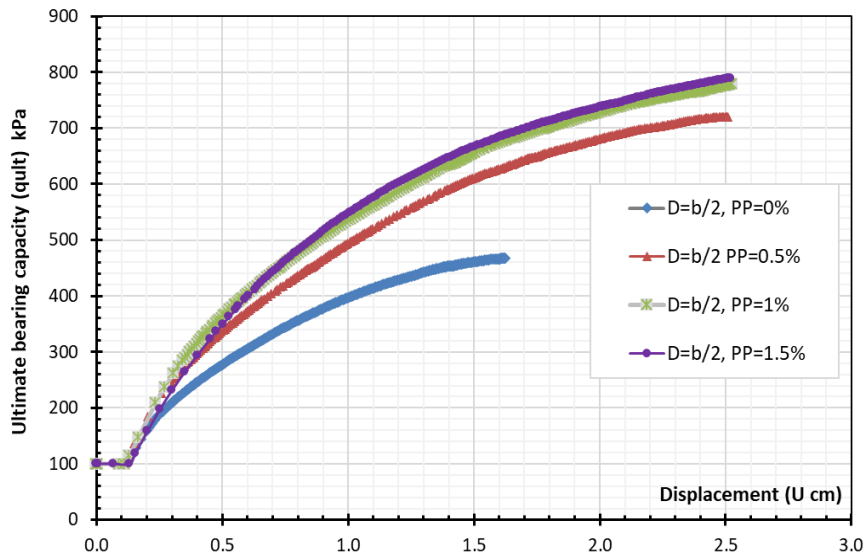
Figure 4.35. Ultimate bearing capacity (q_{ult}) and relevant displacements for (b/2) of fiber-reinforced layer thickness
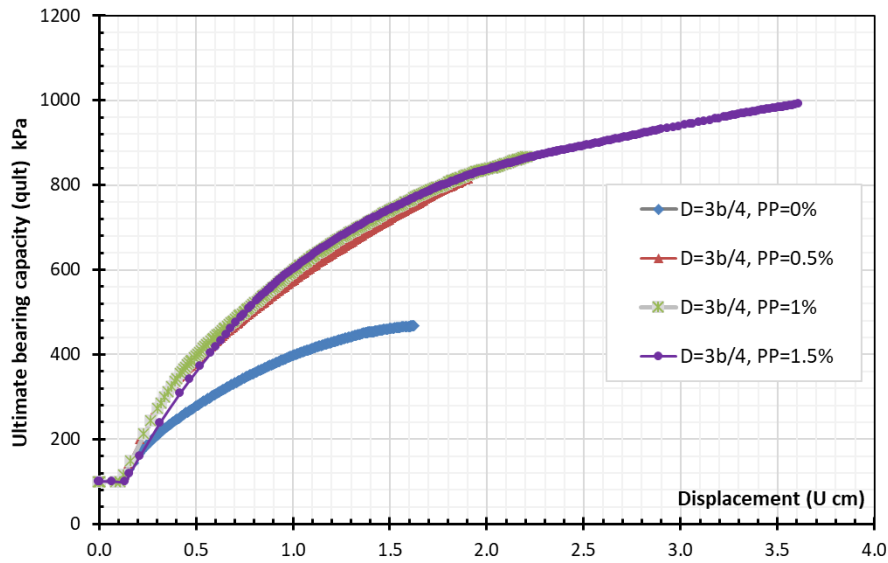
Figure 4.36. Ultimate bearing capacity (q_{ult}) and relevant displacements for (3b/4) of fiber-reinforced layer thickness
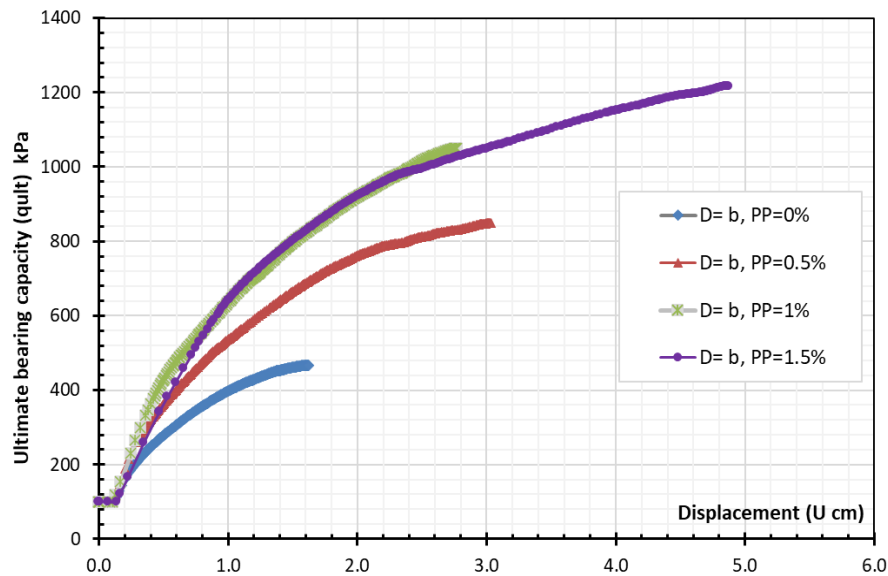
Figure 4.37. Ultimate bearing capacity (q_{ult}) and relevant displacements for (b) of fiber-reinforced layer thickness

Referring to Figs 4.34 to 4.37, it can be easily noticed that regardless of the thickness of the reinforced layer, the ultimate bearing capacity is increased with the increase of fiber inclusion, and this is compatible with previous studies such as (Maheshwari et al. 2011; Mirzababaei, 2017; Alemyparvin, 2020). Table 4.9 shows the ratio of improvement in the

bearing capacity for each fiber content at the layer level, and Figure 4.38 represents the ultimate bearing capacity for each case, It can be inferred that for layer thicknesses less than (b), it is better to reinforce with 1% of fiber content as this content meet the most efficient improvement rate in ultimate bearing capacity.

Table 4.9. Ultimate bearing capacity improvement ratio

Fiber-Soil layer thickness	Improvement Ratio		
	PP=0.5%	PP=1%	PP=1.5%
b/4	1.23	1.37	1.39
b/2	1.53	1.70	1.76
3b/4	1.72	2.02	2.12
b	1.80	2.22	2.58
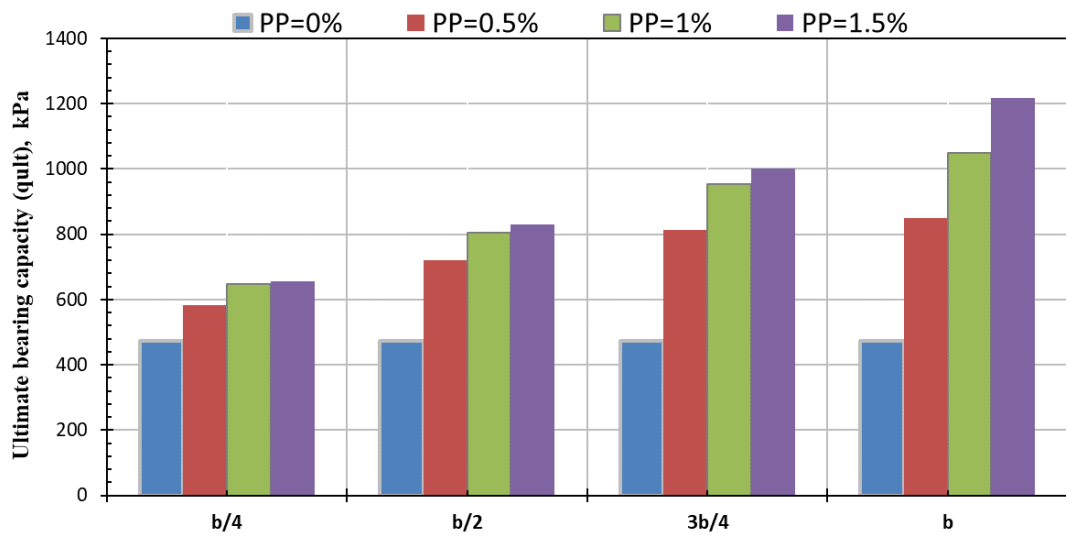
Figure 4.38. Ultimate bearing capacity (q_{ult}) with respect to fiber-reinforced layer thickness and fiber inclusion

5. CHAPTER V: CONCLUSION AND RECOMMENDATIONS

5.1 General Overview

This research presented a comprehensive review and detailed study of soil stabilization techniques, related methods, materials utilization, and field applications that concern stabilizing problematic soils. Both chemical and mechanical stabilization methods were presented and the most recent research results were discussed by highlighting the strength, and weak points for each and flagging the gaps that still needed to be fulfilled. Additionally, extra attention was paid to environmental consideration to maintain the achieved improved properties regardless of the techniques or materials used in soil stabilization, with a full comparative study theoretically and experimentally to evaluate the most appropriate stabilization technique that maintains a sustainable geotechnical solution.

Moreover, with reference to extensive previous studies that were proposing utilizing chemical additives or compositions of chemicals without taking into account the environmental impact of these materials, this research highlighted the devastating effects on the environment resulting from the utilization of chemical additives in soil stabilization and proposed a low-cost, eco-friendly reinforcing material, rapid to perform and easy to work, and the feasibility of its utilization in all weather conditions, and proved through a full set of experiments its efficiency under different applied loads of vertical, horizontal, and triaxial loads and subjected to temperature differences to simulate the environment changes effect in both hot and cold areas.

Also, the feasibility of utilizing PP as reinforcing material under the foundation/footings was inspected by 2D finite element analyses and the influence of fiber inclusion on the bearing capacity was investigated to study all possible applications of this material in practice. This study's key findings are as follows:

This study demonstrates the influence of polypropylene fiber (PP) on the physical, strength, swell, and compressibility properties of high plasticity clay. The results demonstrate that both maximum dry density and liquid limit have been decreased with the increase of fiber content while in contrast, both plastic and shrinkage limits have been increased and these changes have not resulted in a change in soil classification in terms of the investigated fiber content. However, a potential soil classification change could be observed for fiber content higher than 1.5%.

Regarding to its influence on the strength and swelling properties, the findings indicate a significant improvement in both strength and swelling behavior and provide fiber content-based functions to predict all strength and swelling properties. The results show obvious improvement in the shear strength (an average increase of 184% at 1.5% fibers) and shear parameters (cohesion (an increase of 257% at 1.5% fibers) and friction angle (an increase of 62% at 1.5% fibers)) of the reinforced soil, with a possibility of decreasing the friction angle for a fiber content greater than 1.5%. The same behavior was observed in the unconfined compressive strength results (an increase of 86% at 1.5% fibers) after considering the elasticity modulus, which is decreased for a fiber content greater than 0.5%. A like, the unconsolidated undrained (UU) triaxial strength increased with the increase of PP under the specific confined pressure of 200 kPa (an average increase of 112% at 1.5% fibers). The resilient modulus is also increased with the increase of fiber content (an average increase of 80% at 1.5% fibers).

Regarding swell tests, it shows a decrease in swelling stress (a decrease of 46% at 1.5% fibers) and swelling potential (a decrease of 24% at 1.5% fibers) with the increase of fiber content, considering that 1% of fiber content is the optimum fiber content for improving the swelling behavior with respect to the properties of the studied soil. Therefore, it can be inferred that there is a great potential for the utilization of PP to reinforce clayey soils of high plasticity in several areas of geotechnical engineering after applying proper mixing techniques to ensure the homogeneity of the soil-fiber matrix in the field. The fiber contents of 0.5% to 1% are deemed appropriate for the soil in this study to have minimal swell and improve the shear strength and unconfined compressive strength effectively.

Regarding consolidation test results, it shows a decrease in the consolidation settlements for fiber contents up to 1% (a decrease of 15% at 1 % fibers), also the elasticity modulus increases with the increase of fiber content up to 1% (an increase of 22% at 1 % fibers). For fiber content bigger than 1%, it is worth mentioning that the settlements increased in comparison with the unreinforced situation and the same for elasticity modulus that decreased with the increase to 1.5% of fiber. Therefore, 1% of fiber content is the optimum fiber content for improving the compressibility behavior to have a low amount of consolidation settlements.

For environmental effect consideration, the influence of polypropylene fiber, lime, and cement on resisting desiccation cracks and volume changes resulting from drying, and the drying/wetting process was demonstrated, where it was found that cracks' resistance increases with the increase of fiber inclusion. Furthermore, the efficiency of polypropylene fiber utilization to reduce the volume changes was investigated, and different behaviors were observed between the unreinforced samples and reinforced ones. As such, the results highlighted the contraction behavior for fiber-stabilized soil, while it was swelling behavior for both lime/cement stabilized soil and un-stabilized soil. Therefore, the optimum fiber content was identified as 0.38% for improving the resistance of volumetric changes. Besides, the most appropriate ground improvement techniques were assessed by utilizing conventional materials (Lime of 6% and cement of 5%) and comparing their environmental changes' resistance with the fiber-stabilized soil. Thus, it was observed high efficiency of fiber influence in comparison with lime and cement stabilization techniques, and fiber contents between 1% to 1.5% were considered the most effective and suitable contents, after applying proper mixing techniques to ensure the homogeneity of the soil-fiber matrix in the field.

For sustainability and durability aspects, the efficiency of polypropylene fiber utilization to reduce the volume changes, resist the strength reduction, and frost-heave and thawing settlements resulting from freezing-thawing cycles are investigated by using UU triaxial testing. The results highlight strength reduction with the increase of (F–T) cycles and this reduction is decreased with the increase of fiber content, and greatest strength reduction was 51% for unreinforced samples while it was 18% after adding 1% of polypropylene

fibers which is considered as the optimum content for resisting (F–T) cycles. Also, the resilient modulus is decreased with the increase of (F–T) cycles where the reinforced samples exhibited a minimum reduction rate and this rate was decreased with the increase of fiber content. Besides, the durability criteria is investigated by studying the effect of (F–T) cycles on the volume changes resistance where it was observed that volume changes (unit weight variations) are increased with the increase of (F–T) cycles and the volumetric changes' resistance is increased with the increase of fiber content. Therefore, the optimum fiber content is identified as 1% for improving the resistance of volumetric changes resulting from (F–T) cycles.

Ultimately, this study investigated the effect of PP fiber-reinforced clayey soil in a soil-foundation system by utilizing the finite element numerical method through Plaxis 2D software. For this purpose, a set of models have been conducted. Based on the results of numerical modeling, it has been determined that the use of PP fiber is very efficient for the improvement and stabilization of clayey soils where the bearing capacity increases with the increase of fiber inclusion, and 1% of fiber can be considered as optimum content to achieve efficient improvement rate.

5.2 Recommendations for Future Studies

In order to generalize the finding of this research, it is better to extend the current studies to consider different soil properties and types to not be limited to clayey soils with CH classification. Expanding to all clayey and silty soils and considering different soil properties with different densities (from loose to denser soils), can contribute to a better understanding of the fiber-soil behavior, specifically mechanical behavior, where it can end up to a full set of functions based on fiber content to predict all the strength, swell, compressible properties as it was proposed in the current study for the studied soil type only. Also, it is recommended to do additional environmental investigations to compare the impacts of further chemicals or additives with the PP impact as this study was limited to the most conventional chemicals used (lime and cement) only. So thus, further comparisons can contribute to better additives selection and more effective and sustainable solutions in soil stabilization fields.

REFERENCES

Abass I. K. (2013). Lime stabilization of expansive soil. *Journal of Engineering and Development*, 17(1): 219–232. ISSN 1813-7822. http://jeasd.org/images/2013edition/issue_1/18.Lime.

Abdullah A. Sharo, Ahmed S. Alawneh, Hadeel N. Al zghool, and Samer R. Rabab'ah (2022). Effect of Alkali-Resistant Glass Fibers and Cement on the Geotechnical Properties of Highly Expansive Soil. *Journal of Materials in Civil Engineering*, 34 (2). DOI: https://ascelibrary.org/doi/abs/10.1061/%28ASCE%29MT.1943-5533.0004058.

Abu-Hejleh, A. N., and Znidarcic, D. (1995). Desiccation theory for soft cohesive soils. *Journal Geotech. Eng.*, 121(6), 493–502. https://doi.org/10.1061/(ASCE)0733-9410(1995)121:6(493).

Abhishek. T. (2015). Quantification Of Cracks And Shrinkage Using Image Analysis. Department of Civil Engineering National Institute of Technology, Rourkela Odisha, 69008, India.

Ahmad Abdelmawla (2017). Characterization of uniaxial geogrid pullout mechanism for calcareous sand backfill. Researchgate: https://www.researchgate.net/publication/318494867.

Ahmed Abdelraheem Farghaly, A. El-Shater, Mostafa Abdou Abdel Naiem and Fatma Hamdy (2020). Lime addition chemical stabilization of expansive soil at Al- Kawamil city, Sohag region, Egypt. *Advances in Computational Design*, Volume 5, Number 1, pages: 1-11. DOI: https://doi.org/10.12989/acd.2020.5.1.001.

Ahmed M. Al-Mahbashi, Tamer Y. Elkady, Talal O. Alrefeai (2015). Soil water characteristic curve and improvement in lime treated expansive soil. *Geomechanics and Engineering*, 8 (5), pp. 687-696. DOI: https://doi.org/10.12989/gae.2015.8.5.687.

Aiban SA, Al-Ahmad HM, Asi AM, Siddique ZU, Al-Amoudi OSB (2006). Effect of geotextile and cement on the performance of sabkha subgrade. *Building and environment*, 41(6): 807-820. https://doi.org/10.1016/j.buildenv.2005.03.006.

Akbulut, S., Arasan, S. and Kalkan, E. (2007). Modification of clayey soils using scrap tire rubber and synthetic fibers. *Applied Clay Science*, Vol. 38 (1–2), pp. 23–32. https://doi.org/10.1016/j.clay.2007.02.001.

A.K.Haghi (2009). Experimental Analysis Of Geotextiles & Geofibers Composites. *WSEAS Press*, pp: 1-15. https://www.researchgate.net/publication/331000786.

Albrecht, B.A. and C.H. Benson (2001). Effect of desiccation on compacted natural clays. *Journal of Geotechnical and Geoenvironmental Engineering*, 127(1): 67-75.

Asgari, M. R., Baghebanzadeh Dezfuli, A., & Bayat, M. (2013). Experimental study on

stabilization of a low plasticity clayey soil with cement/lime. *Arabian Journal of Geosciences*, vol. 8: 1439–1452. Doi:10.1007/s12517-013-1173-1.

Anagnostopoulos, C.A., Dimitrios, T. and Berketis, K. (2014). Evaluation of the shear strength behaviour of polypropylene and carbon fiber reinforced cohesive soils. *Research Journal of Applied Sciences Engineering and Technology,* 7 (20), pp. 4327–42. https://doi.org/10.19026/rjaset.7.805.

Andersland O. B. and Ladanyi B. (2004). Frozen Ground Engineering. *American Society of Civil Engineers (ASCE Press),* 2nd ed., Reston, VA, and John Wiley & Sons New York.

Aparna R. (2014). Soil Stabilization using rice husk ash and cement. *International Journal of Civil Engineering Research*, ISSN 2278-3652, 5(1): 49-54.

ASTM D698 (2012). Standard Test Methods for Laboratory Compaction Characteristics of Soil. ASTM International, West Conshohocken, Pennsylvania, USA. DOI: 10.1520/D0698-12E02.

ASTM D4318. (2017). Standard Test Methods for Liquid Limit, Plastic Limit, and Plasticity Index of Soils. ASTM International, West Conshohocken, Pennsylvania, USA, DOI: 10.1520/D4318-17E01.

ASTM D2487-17. (2018). Standard Practice for Classification of Soils for Engineering Purposes (Unified Soil Classification System). ASTM International, West Conshohocken, PA 19428-2959, United States. DOI: 10.1520/D2487-17

ASTM D3080-04 (2004). Standard Test Method for Direct Shear Test of Soils Under Consolidated Drained Conditions. ASTM International, West Conshohocken, PA. DOI: 10.1520/D3080-04.

ASTM D2166/D2166M-16 (2016). Standard Test Method for Unconfined Compressive Strength of Cohesive Soil. ASTM International, West Conshohocken, PA. DOI: 10.1520/D2166_D2166M-16.

ASTM D2850– 03a (2007). Standard Test Method for Unconsolidated-Undrained Triaxial Compression Test on Cohesive Soils. ASTM International: West Conshohocken, PA, USA.

ASTM D4546-21 (2021). Standard Test Methods for One-Dimensional Swell or Collapse of Soils. ASTM International, West Conshohocken, PA. DOI: 10.1520/D4546-21.

ASTM D2435_D2435M (2020). Standard Test Methods for One-Dimensional Consolidation Properties of Soils Using Incremental Loading. ASTM International, West Conshohocken, PA. DOI: 10.1520/D2435_D2435M-11

Aykut SENOL, S. Banu IKIZLER, Ehsan ETMINAN, Gokhan DEMIR. (2014). Improvement of Low Plasticity Clayey Soils Using Polypropylene Fibers. In *proceedings of the Geo-*

Hubei International Conference on Sustainable Civil Infrastructure, China. https://doi.org/10.1061/9780784478547.001

Bachmann, J. & Van, D. P. R. R. (2015). A review on recent developments in soil water retention theory: Interfacial tension and temperature effects. *J. Plant Nutr. Soil Sci*., 165(4), 468–478. https:// doi. org/ 10. 1002/ 1522- 2624(200208) 165:4% 3c468:: AID-JPLN4 68% 3e3.0.CO;2-G.

Baker R. (1981). Tensile strength, tension cracks, and stability of slopes. Japanese Society of Soil Mechanics and Foundation Engineering, *Soils and Foundations*, 21(2): 1–17. Doi:10.3208/sandf1972.21.2_1.

Behzad Isazadeh-Khiav, Tohid Akhlaghi, Masoud Hajialilue-Bonab (2022). Studying the Failure Behavior of Cement-fiber-treated Sand under Triaxial Direct Tension Tests. *Periodica Polytechnica Civil Engineering*, 66(2), pp. 384–397. https://doi.org/10.3311/PPci.18469

Benson, C.H. and D.E. Daniel, (1994). Minimum Thickness of Compacted Soil Liners: II. Analysis and Case Histories. *Journal of Geotechnical Engineering*, 120(1): 153-172.

Bozbey, I., & Garaisayev, S. (2010). Effects of soil pulverization quality on lime stabilization of an expansive clay. *Environmental Earth Sciences*, 60: 1137–1151. DOI:10.1007/s12665-009-0256-5

Brown, R., Shukla, A. and Natarajan K.R. (2002). Fiber Reinforcement Of Concrete Structures, Kingston, RI: University of Rhode Island Trans Center, Kingston, RI, USA.

Cai, Y., Shi, B., Ng, C.W.W. and Tang, C. (2006). Effect of polypropylene fiber and lime admixture on engineering properties of clayey soil. *Engineering Geology,* 87 (3–4), pp. 230–40. https://doi.org/10.1016/j.enggeo.2006.07.007.

Caravaca F., Lozano Z., Rodríguez-Caballero G., Rold A. (2017). Spatial shifts in soil microbial activity and degradation of pasture cover caused by prolonged exposure to cement dust. *Land Degrad. Dev.,* 28 (4), pages:1329-1335. https://doi.org/10.1002/ldr.2564.

Cao, L.; Zhang, D.; Fang, Q.; Yu, L. (2020). Movements of ground and existing structures induced by slurry pressure-balance tunnel boring machine (SPB TBM) tunnelling in clay. *Tunn. Undergr. Space Technol.*, 97, 103278. https://doi.org/10.1016/j.tust.2019.103278.

Chao-Sheng Tang, Bin Shi, Chun Liu, Lei Gao, Hilary I. Inyang (2011). Experimental Investigation of the Desiccation Cracking Behavior of Soil Layers during Drying. *Journal of materials in civil engineering (ASCE)*, Pages: 873-878. DOI: 10.1061/(ASCE) MT.1943-5533.0000242

Chuang Lin, S.M.ASCE; and Xiong Zhang (2018). Laboratory Drainage Performance of a New Geotextile with Wicking Fabric. *Journal of Materials in Civil Engineering (ASCE)*, 30 (11), pp:1-15. https://doi.org/10.1061/(ASCE)MT.1943-5533.0002476

Corte, A., and Higashi, A. (1960). Experimental research on desiccation cracks in soil. *Research Rep*. 66: U.S. Army Snow Ice and Permafrost Research Establishment, Wilmette, IL.

Daniel, D.E. and Y.-K. Wu, (1993). Compacted Clay Liners and Covers for Arid Sites. *Journal of Geotechnical Engineering*, 119(2): 223-237.

Dasog, G.S., and Mermut, A.R. (2013). Expansive Soils and Clays, In: Bobrowsky P.T. (eds) Encyclopedia of Natural Hazards. Springer: Dordrecht, Netherlands. https://doi.org/10.1007/978-1-4020-4399-4_124.

Degirmenci N, Okucu A, Turabib A. (2007). Application of phosphogypsum in soil stabilization. *Building and environment*, 42:3393–3398. DOI: 10.1016/j.buildenv.2006.08.010.

El-Attar M.M., Sadek D.M., Salah A.M. (2017). Recycling of high volumes of cement kiln dust in bricks industry. *J. Clean. Prod.,* Volume143, pages: 506-515. https://doi.org/10.1016/j.jclepro.2016.12.082.

El-Soud S.A., Belal A.M., (2018). Bearing capacity of rigid shallow footing on geogrid-reinforced fine sand experimental modeling. *Arabian Journal of Geosciences*, 11: 247.

Ghazavi M. and Roustaei M. (2013). Freeze-thaw performance of clayey soil reinforced with geotextile layer. *Cold Regions Science and Technology*, Vol. 89, pp. 22-29. https://doi.org/10.1016/j.coldregions.2013.01.002.

Ghobadi, M. H., Abdilor, Y., & Babazadeh, R. (2013). Stabilization of clay soils using lime and effect of pH variations on shear strength parameters. *Bulletin of Engineering Geology and the Environment*, 73(2): 611–619. DOI 10.1007/s10064-013-0563-7

Guney Y, Sari D, Cetin M, Tuncan M. (2007). Impact of cyclic wetting - drying on swelling behavior of lime-stabilized soil. *Building and environment*, 42(2): 681–688. https://doi.org/10.1016/j.buildenv.2005.10.035

Hao Wu, Chongkai Yao , Chenghan Li, Miao Miao, Yujian Zhong, Yuquan Lu and Tong Liu (2020). Review of Application and Innovation of Geotextiles in Geotechnical Engineering. *Materials*, 13, 1774, pp: 1-21. doi:10.3390/ma13071774

Harichane K., Ghrici M., Missoum H. (2011). Influence of natural pozzolana and lime additives on the temporal variation of soil compaction and shear strength. *Frontiers of Earth Science*, 5: 162–169. DOI: 10.1007/s11707-011-0166-1.

Hejazi, S.M., Sheikhzadeh, M., Abtahi, S.M. and Zadhoush, A. (2012). A simple review of soil reinforcement by using natural and synthetic fibers. *Constr. Build. Material*, Vol. 30, pp.100-116.

Hohmann-Porebska M. (2002). Microfabric effects in frozen clays in relation to geotechnical parameters. *Applied Clay Science*, 21 (1–2), pages: 77–87.

Howard L. Needles (1980). Textile Fibers, Dyes, Finishes, And Processes. University of California, Published by Noyes Publications, USA, ISBN 0-8155-1076-4, pp: 1-175

Hoy, M., Rachan, R., Horpibulsuk, S. Arulrajah, A. and Mirzababaei, M. (2017). Effect of wetting–drying cycles on compressive strength and microstructure of recycled asphalt pavement – fly ash geopolymer. *Construction and Building Materials,* Vol. 144, pp. 624–34. https://doi.org/10.1016/j.conbuildmat.2017.03.243.

Huffman, John E. (1995). Base/Subgrade Stabilization. Salina, KS: The Asphalt Institute, Kansas State University at Salina.

Ikhlef NS, Ghembaza MS, Dadouch M. (2015). Effect of treatment with cement on the mechanical characteristics of silt from Telagh region of Sidi Belabes Algeria. *Geotech Geol Eng*, 33(4), pages 1067–1079. DOI:10.1007/s10706-015-9888-2

Imran Khan and Rashid Umar (2018). Environmental risk assessment of coal fly ash on soil and groundwater quality. *Groundwater for Sustainable Development*, Volume 8, pp. 346-357. DOI: https://doi.org/10.1016/j.gsd.2018.12.002

Indiana devlopment of transportation (INDOT) (2020). Design Procedures for Soil Modification or Stabilization. Division of Engineering and Asset Management Division of Geotechnical Services,120 South Shortridge Road Indianapolis, pp. 1-18.

Jianwei Yue, Xuanjia Huang, Limin Zhao, and Zifa Wang. (2022). Study on the factors affecting cracking of earthen soil under dry shrinkage and freeze–thaw conditions. Sci Rep 12, 1816. https://doi.org/10.1038/s41598-022-05946-w.

Jones, D.E. and K.A. Jones (1987). Treating expansive soils. Civil Engineering, 57(8): 62-65.

Kalkan E. (2006). Utilization of red mud as a stabilization material for the preparation of clay liners. *Eng Geo*, 87(3–4), pages 220–229. https://doi.org/10.1016/j.enggeo.2006.07.002

Kalpana Maheshwari, A. K. Desai, C. H. Solanki (2011). Application And Modeling Of Fiber Reinforced Soil. *Proceedings of Indian Geotechnical Conference*, Kochi (Paper No H - 362).

Kiliç Recep, Özgür Küçükali, and Koray Ulamiş (2016). Stabilization of high plasticity clay with lime and gypsum. *Bulletin of Engineering Geology and the Environment*, 75(2), pages 735-744.

Kleppe, J.H. and R.E. Olson (1985). Desiccation Cracking of Soil Barriers. ASTM SPT 874, A. I. Johnson

Kolay P.K., Kumar S., Tiwari D., (2013). Improvement of bearing capacity of shallow foundation on geogrid reinforced silty clay and sand. *Journal of Construction Engineering*, 293809: 1-10.

Konrad, J. M., and Ayad, R. (1997). An idealized framework for the analysis of cohesive soils

undergoing desiccation. *Can. Geotech. J.,* 34, 477–488.

Kua, T.A., Arulrajah, A., Mohammadinia, A., Horpibulsuk, S., Mirzababaei, M. (2017). Stiffness and deformation properties of spent coffee grounds based geopolymers. *J. Constr. Build. Mater.*, Vol. 138, pp. 79-87. doi:10.1016/j.conbuildmat.2017.01.082

Kumar, A., Walia, B.S. and Bajaj, A. (2007). Influence of fly ash, lime, and polyester fibers on compaction and strength properties of expansive soil. *Journal of Materials in Civil Engineering*, 19 (3), pp. 242–48. https://doi.org/10.1061/(asce)0899-1561(2007)19:3(242).

Leng, T. et al. (2018). Advance on the engineering geological characteristics of expansive soil. *J. Eng. Geol.,* 26(1), 112–128. https:// doi. org/10. 13544/j. cnki. jeg. 2018. 01. 013.

Liu, T.; Zhong, Y.; Feng, Z.; Xu,W.; Song, F. (2020). New Construction Technology of a Shallow Tunnel in Boulder-Cobble Mixed Grounds. *Advances in Civil Engineering*, vol. 2020, Article ID 5686042, pages: 1-20. https://doi.org/10.1155/2020/5686042.

Maheshwari, K., Solanki, C.H., and Desai, A.K. (2013). Effect of polyester fibers on strength properties of clayey soil of high plasticity. *International Journal of Scientific and Engineering Research*, 4 (6), pp. 486-490.

Mali, S. and Singh, B. (2014). Strength behaviour of cohesive soils reinforced with fibers. *International Journal of Civil Engineering Research*, 5 (4), pp. 353–360. https://doi.org/ISSN 2278-3652.

Miller C. J., Mi H., and Yesiller N. (1998). Experimental analysis of desiccation crack propagation in clay liners. J. Am. Water Resour.Assoc. (JAWRA), 34(3), pages 677–686. https://doi.org/10.1111/j.1752-1688.1998.tb00964.x

Mirzababaei, M., Arulrajah, A., Haque, A., Nimbalkar, S. and Mohajerani, A. (2018). Effect of fiber reinforcement on shear strength and void ratio of soft clay. *Geosynthetics International,* 25 (4), pp. 471–80. https://doi.org/10.1680/jgein.18.00023.

Mirzababaei M., Mohamed M., Miraftab M. (2017). Analysis of strip footings on fiber-reinforced slopes with the aid of particle image velocimetry. *Journal of Materials in Civil Engineering*, 29(4). https://doi.org/10.1061/(asce)mt.1943-5533.0001758.

Mohammed A. M. Al-Bared, Indra S. H. Harahap, Aminaton Marto, Seyed Vahid Abad, Zahiraniza Mustaffa, Montasir O. A. Al (2019). Mechanical behaviour of waste powdered tiles and Portland cement treated soft clay. *Geomechanics and Engineering*, 19 (1), pp. 37-47. DOI: https://doi.org/10.12989/gae.2019.19.1.037

Mona Malekzadeh, Huriye Bilsel (2012). Effect of Polypropylene Fiber on Mechanical Behaviour of Expansive soils. *EJGE*, Vol. 17, Bund. A, pp. 55-63.

Morris, P. H., Graham, J., and Williams, D. J. (1992). Cracking in drying soils. *Can. Geotech. J.,* 29, 263–277. https://cdnsciencepub.com/doi/10.1139/t92-030

Morteza Alemyparvin (2020). Finite element numerical modeling of geogrid-reinforced shallow foundation's behavior on loose soils. *Journal of Geotechnical Geology,* 16(1), pp: 339–345. https://doi.org/10.30495/GEOTECH.2020.679340

Mosallanezhad M., Alfaro M.C., Hataf N., Taghavi S.H. (2016). Performance of the new reinforcement system in the increase of shear strength of typical geogrid interface with soil. *Geotextiles and Geomembranes*, 44(3): 457-462.

Nelson, J.D. and Miller, D.J. (1992). Expansive Soils: Problems and Practice in Foundation and Pavement Engineering. John Wiley & Sons Inc., New York, NY, USA.

Nguyen T. T. H. (2015). Stabilisation des sols traités à la chaux et leur comportement au gel [Stabilization of soils treated with lime and their freezing behaviour]. Ph.D thesis; Université Paris Est, Paris, France.

Office of Geotechnical Engineering (2008). Design Procedures for Soil Modification or Stabilization. Indianapolis. http://messerconstruction.com/smod.pdf

Omidi, G. (1993). Desiccation shrinkage and cracking in soil liner. Civil Engineering. Texas A&M University.

Osinubi, K.J. and A.O. Eberemu (2010). Desiccation Induced Shrinkage of Compacted Lateritic Soil Treated with Blast Furnace Slag. *Geotechnical and Geological Engineering*, 28(5): 537-547.

Pakbaz MS, Alipour R. (2012). Influence of cement addition on the geotechnical properties of an Iranian clay. *Applied Clay Science,* 1(4), pp: 67–68:. https://doi.org/10.1016/j.clay.2012.07.006

Panchal, J.P., McNamara, A.M. and Stallebrass, S.E. (2018). Physical modelling of lime stabilisation in soft soils around deep excavations. *Journal of the Deep Foundations Institute (DFI)*, pp. 1-11.

Péron, H., Herchel, T., Laloui, L., and Hu, L. B. (2009). Fundamentals of desiccation cracking of fine-grained soils: Experimental characterization and mechanisms identification. *Can. Geotech. J.,* 46, 1177–1201. https://cdnsciencepub.com/doi/10.1139/T09-054

Portelinha FHM, Lima DC, Fontes MPF, Carvalho CAB. (2012). Modification of a lateritic soil with lime and cement: an economical alternative for flexible pavement layers. *Soils and Rocks*, Brazil Sa˜o Paulo V.35, N.1, pp: 51–63.

Puljan, V. (2010). Experimental Studies on Shrinkage Induced Pressure Measurements of Four Expansive Soils. University of Texsas.

Rabindra Kumar Kar, Pradip Kumar Pradhan and Ashutosh Naik (2012). Consolidation Characteristics of Fiber Reinforced Cohesive Soil. *EGJE,* Vol. 17, pp. 3861-3874.

Raddi M. AlZubaidi, Kawkab H. AlRawi, Ahmed J. AlFalahi (2013). Using cement dust to reduce swelling of expansive soil. *Geomechanics and Engineering*, Volume 5, Number 6, pp. 565-574. DOI: https://doi.org/10.12989/gae.2013.5.6.565.

Rios, S., Cristelo, N., Viana da Fonseca, A. and Ferreira, C. (2015). Structural performance of alkali-activated soil ash versus soil cement. *Journal of Materials in Civil Engineering*, 28 (2).

Rios, S., Cristelo, N., Viana, A. and Ferreira, C. (2016). Stiffness behavior of soil stabilized with alkali-activated fly ash from small to large strains. *International Journal of Geomechanics*, 17 (3).

Robert D. Holtz (2001). Geosynthetics For Soil Reinforcement. College Station Hilton, University of Washington Seattle, Washington 98195-2700 USA, pp: 1-20.

Rodríguez, R., Sánchez, M., Ledesma, A., and Lloret, A. (2007). Experimental and numerical analysis of desiccation of a mining waste. *Can.Geotech. J.,* 44, 644–658. https://cdnsciencepub.com/doi/10.1139/t07-016.

Rogers C.D., Thomas A.M., Jefferson I., Gaterell M. (2009). Carbon dioxide emissions due to highway subgrade improvements. *Transport. Res. Rec.,* vol 2104 (1), pages: 80-87. https://doi.org/10.3141/2104-09.

Sabat, A.K. (2012). Effect of polypropylene fiber on engineering properties of rice husk ash - lime stabilized expansive soil. *Electronic Journal of Geotechnical Engineering*, Vol. 17, pp. 651–660.

Segetin M, Jayaraman K, Xu X. (2007). Harakeke reinforcement of soil–cement building materials: manufacturability and properties. *Building and environment*, Volume 42, issue 8, pp:3066–3079. https://doi.org/10.1016/j.buildenv.2006.07.033

Seyhan Firat, Jamal M Khatib, Gulgun Yilmaz, and AT Comert (2017). Effect of curing time on selected properties of soil stabilized with fly ash, marble dust and waste sand for road sub-base materials. *Waste Management & Research Journal*, pp. 1-10. https://doi.org/10.1177/0734242X17705726.

Sharma, T. and Kaushik, R. (2019). Effect of Polypropylene Fiber on Properties of Bagasse Ash-Cement Stabilized Clay Soil. *International Journal of Emerging Technologies*, 10(2), pp: 255–266.

Shi, Z. F. et al. (2021). Mechanical properties and normalized stress-strain behaviour of Yellow River embankment silt under freezing thawing cycle. *J. Arid Land Resources Environ*, 35(09), 126–134. https:// doi. org/ 10. 13448/j. cnki. jalre. 2021. 251.

Shukla S. K. (2017). Engineering Behaviour of Fibre-Reinforced Soil. *In: Fundamentals of Fibre-Reinforced Soil Engineering*, Springer, Singapore, pp. 45–110. https://doi.org/10.1007/978-981-10-3063-5_3

Silvestri V., Sarkis G., Bekkouche N., Soulié M. (1992). Evapotranspiration, trees and damage to foundations in sensitive clays. In *Proc Canadian Geotechnical Conf.,* Vol. II, pp: 533–538.

Sitharam T.G., Sireesh S., (2006). Effects of geogrid on geocellreinforced foundation beds. *Geomechanics and Geoengineering*, 1(3): 207-216.

Sivakumar Babu, G.L., and Vasudevan, A.K. (2008). Strength and stiffness response of coir fiber-reinforced tropical soil. *Journal of Materials in Civil Engineering*, 20 (9), pp. 571–77. https://doi.org/10.1061/(asce)0899-1561(2008)20:9(571).

Sridharan, A., and Gurtug, Y. (2004). Swelling behaviour of compacted fine-grained soils. *Engineering* Geology, Vol. 72 (1–2), pp. 9–18. https://doi.org/10.1016/S0013-7952(03)00161-3.

Stoltz G., Cuisinier O., Masrouri F. (2012). Multi-scale analysis of the swelling and shrinkage of a lime-treated expansive clayey soil. *Applied Clay Science,* 61, pp: 44–51. DOI: 10.1016/j.clay.2012.04.001

Sunitsakul J, Sawatparnich A, Sawangsuriya A (2012). Prediction of unconfined compressive strength of soil–cement at 7 days. *Geotech Geo Eng*, 30(1), pages 263–268. DOI:10.1007/s10706-011-9460-7

Tang, C. S. et al. (2018). Characterizing drying-induced clayey soil desiccation cracking process using electrical resistivity method. *Appl.Clay Sci.,* 152(feb), 101–112. https:// doi. org/ 10. 1016/j. clay. 2017. 11. 001.

Temel Yetimoglu, Omer Salbas (2003). A study on shear strength of sands reinforced with randomly distributed discrete fibers. *Geotextiles and Geomembranes*, Volume 21, Issue 2, Pages 103-110. https://doi.org/10.1016/S0266-1144(03)00003-7.

Tran TD, Cui Y-J, Tang A-M, Audiguier M, Cojean R (2014). Effects of lime treatment on the microstructure and hydraulic conductivity of Héricourt clay. *J Rock Mech Geotech Eng*, 6(5), pages 399–404. https://doi.org/10.1016/j.jrmge.2014.07.001

Vaibhav Sharma & Arvind Kumar (2019). Numerical study of ring and circular foundations resting on fibre-reinforced soil. *International Journal of Geotechnical Engineering*, pp:1-15. https://doi.org/10.1080/19386362.2019.1603680

Vessely, M.J. and Wu, J.T.H. (2002). Feasibility of geosynthetic inclusion for reducing swelling of expansive soils. *Trans Res Rec J. of the Trans Res Board,* Vol. 1787, pp. 42–52. https://doi.org/10.3141/1787-05.

Viswanadham, B.V.S., Phanikumar, B.R. and Mukherjee, R.V. (2009). Swelling behaviour of a geofiber-reinforced expansive soil. *Geotextiles and Geomembranes,* 27 (1), pp. 73–76. https://doi.org/10.1016/j.geotexmem.2008.06.002.

Wang D., Abriak N., and Zentar R. (2013). Strength and deformation properties of Dunkirk

marine sediments solidified with cement, lime and fly ash", *Engineering Geology*, 166, pp: 90–99. https://doi.org/10.1016/j.enggeo.2013.09.007.

Wang D., Ma W., Niu Y. H., Chang X., and Wen Z. (2007). Effects of cyclic freezing and thawing on mechanical properties of Qinghai-Tibet clay. *Cold Regions Science and Technology*, Vol. 48, pp. 34-43, DOI: 10.1016/j.coldregions.2006.09.008.

Wang, L. L. et al. (2018). Nucleation and propagation mechanisms of soil desiccation cracks. *Eng. Geol.,* 238, 27–35. https:// doi. org/ 10.1016/j. enggeo.2018.03.004.

Weiss, T., Slavik, M. & Bruthans, J. (2018). Use of sodium fluorescein dye to visualize the vaporization plane within porous media. *J. Hydrol.,* 565, 331–340. https:// doi. org/ 10. 1016/j. jhydr ol. 2018. 08. 028.

Xue, K. et al. (2017). Relationship between matric potential, moisture migration and frost heave in freezing process of soil. *Trans. Chin.Soc. Agric. Eng.,* 33(10), 176–183. https:// doi. org/ 10. 11975/j. issn. 1002- 6819. 2017. 10. 023.

YANG Bo-han, WENG Xing-zhong, LIU Jun-zhong, KOU Ya-nan, JIANG Le, LI Hong-lei, YAN Xiang-cheng, (2017). Strength characteristics of modified polypropylene fiber and cement-reinforced loess. Journal of Central South University, 24 (2), pp. 560−568. DOI: 10.1007/s11771-017-3458-0.

Yao, D. T. C., Oliveira-Filho, W. L., Cai, X. C., and Znidarcic, D. (2002). Numerical solution for consolidation and desiccation of soft soils. *Int.J. Numer. Anal. Methods Geomech.*, 26(2), 139–161. https://doi.org/10.1002/nag.196

Yilmaz, Y. (2015). Compaction and strength characteristics of fly ash and fiber amended clayey soil. *Engineering Geology*, Vol. 188, pp. 168–77. https://doi.org/10.1016/j.enggeo.2015.01.018.

Yilmaz Y, and Ozaydin V. (2013). Compaction and shear strength characteristics of colemanite ore waste modified active belite cement stabilized high plasticity soils. *Engineering Geology*, 155, pages 45–53. https://doi.org/10.1016/j.enggeo.2013.01.003.

Zhang, Z., Wang, H., Provis, J.L. (2012). Quantitative study of the reactivity of fly ash in *geopolymerization* by ftir. *J. Sustain. Cem. Material*, Vol. 1, pp.154-166. Doi:10.1080/21650373.2012.752620.

Zhao, G. T. et al. (2021). Evolution of soil-water and shrinkage characteristics of an expansive clay during freeze-thaw and drying-wetting cycles. *Cold Reg. Sci. Technol*., 186(4), 103275. https:// doi. org/ 10. 1016/j. coldr egions. 2021. 103275.

APPENDIX

APPX 1: Physical tests' readings and calculations

1. Specific gravity test

Number of pycnometer	1	2	3
Empty weight of the pycnometer (gr)	159.57	163.22	163.32
Weight of the pycnometer with dry soil (gr)	262.44	261.25	213.32
Weight of the pycnometer with water (gr)	656.48	659.93	660.6
Weight of the pycnometer with dry soil and soil (gr)	720.9	721.62	692.35
Solid weight(gr)	102.87	98.03	50
Volume of the pycnometer (cm^3)	496.91	496.71	497.28
Volume/weight of the water (cm^3)	458.46	460.37	479.03
Solid volume of soil (cm^3)	38.45	36.34	18.25
Specific gravity value	2.675	2.698	2.740

2. Atterberg limits test

2.1 Liquid limit

Weight of container (gr)	Weight of container with bulk soil (gr)	Weight of container with dry soil (gr)	Weight of dry soil (gr)	Weight of water (gr)	W%	No. of blows
11.73	37.25	27.67	15.94	9.58	60.10	12
11.68	42.55	31.35	19.67	11.2	56.94	33
11.79	41.74	31.12	19.33	10.62	54.94	30
11.72	42.61	32.42	20.7	10.19	49.23	47

From the figure below LL= 12.3% when the shrinkage is zero.
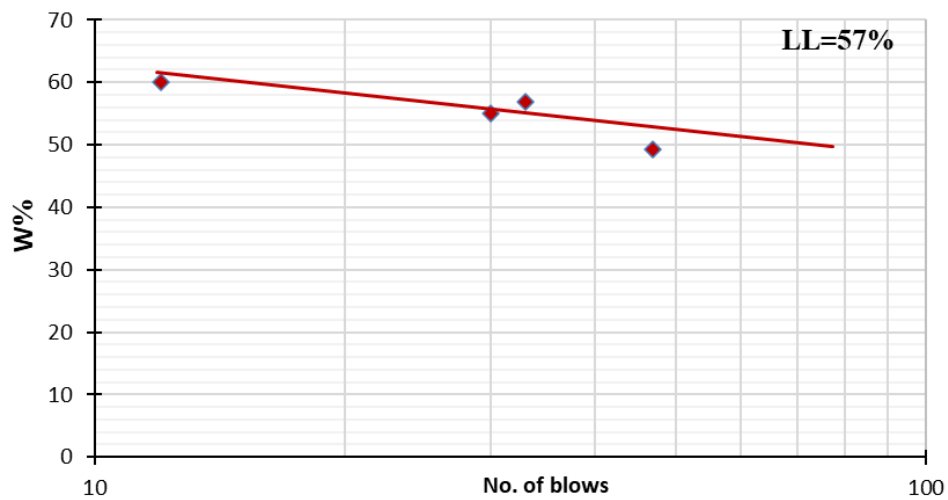
2.2 Plastic limit

Number of container	1	2
Empty weight of the container (gr)	11.63	11.59
Weight of the pycnometer with bulk soil (gr)	16.13	18.73
Weight of the container with dry soil (gr)	15.28	17.44
W%	23.29	22.05
Average w%	22.67	

2.3 Linear shrinkage (SL)

Number of container (gr)	Empty weight of the container (gr)	Weight of container with bulk soil (gr)	Weight of container with dry soil (gr)	W%	Shrinkage length, dL (cm)	dL/L
1	18.29	36.92	32.61	30.10	1	0.079
2	17.76	38.66	33.28	34.66	1.105	0.087
3	18.28	44.2	36.92	39.06	1.3	0.102

From the figure below SL= 12.3% when the shrinkage is zero.
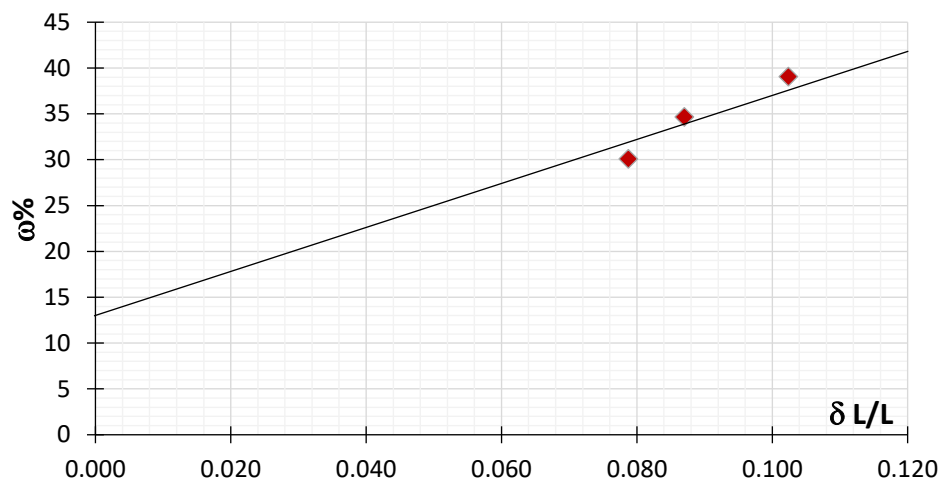
3. Standard Proctor test

Number of sample	1	2	3	4	5
Empty weight of the mold (gr)	4214.6	4214.6	4248.3	4245.6	4252.2
Weight of the mold with bulk soil (gr)	5930	6045	6053.1	5897.9	6011.2
Volume of the mold (cm^3)	944	944	944	944	944
Density (g/cm^3)	1.520	1.588	1.568	1.458	1.492

For water content calculations the table below shows the moisture content readings for each of the above samples

Number of container	1	2	3	4	5
Empty weight of the container (gr)	35	35	18.36	18.18	18.39
Weight of the pycnometer with bulk soil (gr)	79.7	119.8	44.37	46.17	48.81
Weight of the container with dry soil (gr)	70.4	104.6	39.56	41.26	42.58
W%	26.27	21.84	22.69	21.27	25.75

From the figure below, we can find both MDD and OMC
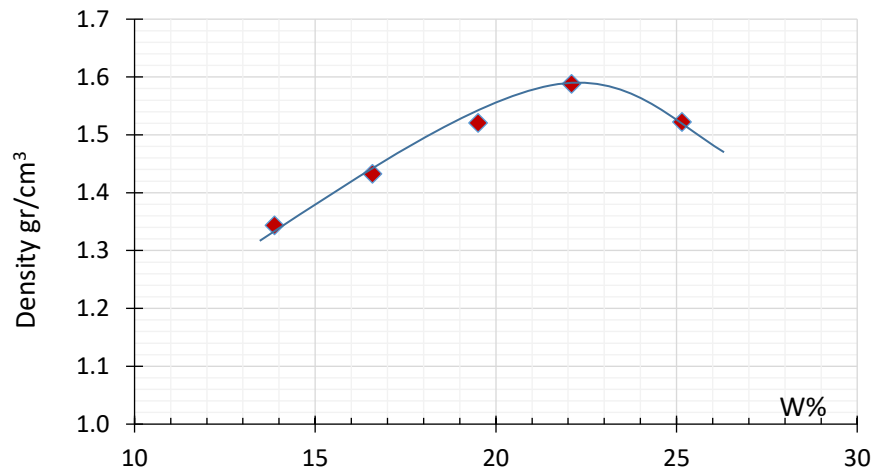
4. Direct shear test

Unreinforcement case, 0% of fiber and vertical stress equal to 50 kPa				
Shear stress	Load value in kg	Horizontal load reading	L in mm	Displacement reading, L
0	0	0	0	0
8.02	2.5	1.8	0.127	5
10.69	3.4	2.4	0.254	10
14.70	4.6	3.3	0.381	15
20.05	6.3	4.5	0.508	20
24.51	7.7	5.5	0.635	25
28.07	8.8	6.3	0.762	30
30.74	9.7	6.9	0.889	35
34.31	10.8	7.7	1.016	40
36.09	11.3	8.1	1.143	45
37.87	11.9	8.5	1.27	50
38.77	12.2	8.7	1.397	55
39.21	12.32	8.8	1.524	60
39.21	12.3	8.8	1.651	65

Unreinforcement case, 0% of fiber and vertical stress equal to 100 kPa				
Shear stress	Load value in kg	Horizontal load reading	L in mm	Displacement reading, L

Shear stress	Load value in kg	Horizontal load reading	L in mm	Displacement reading, L
0	0	0	0	0
13.81	4.3	3.1	0.1270	5
18.27	5.7	4.1	0.2540	10
20.94	6.6	4.7	0.3810	15
24.06	7.6	5.4	0.5080	20
29.41	9.2	6.6	0.6350	25
35.20	11.1	7.9	0.7620	30
41.44	13.0	9.3	0.8890	35
45.00	14.1	10.1	1.0160	40
47.23	14.8	10.6	1.1430	45
52.13	16.4	11.7	1.2700	50
55.25	17.4	12.4	1.3970	55
57.03	17.9	12.8	1.5240	60
59.71	18.8	13.4	1.6510	65
61.49	19.3	13.8	1.7780	70
62.38	19.6	14.0	1.9050	75
63.27	19.9	14.2	2.0320	80
63.27	19.9	14.2	2.1590	85
63.27	19.9	14.2	2.2860	90

Unreinforcement case, 0% of fiber and vertical stress equal to 150 kPa				
Shear stress	Load value in kg	Horizontal load reading	L in mm	Displacement reading, L
0	0	0	0	0
18.71	5.9	4.2	0.1270	5
21.83	6.9	4.9	0.2540	10
23.62	7.4	5.3	0.3810	15
27.18	8.5	6.1	0.5080	20
32.53	10.2	7.3	0.6350	25
38.77	12.2	8.7	0.7620	30
44.11	13.9	9.9	0.8890	35

47.23	14.8	10.6	1.0160	40
50.80	16.0	11.4	1.1430	45
57.03	17.9	12.8	1.2700	50
60.15	18.9	13.5	1.3970	55
65.95	20.7	14.8	1.5240	60
71.74	22.5	16.1	1.6510	65
77.08	24.2	17.3	1.7780	70
78.87	24.8	17.7	1.9050	75
79.76	25.1	17.9	2.0320	80
79.76	25.1	17.9	2.1590	85
79.76	25.1	17.9	2.2860	90

5. UCS test

Unreinforcement case, 0% of fiber _ Sample No.1					
Stress kPa	Corrected Area A' cm^2	strain %	strain $\Delta L/L$	load reading	Displacement reading, L mm
0	19.635	0	0	0	0
1.02	19.647	0.06	0.0006	2	0.06
11.19	19.666	0.16	0.0016	22	0.16
35.04	19.694	0.3	0.003	69	0.3
95.12	19.765	0.66	0.0066	188	0.66
156.35	19.827	0.97	0.0097	310	0.97
206.55	19.898	1.32	0.0132	411	1.32
240.41	19.966	1.66	0.0166	480	1.66
261.06	20.034	1.99	0.0199	523	1.99
271.18	20.097	2.3	0.023	545	2.3
275.34	20.157	2.59	0.0259	555	2.59
274.35	20.230	2.94	0.0294	555	2.94
269.50	20.297	3.26	0.0326	547	3.26
260.65	20.372	3.62	0.0362	531	3.62

Stress kPa	Corrected Area A' cm²	strain %	strain ΔL/L	load reading	Displacement reading, L mm
245.54	20.445	3.96	0.0396	502	3.96
226.18	20.515	4.29	0.0429	464	4.29

Unreinforcement case, 0% of fiber _ Sample No.2					
Stress kPa	Corrected Area A' cm²	strain %	strain ΔL/L	load reading	Displacement reading, L mm
0	19.635	0	0	0	0
1.53	19.641	0.03	0.0003	3	0.03
12.72	19.661	0.13	0.0013	25	0.13
29.95	19.700	0.33	0.0033	59	0.33
88.58	19.757	0.62	0.0062	175	0.62
150.88	19.817	0.92	0.0092	299	0.92
191.11	19.884	1.25	0.0125	380	1.25
235.77	19.977	1.71	0.0171	471	1.71
242.39	20.009	1.87	0.0187	485	1.87
254.66	20.105	2.34	0.0234	512	2.34
263.30	20.167	2.64	0.0264	531	2.64
263.64	20.217	2.88	0.0288	533	2.88
262.77	20.284	3.2	0.032	533	3.2
260.31	20.360	3.56	0.0356	530	3.56
252.08	20.430	3.89	0.0389	515	3.89
239.27	20.479	4.12	0.0412	490	4.12

Unreinforcement case, 0% of fiber _ Sample No.3					
Stress kPa	Corrected Area A' cm²	strain %	strain ΔL/L	load reading	Displacement reading, L mm
0	19.635	0	0	0	0
2.55	19.637	0.01	0.0001	5	0.01
9.16	19.647	0.06	0.0006	18	0.06

27.46	19.663	0.14	0.0014	54	0.14
81.14	19.720	0.43	0.0043	160	0.43
133.80	19.805	0.86	0.0086	265	0.86
163.59	19.867	1.17	0.0117	325	1.17
198.13	19.936	1.51	0.0151	395	1.51
223.90	20.009	1.87	0.0187	448	1.87
245.95	20.085	2.24	0.0224	494	2.24
259.54	20.151	2.56	0.0256	523	2.56
263.94	20.232	2.95	0.0295	534	2.95
261.54	20.303	3.29	0.0329	531	3.29
251.78	20.375	3.63	0.0363	513	3.63
242.66	20.440	3.94	0.0394	496	3.94
233.12	20.462	4.04	0.0404	477	4.04

6. UU triaxial test

Axial strain %	UU triaxial strength kPa
0	0
0.25	94.00978181
0.5	143.6260555
0.75	201.0764778
1	248.0813687
1.25	295.0862596
1.5	339.4797676
1.75	391.7074242
2	433.4895494
2.25	475.2716747
2.5	514.4424171
2.75	543.1676282
3	571.8928393
3.25	598.0066676
3.5	616.2863474

3.75	634.5660272
3.75	645.0115585
4	652.845707
4.25	658.0684726
4.5	660.6798555
4.75	663.2912383
5	663.2912383
5.25	663.2912383
5.5	663.2912383
5.75	663.2912383
6	0

7. UU triaxial test under (F-T) cycles

Axial strain %	UU triaxial strength kPa		
	3 cycles	6 cycles	10 cycles
0	0	0	0
0.25	15.66829697	41.78212525	36.55935959
0.5	54.83903939	75.73010201	62.67318787
0.75	83.56425049	112.2894616	88.78701615
1	112.2894616	143.6260555	114.9008444
1.25	141.0146727	177.5740323	141.0146727
1.5	169.7398838	216.7447747	167.128501
1.75	198.4650949	250.6927515	188.0195636
2	232.4130717	292.4748767	208.9106262
2.25	258.5269	331.6456192	229.8016889
2.5	284.6407282	365.5935959	245.4699858
2.75	310.7545565	391.7074242	263.7496656
3	334.257002	417.8212525	279.4179626
3.25	360.3708303	438.7123151	292.4748767
3.5	386.4846585	459.6033777	302.920408

3.75	412.5984868	470.048909	310.7545565
3.75	433.4895494	480.4944403	318.588705
4	454.3806121	485.717206	323.8114707
4.25	470.048909	485.717206	326.4228535
4.5	483.1058232	485.717206	326.4228535
4.75	493.5513545	483.1058232	323.8114707
5	503.9968858	483.1058232	-
5.25	511.8310343	480.4944403	-
5.5	519.6651828	-	-
5.75	522.2765656	-	-
6	532.7220969	-	-
6.25	537.9448626	-	-
6.5	540.5562454	-	-
6.75	543.1676282	-	-
7	532.7220969	-	-
7.25	532.7220969	-	-

8. Free swelling test

Time (min)	Swell Strain $\delta H/H\%$
0	0
0.25	0.02
1	0.04
4	0.05
9	0.07
16	0.105
25	0.165
36	0.25
49	0.285
64	0.34
81	0.4
100	0.5

121	0.59
169	0.76
196	0.955
225	1.16
1200	1.6
1440	1.6
1600	1.6

9. Oedometer/consolidation test

Unreinforcement case, 0% of fiber. Applied vertical stress is 80 kPa		
Sqrt (time)	Time (min)	Axial Strain δH/H%
0	0	0
0.5	0.25	0.3
1	1	0.41
2	4	0.45
3	9	0.465
4	16	0.485
5	25	0.5
6	36	0.52
7	49	0.545
8	64	0.55
9	81	0.57
10	100	0.585
11	121	0.6
13	169	0.605
14	196	0.615
15	225	0.63
34.64	1200	0.665
38	1440	0.675

Unreinforcement case, 0% of fiber. Applied vertical stress is 160 kPa		
Sqrt (time)	Time (min)	Axial Strain δH/H%
0	0	0
0.5	0.25	0.725
1	1	0.775
2	4	0.875
3	9	0.915
4	16	0.945
5	25	0.97
6	36	1.005
7	49	1.03
8	64	1.065
9	81	1.1
10	100	1.13
11	121	1.17
13	169	1.26
14	196	1.285
15	225	1.315
34.64	1200	1.4
38	1440	1.425

Unreinforcement case, 0% of fiber. Applied vertical stress is 320 kPa		
Sqrt (time)	Time (min)	Axial Strain δH/H%
0	0	0
0.5	0.25	1.65
1	1	1.8
2	4	1.865
3	9	1.91
4	16	2.005
5	25	2.05
6	36	2.075

7	49	2.1
8	64	2.12
9	81	2.14
10	100	2.15
11	121	2.185
13	169	2.2
14	196	2.225
15	225	2.25
34.64	1200	2.4
38	1440	2.425

The calculated void ratio for each vertical applied load is in the tables below:

Unreinforcement case, 0% of fiber. Void ratio under the applied vertical stress is 80 kPa		
Sqrt (time)	Time (min)	Axial Strain δH/H%
0	0	0.7197
0.5	0.25	0.6682
1	1	0.6492
2	4	0.6424
3	9	0.6398
4	16	0.6363
5	25	0.6338
6	36	0.6303
7	49	0.6260
8	64	0.6252
9	81	0.6217
10	100	0.6191
11	121	0.6166
13	169	0.6157
14	196	0.6140

15	225	0.6114
34.64	1200	0.6054
38	1440	0.6037

Unreinforcement case, 0% of fiber. Void ratio under the applied vertical stress is 160 kPa		
Sqrt (time)	Time (min)	Axial Strain δH/H%
0	0	0.7197
0.5	0.25	0.5951
1	1	0.5865
2	4	0.5693
3	9	0.5624
4	16	0.5572
5	25	0.5529
6	36	0.5469
7	49	0.5426
8	64	0.5366
9	81	0.5306
10	100	0.5254
11	121	0.5185
13	169	0.5031
14	196	0.4988
15	225	0.4936
34.64	1200	0.4790
38	1440	0.4747

Unreinforcement case, 0% of fiber. Void ratio under the applied vertical stress is 320 kPa		
Sqrt (time)	Time (min)	Axial Strain δH/H%
0	0	0.7197
0.5	0.25	0.4360

1	1	0.4102
2	4	0.3990
3	9	0.3913
4	16	0.3749
5	25	0.3672
6	36	0.3629
7	49	0.3586
8	64	0.3552
9	81	0.3517
10	100	0.3500
11	121	0.3440
13	169	0.3414
14	196	0.3371
15	225	0.3328
34.64	1200	0.3070
38	1440	0.3027

APPX 2: Fiber-reinforced testing' readings and calculations

1. Atterberg limits test

1.1 Liquid limit

Reinforcement case, 0.5% of fiber						
Weight of container (gr)	Weight of container with bulk soil (gr)	Weight of container with dry soil (gr)	Weight of dry soil (gr)	Weight of water (gr)	W%	No. of blows
11.84	32.65	25.04	13.2	7.61	57.65	16
11.68	38.91	29.52	17.84	9.39	52.63	21
11.67	43.59	32.72	21.05	10.87	51.64	37
11.62	34.79	26.72	15.1	8.07	53.44	43

And from the figure below we can find the LL= 54.4% that meets 25 blows.
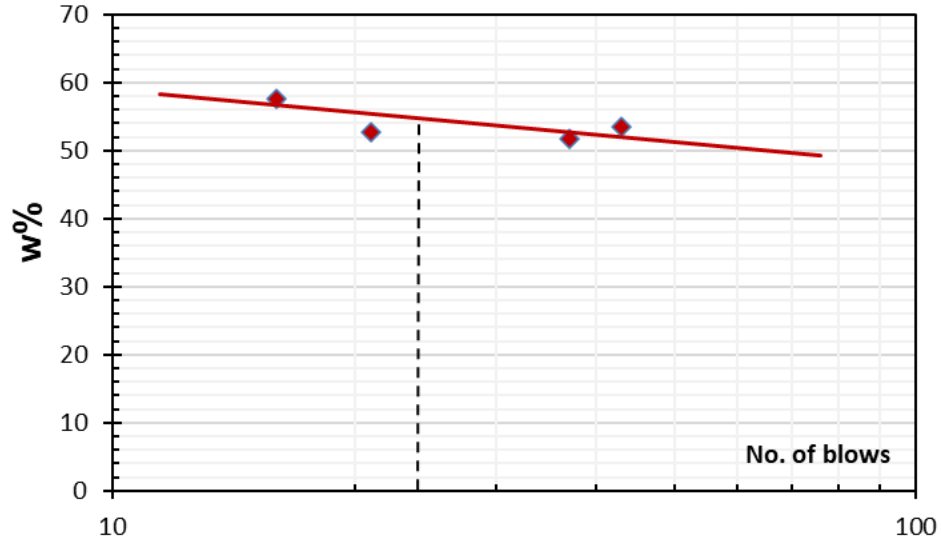
Reinforcement case, 1% of fiber						
Weight of container (gr)	Weight of container with bulk soil (gr)	Weight of container with dry soil (gr)	Weight of dry soil (gr)	Weight of water (gr)	W%	No. of blows

11.67	31.43	24.43	12.76	7	54.86	17
11.23	38.59	29.23	18	9.36	52.00	33
11.77	30.16	23.93	12.16	6.23	51.23	21
11.81	41.59	31.47	19.66	10.12	51.48	41

And from the figure below we can find the LL= 53% that meets 25 blows.
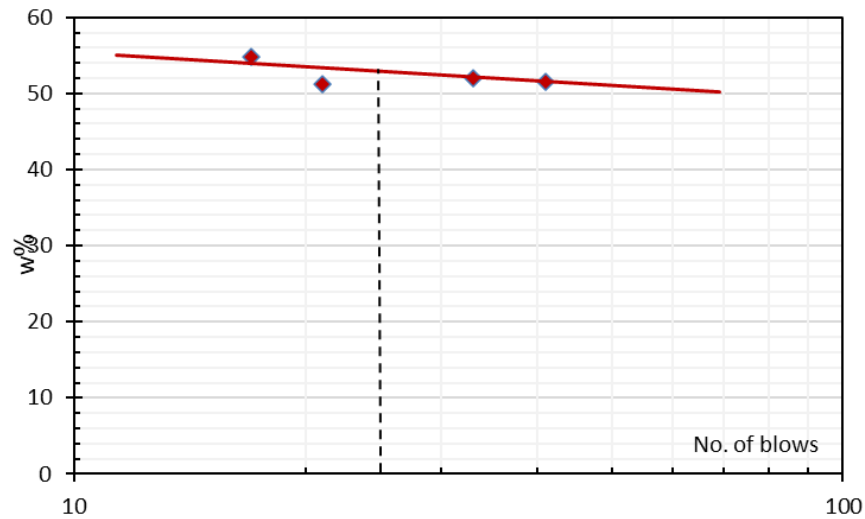
Reinforcement case, 1.5% of fiber						
Weight of container (gr)	Weight of container with bulk soil (gr)	Weight of container with dry soil (gr)	Weight of dry soil (gr)	Weight of water (gr)	W%	No. of blows
18.47	40.59	33.62	15.15	6.97	46.01	44
17.83	41.15	33.17	15.34	7.98	52.02	28
18.16	45.23	35.98	17.82	9.25	51.91	21
11.87	42.34	31.48	19.61	10.86	55.38	14

And from the figure below we can find the LL= 52% that meets 25 blows.
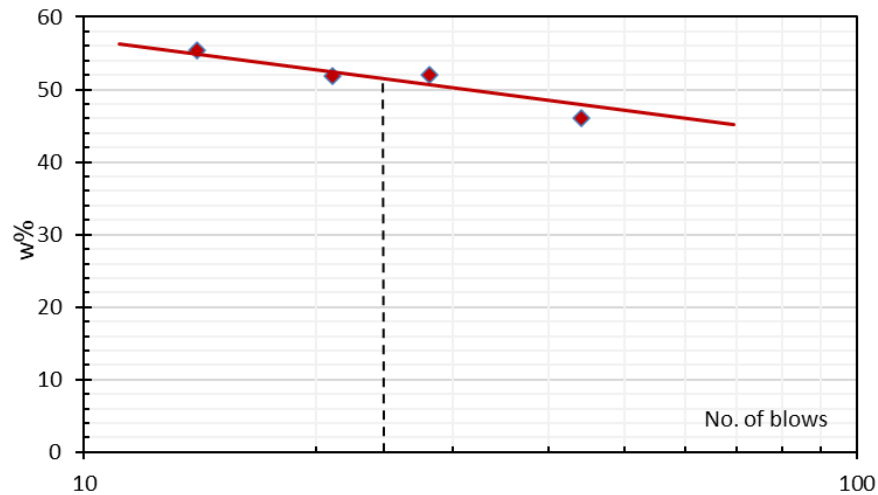
1.2 Plastic limit

Reinforcement case, 0.5% of fiber		
Number of container	1	2
Empty weight of the container (gr)	11.52	11.59
Weight of the pycnometer with bulk soil (gr)	15.23	15.57
Weight of the container with dry soil (gr)	14.53	14.74
W%	23.26	26.35
Average w%	24.80	

Reinforcement case, 1 % of fiber		
Number of container	1	2
Empty weight of the container (gr)	11.57	11.54
Weight of the pycnometer with bulk soil (gr)	15.74	17.12
Weight of the container with dry soil (gr)	14.89	15.92
W%	25.60	27.40
Average w%	25.6	

Reinforcement case, 1.5 % of fiber		
Number of container	1	2
Empty weight of the container (gr)	11.52	11.61
Weight of the pycnometer with bulk soil (gr)	16.73	15.54

Weight of the container with dry soil (gr)	15.67	14.75
W%	25.54	25.16
Average w%	25.35	

1.3 linear shrinkage (SL)

Number of container (gr)	Empty weight of the container (gr)	Weight of container with bulk soil (gr)	Weight of container with dry soil (gr)	W%	Shrinkage length, dL (cm)	dL/L
Reinforcement case, 0.5 % of fiber						
1	18.39	32.81	29.70	27.50	0.765	0.060
2	17.83	38.13	33.20	32.08	1	0.079
3	18.34	61.72	49.67	38.46	1.215	0.096

Number of container (gr)	Empty weight of the container (gr)	Weight of container with bulk soil (gr)	Weight of container with dry soil (gr)	W%	Shrinkage length, dL (cm)	dL/L
Reinforcement case, 1 % of fiber						
1	17.62	34.39	30.41	31.12	0.725	0.057
2	18.29	34.43	30.36	33.72	0.825	0.065
3	18.16	33.59	29.57	35.23	0.94	0.074

Number of container (gr)	Empty weight of the container (gr)	Weight of container with bulk soil (gr)	Weight of container with dry soil (gr)	W%	Shrinkage length, dL (cm)	dL/L
Reinforcement case, 1.5 % of fiber						

1	17.69	32.61	28.85	33.69	0.73	0.057
2	18.17	35.42	31.48	29.60	0.55	0.043
3	18.44	48.31	39.91	39.12	0.905	0.071

From the figures below SL can be found for each fiber content when the shrinkage is zero.
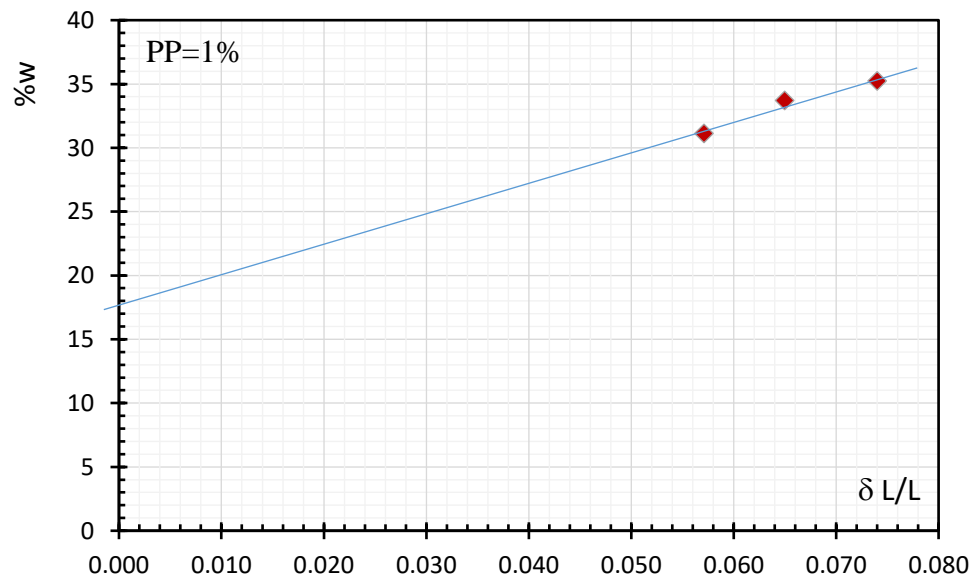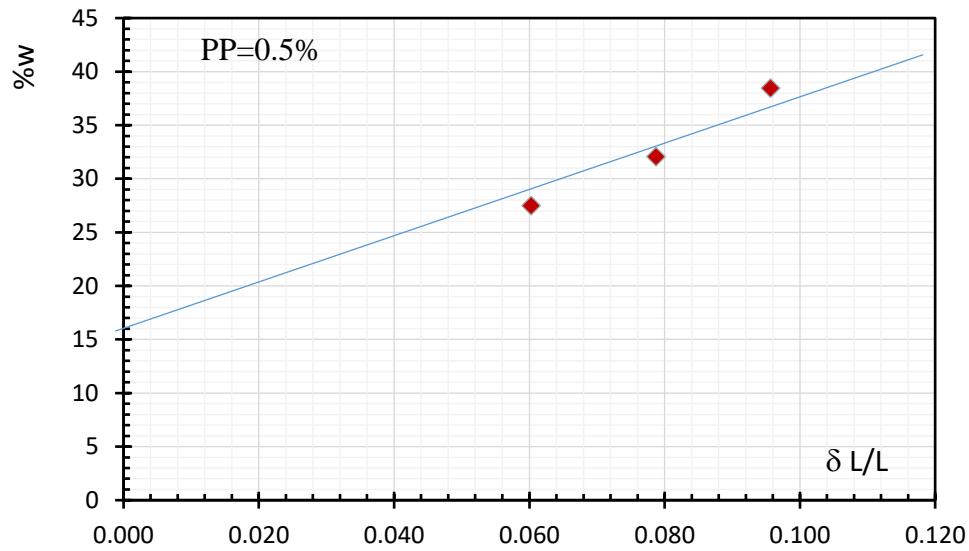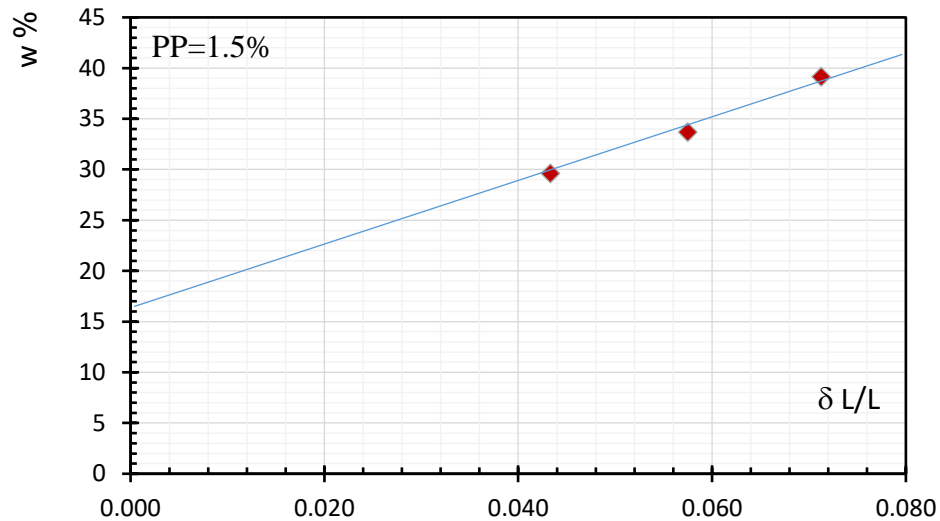
6. Standard Proctor test

Reinforcement case, 0.5 % of fiber				
Number of sample	1	2	3	4
Empty weight of the mold (gr)	4214.6	4249	4252	4253
Weight of the mold with bulk soil (gr)	5578.6	5844	6048	6011
Volume of the mold (cm^3)	944	944	944	944
Density (g/cm^3)	1.230	1.408	1.552	1.472

For water content calculations the table below shows the moisture content readings for each of the above samples

Number of container	1	2	3	4
Empty weight of the container (gr)	37.4	18.52	18.36	17.86
Weight of the pycnometer with bulk soil (gr)	104.8	42.83	48.92	52.7
Weight of the container with dry soil (gr)	94.8	38.88	43.22	45.14
W%	17.42	19.40	22.93	27.71

From the figure below, we can find both MDD and OMC
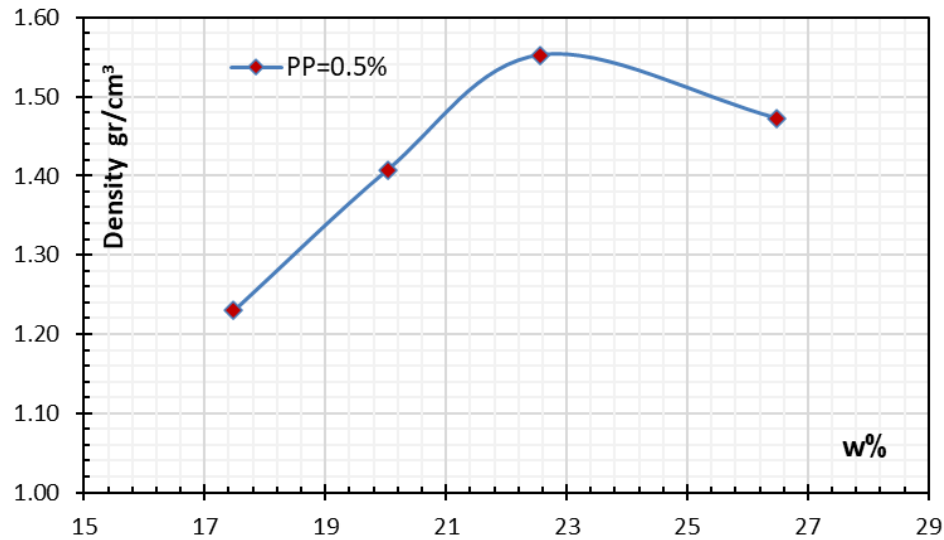
Reinforcement case, 1 % of fiber				
Number of sample	1	2	3	4
Empty weight of the mold (gr)	4248.4	4249	4253	4253
Weight of the mold with bulk soil (gr)	5674.4	5944	6045	6020
Volume of the mold (cm^3)	944	944	944	944
Density (g/cm^3)	1.275	1.480	1.534	1.491

For water content calculations the table below shows the moisture content readings for each of the above samples

Number of container	1	2	3	4
Empty weight of the container (gr)	35.4	18.52	17.89	17.73
Weight of the pycnometer with bulk soil (gr)	107.7	64.33	49.56	85.71
Weight of the container with dry soil (gr)	95.98	56.11	43.52	72.14
W%	19.35	21.87	23.57	24.94

From the figure below, we can find both MDD and OMC
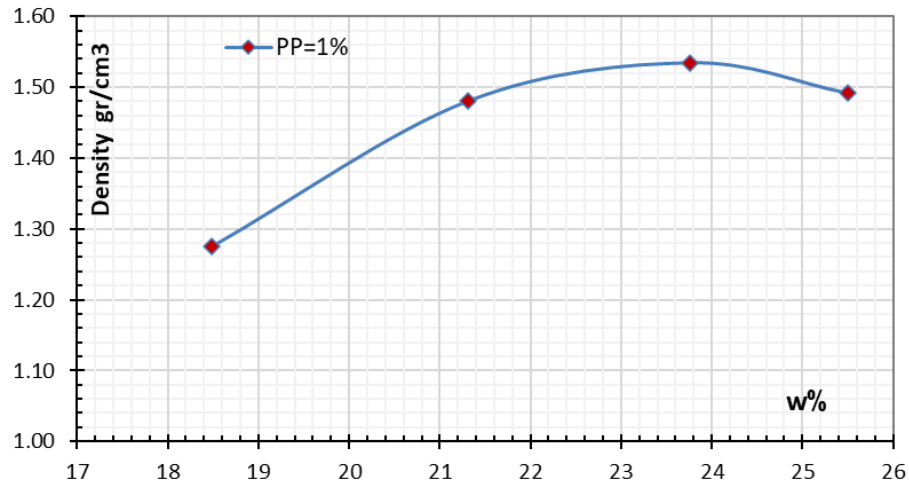
Reinforcement case, 1.5 % of fiber				
Number of sample	1	2	3	4
Empty weight of the mold (gr)	4247	4247	4246	4246
Weight of the mold with bulk soil (gr)	5509	5725	5983	5992
Volume of the mold (cm^3)	944	944	944	944
Density (g/cm^3)	1.147	1.295	1.486	1.452

For water content calculations the table below shows the moisture content readings for each of the above samples

Number of container	1	2	3	4
Empty weight of the container (gr)	17.73	31.28	30.74	30.45
Weight of the pycnometer with bulk soil (gr)	49.31	80.31	89.26	103.39
Weight of the container with dry soil (gr)	44.69	72.16	77.64	87.72
W%	17.14	19.94	24.78	27.36

From the figure below, we can find both MDD and OMC
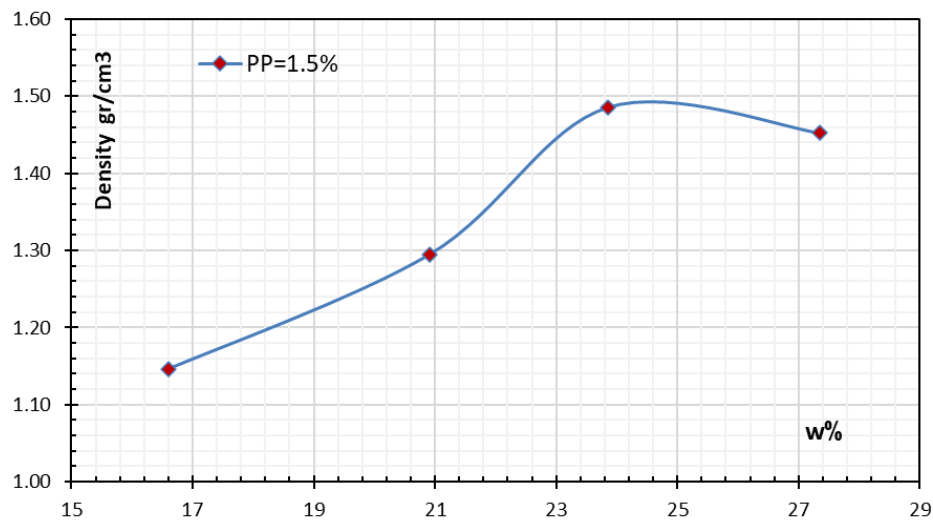
7. Direct shear test

Reinforcement case, 0.5% of fiber and vertical stress equal to 25 kPa				
Shear stress	Load value in kg	Horizontal load reading	L in mm	Displacement reading, L
0	0	0	0	0
10.69	3.36	2.4	0.127	5
18.71	5.88	4.2	0.254	10
23.62	7.42	5.3	0.381	15
29.85	9.38	6.7	0.508	20
38.32	12.04	8.6	0.635	25
45.45	14.28	10.2	0.762	30
54.81	17.22	12.3	0.889	35
58.37	18.34	13.1	1.016	40
63.27	19.88	14.2	1.143	45
63.27	19.88	14.2	1.27	50
63.27	19.88	14.2	1.397	55

Reinforcement case, 0.5% of fiber and vertical stress equal to 50 kPa				
Shear stress	Load value in kg	Horizontal load reading	L in mm	Displacement reading, L
0	0	0	0	0

14.26	4.48	3.2	0.127	5
19.16	6.02	4.3	0.254	10
27.18	8.54	6.1	0.381	15
32.08	10.08	7.2	0.508	20
39.21	12.32	8.8	0.635	25
51.24	16.1	11.5	0.762	30
61.49	19.32	13.8	0.889	35
71.74	22.54	16.1	1.016	40
79.76	25.06	17.9	1.143	45
80.65	25.34	18.1	1.27	50
80.65	25.34	18.1	1.397	55
80.65	25.34	18.1	1.524	60

Reinforcement case, 0.5% of fiber and vertical stress equal to 100 kPa				
Shear stress	Load value in kg	Horizontal load reading	L in mm	Displacement reading, L
0	0	0	0	0
31.64	9.94	7.1	0.127	5
45.00	14.14	10.1	0.254	10
64.16	20.16	14.4	0.381	15
79.31	24.92	17.8	0.508	20
91.34	28.7	20.5	0.635	25
99.36	31.22	22.3	0.762	30
105.16	33.04	23.6	0.889	35
106.49	33.46	23.9	1.016	40
107.38	33.74	24.1	1.143	45
107.83	33.88	24.2	1.270	50
107.83	33.88	24.2	1.397	55
107.83	33.88	24.2	1.524	60

Reinforcement case, 0.5% of fiber and vertical stress equal to 150 kPa				
Shear stress	Load value in kg	Horizontal load reading	L in mm	Displacement reading, L
0	0	0	0	0
33.86	10.64	7.6	0.127	5
45.89	14.42	10.3	0.254	10
61.04	19.18	13.7	0.381	15
71.74	22.54	16.1	0.508	20
81.99	25.76	18.4	0.635	25
97.14	30.52	21.8	0.762	30
110.06	34.58	24.7	0.889	35
118.52	37.24	26.6	1.016	40
126.10	39.62	28.3	1.143	45
137.68	43.26	30.9	1.270	50
137.68	43.26	30.9	1.397	55
137.68	43.26	30.9	1.524	60

Reinforcement case, 1% of fiber and vertical stress equal to 25 kPa				
Shear stress	Load value in kg	Horizontal load reading	L in mm	Displacement reading, L
0	0	0	0	0
14.70	4.62	3.3	0.127	5
25.84	8.12	5.8	0.254	10
33.86	10.64	7.6	0.381	15
47.68	14.98	10.7	0.508	20
59.71	18.76	13.4	0.635	25
69.06	21.7	15.5	0.762	30
76.64	24.08	17.2	0.889	35
81.54	25.62	18.3	1.016	40
81.54	25.62	18.3	1.143	45
81.54	25.62	18.3	1.27	50

Reinforcement case, 1% of fiber and vertical stress equal to 50 kPa				
Shear stress	Load value in kg	Horizontal load reading	L in mm	Displacement reading, L
0	0	0	0	0
24.51	7.7	5.5	0.127	5
39.21	12.32	8.8	0.254	10
52.58	16.52	11.8	0.381	15
61.94	19.46	13.9	0.508	20
73.07	22.96	16.4	0.635	25
84.21	26.46	18.9	0.762	30
92.23	28.98	20.7	0.889	35
97.58	30.66	21.9	1.016	40
100.25	31.5	22.5	1.143	45
101.59	31.92	22.8	1.27	50
102.93	32.34	23.1	1.397	55
102.93	32.34	23.1	1.524	60

Reinforcement case, 1% of fiber and vertical stress equal to 100 kPa				
Shear stress	Load value in kg	Horizontal load reading	L in mm	Displacement reading, L
0	0	0	0	0
34.75	10.92	7.8	0.127	5
54.81	17.22	12.3	0.254	10
78.87	24.78	17.7	0.381	15
94.91	29.82	21.3	0.508	20
116.30	36.54	26.1	0.635	25
122.98	38.64	27.6	0.762	30
127.88	40.18	28.7	0.889	35
131.00	41.16	29.4	1.016	40
133.23	41.86	29.9	1.143	45

134.12	42.14	30.1	1.270	50
134.12	42.14	30.1	1.397	55
134.12	42.14	30.1	1.524	60

Reinforcement case, 1% of fiber and vertical stress equal to 150 kPa				
Shear stress	Load value in kg	Horizontal load reading	L in mm	Displacement reading, L
0	0	0	0	0
36.54	11.48	8.2	0.127	5
61.94	19.46	13.9	0.254	10
85.11	26.74	19.1	0.381	15
103.82	32.62	23.3	0.508	20
123.87	38.92	27.8	0.635	25
131.00	41.16	29.4	0.762	30
144.81	45.5	32.5	0.889	35
155.51	48.86	34.9	1.016	40
163.53	51.38	36.7	1.143	45
165.75	52.08	37.2	1.270	50
165.75	52.08	37.2	1.397	55
165.75	52.08	37.2	1.524	60

Reinforcement case, 1.5% of fiber and vertical stress equal to 25 kPa				
Shear stress	Load value in kg	Horizontal load reading	L in mm	Displacement reading, L
0	0	0	0	0
15.60	4.9	3.5	0.127	5
26.29	8.26	5.9	0.254	10
56.59	17.78	12.7	0.381	15
76.64	24.08	17.2	0.508	20
90.45	28.42	20.3	0.635	25
103.82	32.62	23.3	0.762	30

114.51	35.98	25.7	0.889	35
122.98	38.64	27.6	1.016	40
124.32	39.06	27.9	1.143	45
124.32	39.06	27.9	1.27	50

Reinforcement case, 1.5% of fiber and vertical stress equal to 50 kPa				
Shear stress	Load value in kg	Horizontal load reading	L in mm	Displacement reading, L
0	0	0	0	0
27.63	8.68	6.2	0.127	5
34.75	10.92	7.8	0.254	10
58.37	18.34	13.1	0.381	15
69.96	21.98	15.7	0.508	20
88.22	27.72	19.8	0.635	25
109.61	34.44	24.6	0.762	30
127.88	40.18	28.7	0.889	35
139.47	43.82	31.3	1.016	40
143.92	45.22	32.3	1.143	45
145.26	45.64	32.6	1.27	50
145.26	45.64	32.6	1.397	55
145.26	45.64	32.6	1.524	60

Reinforcement case, 1.5% of fiber and vertical stress equal to 100 kPa				
Shear stress	Load value in kg	Horizontal load reading	L in mm	Displacement reading, L
0	0	0	0	0
31.19	9.8	7	0.127	5
36.09	11.34	8.1	0.254	10
56.59	17.78	12.7	0.381	15
81.99	25.76	18.4	0.508	20
103.82	32.62	23.3	0.635	25

118.52	37.24	26.6	0.762	30
139.02	43.68	31.2	0.889	35
154.61	48.58	34.7	1.016	40
161.30	50.68	36.2	1.143	45
165.31	51.94	37.1	1.27	50
166.65	52.36	37.4	1.397	55
166.65	52.36	37.4	1.524	60

Reinforcement case, 1.5% of fiber and vertical stress equal to 150 kPa				
Shear stress	Load value in kg	Horizontal load reading	L in mm	Displacement reading, L
0	0	0	0	0
35.65	11.2	8	0.127	5
48.12	15.12	10.8	0.254	10
65.05	20.44	14.6	0.381	15
94.02	29.54	21.1	0.508	20
115.40	36.26	25.9	0.635	25
134.56	42.28	30.2	0.762	30
156.40	49.14	35.1	0.889	35
172.44	54.18	38.7	1.016	40
183.13	57.54	41.1	1.143	45
191.15	60.06	42.9	1.27	50
195.16	61.32	43.8	1.397	55
195.16	61.32	43.8	1.524	60

8. UCS test

Reinforcement case, 0.5% of fiber _ Sample No.1					
Stress kPa	Corrected Area A' cm^2	strain %	strain ΔL/L	load reading	Displacement reading, L mm
0	19.635	0	0	0	0
3.06	19.637	0.01	0.0001	6	0.01
5.60	19.641	0.03	0.0003	11	0.03
12.72	19.647	0.06	0.0006	25	0.06
19.33	19.663	0.14	0.0014	38	0.14
35.04	19.694	0.3	0.003	69	0.3
77.41	19.765	0.66	0.0066	153	0.66
128.11	19.827	0.97	0.0097	254	0.97
173.40	19.896	1.31	0.0131	345	1.31
213.93	19.960	1.63	0.0163	427	1.63
245.72	20.023	1.94	0.0194	492	1.94
266.71	20.097	2.3	0.023	536	2.3
279.14	20.169	2.65	0.0265	563	2.65
284.58	20.240	2.99	0.0299	576	2.99
287.12	20.305	3.3	0.033	583	3.3
286.11	20.377	3.64	0.0364	583	3.64
284.15	20.447	3.97	0.0397	581	3.97
281.23	20.517	4.3	0.043	577	4.3
277.83	20.588	4.63	0.0463	572	4.63
273.99	20.658	4.95	0.0495	566	4.95

Reinforcement case, 0.5% of fiber _ Sample No.2					
Stress kPa	Corrected Area A' cm^2	strain %	strain ΔL/L	load reading	Displacement reading, L mm
0.00	19.635	0	0	0	0

4.58	19.637	0.01	0.0001	9	0.01
8.15	19.641	0.03	0.0003	16	0.03
15.78	19.649	0.07	0.0007	31	0.07
29.50	19.664	0.15	0.0015	58	0.15
60.92	19.698	0.32	0.0032	120	0.32
121.48	19.757	0.62	0.0062	240	0.62
171.99	19.827	0.97	0.0097	341	0.97
213.17	19.890	1.28	0.0128	424	1.28
243.08	19.952	1.59	0.0159	485	1.59
262.70	20.023	1.94	0.0194	526	1.94
276.22	20.093	2.28	0.0228	555	2.28
284.71	20.161	2.61	0.0261	574	2.61
289.73	20.226	2.92	0.0292	586	2.92
292.60	20.301	3.28	0.0328	594	3.28
294.61	20.366	3.59	0.0359	600	3.59
295.50	20.440	3.94	0.0394	604	3.94
296.59	20.500	4.22	0.0422	608	4.22
296.93	20.577	4.58	0.0458	611	4.58
297.86	20.647	4.9	0.049	615	4.9
296.77	20.723	5.25	0.0525	615	5.25
296.71	20.795	5.58	0.0558	617	5.58
295.70	20.866	5.9	0.059	617	5.9
295.13	20.940	6.23	0.0623	618	6.23
293.08	21.018	6.58	0.0658	616	6.58
290.16	21.092	6.91	0.0691	612	6.91
287.77	21.163	7.22	0.0722	609	7.22
285.36	21.236	7.54	0.0754	606	7.54
282.47	21.312	7.87	0.0787	602	7.87
279.56	21.391	8.21	0.0821	598	8.21
275.78	21.466	8.53	0.0853	592	8.53

Reinforcement case, 0.5% of fiber _ Sample No.3					
Stress kPa	Corrected Area A' cm^2	strain %	strain ΔL/L	load reading	Displacement reading, L mm
0.00	19.635	0	0	0	0
5.60	19.637	0.01	0.0001	11	0.01
7.64	19.641	0.03	0.0003	15	0.03
15.78	19.649	0.07	0.0007	31	0.07
31.02	19.666	0.16	0.0016	61	0.16
65.48	19.700	0.33	0.0033	129	0.33
128.54	19.761	0.64	0.0064	254	0.64
170.42	19.833	1	0.01	338	1
219.16	19.894	1.3	0.013	436	1.3
248.02	19.958	1.62	0.0162	495	1.62
271.22	20.021	1.93	0.0193	543	1.93
286.58	20.099	2.31	0.0231	576	2.31
288.09	20.167	2.64	0.0264	581	2.64
295.05	20.234	2.96	0.0296	597	2.96
299.93	20.305	3.3	0.033	609	3.3
305.41	20.366	3.59	0.0359	622	3.59
306.84	20.434	3.91	0.0391	627	3.91
307.67	20.509	4.26	0.0426	631	4.26
308.49	20.584	4.61	0.0461	635	4.61
310.88	20.651	4.92	0.0492	642	4.92
310.83	20.719	5.23	0.0523	644	5.23
311.25	20.787	5.54	0.0554	647	5.54
310.93	20.873	5.93	0.0593	649	5.93
310.83	20.944	6.25	0.0625	651	6.25
309.68	21.022	6.6	0.066	651	6.6
308.20	21.090	6.9	0.069	650	6.9
307.14	21.163	7.22	0.0722	650	7.22

Stress kPa	Corrected Area A' cm²	strain %	strain ΔL/L	load reading	Displacement reading, L mm
305.04	21.243	7.57	0.0757	648	7.57
303.12	21.312	7.87	0.0787	646	7.87
299.49	21.403	8.26	0.0826	641	8.26

Reinforcement case, 1% of fiber _ Sample No.1					
Stress kPa	Corrected Area A' cm²	strain %	strain ΔL/L	load reading	Displacement reading, L mm
0.00	19.635	0	0	0	0
1.53	19.637	0.01	0.0001	3	0.01
6.11	19.639	0.019	0.00019	12	0.019
12.72	19.647	0.06	0.0006	25	0.06
22.88	19.666	0.16	0.0016	45	0.16
39.60	19.698	0.32	0.0032	78	0.32
77.94	19.759	0.63	0.0063	154	0.63
119.05	19.823	0.95	0.0095	236	0.95
161.34	19.896	1.31	0.0131	321	1.31
203.33	19.968	1.67	0.0167	406	1.67
241.61	20.032	1.98	0.0198	484	1.98
276.05	20.105	2.34	0.0234	555	2.34
307.33	20.174	2.67	0.0267	620	2.67
333.43	20.244	3.01	0.0301	675	3.01
356.49	20.309	3.32	0.0332	724	3.32
376.29	20.383	3.67	0.0367	767	3.67
393.17	20.449	3.98	0.0398	804	3.98
407.37	20.522	4.32	0.0432	836	4.32
420.49	20.595	4.66	0.0466	866	4.66
431.10	20.668	5	0.05	891	5
440.78	20.736	5.31	0.0531	914	5.31
448.76	20.813	5.66	0.0566	934	5.66
456.85	20.882	5.97	0.0597	954	5.97

Stress kPa	Corrected Area A' cm²	strain %	strain ΔL/L	load reading	Displacement reading, L mm
463.22	20.962	6.33	0.0633	971	6.33
468.29	21.034	6.65	0.0665	985	6.65
472.27	21.111	6.99	0.0699	997	6.99
478.06	21.190	7.34	0.0734	1013	7.34
479.59	21.268	7.68	0.0768	1020	7.68
482.03	21.347	8.02	0.0802	1029	8.02
484.50	21.424	8.35	0.0835	1038	8.35
485.14	21.499	8.67	0.0867	1043	8.67
486.63	21.577	9	0.09	1050	9
488.62	21.653	9.32	0.0932	1058	9.32
486.38	21.732	9.65	0.0965	1057	9.65
484.55	21.814	9.99	0.0999	1057	9.99
483.58	21.899	10.34	0.1034	1059	10.34
479.07	21.980	10.67	0.1067	1053	10.67
475.54	22.059	10.99	0.1099	1049	10.99
471.07	22.141	11.32	0.1132	1043	11.32
465.82	22.219	11.63	0.1163	1035	11.63
461.50	22.297	11.94	0.1194	1029	11.94
452.51	22.386	12.29	0.1229	1013	12.29

Reinforcement case, 1% of fiber _ Sample No.2					
Stress kPa	Corrected Area A' cm²	strain %	strain ΔL/L	load reading	Displacement reading, L mm
0.00	19.635	0	0	0	0
2.04	19.637	0.01	0.0001	4	0.01
7.13	19.639	0.02	0.0002	14	0.02
16.80	19.647	0.06	0.0006	33	0.06
26.96	19.657	0.11	0.0011	53	0.11
42.66	19.690	0.28	0.0028	84	0.28
60.84	19.724	0.45	0.0045	120	0.45

81.98	19.761	0.64	0.0064	162	0.64
106.10	19.793	0.8	0.008	210	0.8
130.66	19.823	0.95	0.0095	259	0.95
143.56	19.853	1.1	0.011	285	1.1
155.35	19.890	1.28	0.0128	309	1.28
174.68	19.922	1.44	0.0144	348	1.44
195.51	19.948	1.57	0.0157	390	1.57
209.57	19.993	1.79	0.0179	419	1.79
233.73	20.023	1.94	0.0194	468	1.94
247.31	20.056	2.1	0.021	496	2.1
259.90	20.085	2.24	0.0224	522	2.24
276.29	20.124	2.43	0.0243	556	2.43
297.11	20.161	2.61	0.0261	599	2.61
304.08	20.192	2.76	0.0276	614	2.76
312.90	20.230	2.94	0.0294	633	2.94
330.59	20.267	3.12	0.0312	670	3.12
336.47	20.299	3.27	0.0327	683	3.27
344.73	20.335	3.44	0.0344	701	3.44
354.85	20.375	3.63	0.0363	723	3.63
367.54	20.406	3.78	0.0378	750	3.78
379.65	20.440	3.94	0.0394	776	3.94
386.46	20.468	4.07	0.0407	791	4.07
391.42	20.515	4.29	0.0429	803	4.29
392.76	20.547	4.44	0.0444	807	4.44
400.04	20.573	4.56	0.0456	823	4.56
404.17	20.610	4.73	0.0473	833	4.73
410.67	20.649	4.91	0.0491	848	4.91
419.27	20.679	5.05	0.0505	867	5.05
426.01	20.727	5.27	0.0527	883	5.27
431.12	20.760	5.42	0.0542	895	5.42
436.10	20.798	5.59	0.0559	907	5.59

Stress kPa	Corrected Area	strain %	strain ΔL/L	load reading	Displacement reading
438.20	20.835	5.76	0.0576	913	5.76
440.91	20.866	5.9	0.059	920	5.9
446.09	20.915	6.12	0.0612	933	6.12
452.68	20.942	6.24	0.0624	948	6.24
460.48	20.978	6.4	0.064	966	6.4
467.65	21.020	6.59	0.0659	983	6.59
468.32	21.054	6.74	0.0674	986	6.74
469.06	21.106	6.97	0.0697	990	6.97
470.01	21.127	7.06	0.0706	993	7.06
471.42	21.170	7.25	0.0725	998	7.25
473.97	21.204	7.4	0.074	1005	7.4
476.44	21.241	7.56	0.0756	1012	7.56
477.44	21.280	7.73	0.0773	1016	7.73
476.97	21.322	7.91	0.0791	1017	7.91
476.26	21.354	8.05	0.0805	1017	8.05
475.90	21.391	8.21	0.0821	1018	8.21
474.97	21.433	8.39	0.0839	1018	8.39
472.98	21.523	8.77	0.0877	1018	8.77
472.06	21.565	8.95	0.0895	1018	8.95
471.34	21.577	9	0.09	1017	9
469.54	21.617	9.17	0.0917	1015	9.17
466.04	21.672	9.4	0.094	1010	9.4
462.15	21.768	9.8	0.098	1006	9.8
458.21	21.846	10.12	0.1012	1001	10.12

Reinforcement case, 1% of fiber _ Sample No.3					
Stress kPa	Corrected Area A' cm^2	strain %	strain ΔL/L	load reading	Displacement reading, L mm
0.00	19.635	0	0	0	0
2.04	19.637	0.01	0.0001	4	0.01

6.62	19.641	0.03	0.0003	13	0.03
14.25	19.649	0.07	0.0007	28	0.07
19.35	19.638	0.015	0.00015	38	0.015
34.01	19.700	0.33	0.0033	67	0.33
72.36	19.761	0.64	0.0064	143	0.64
111.95	19.831	0.99	0.0099	222	0.99
156.23	19.906	1.36	0.0136	311	1.36
193.59	19.991	1.78	0.0178	387	1.78
237.31	20.058	2.11	0.0211	476	2.11
258.84	20.128	2.45	0.0245	521	2.45
301.75	20.182	2.71	0.0271	609	2.71
328.61	20.267	3.12	0.0312	666	3.12
350.10	20.337	3.45	0.0345	712	3.45
367.54	20.406	3.78	0.0378	750	3.78
390.19	20.477	4.11	0.0411	799	4.11
394.22	20.547	4.44	0.0444	810	4.44
411.82	20.640	4.87	0.0487	850	4.87
428.96	20.701	5.15	0.0515	888	5.15
432.44	20.789	5.55	0.0555	899	5.55
437.12	20.864	5.89	0.0589	912	5.89
445.19	20.935	6.21	0.0621	932	6.21
450.66	21.036	6.66	0.0666	948	6.66
452.97	21.083	6.87	0.0687	955	6.87
457.94	21.138	7.11	0.0711	968	7.11
462.92	21.213	7.44	0.0744	982	7.44
469.30	21.287	7.76	0.0776	999	7.76
474.18	21.342	8	0.08	1012	8
476.26	21.417	8.32	0.0832	1020	8.32
478.36	21.490	8.63	0.0863	1028	8.63
479.52	21.584	9.03	0.0903	1035	9.03
478.85	21.677	9.42	0.0942	1038	9.42

477.53	21.737	9.67	0.0967	1038	9.67
474.40	21.817	10	0.1	1035	10
471.43	21.912	10.39	0.1039	1033	10.39
467.38	21.995	10.73	0.1073	1028	10.73
463.24	22.062	11	0.11	1022	11

Reinforcement case, 1.5% of fiber _ Sample No.1					
Stress kPa	Corrected Area A' cm^2	strain %	strain ΔL/L	load reading	Displacement reading, L mm
0.00	19.635	0	0	0	0
5.09	19.637	0.01	0.0001	10	0.01
8.65	19.649	0.07	0.0007	17	0.07
13.73	19.666	0.16	0.0016	27	0.16
26.39	19.702	0.34	0.0034	52	0.34
61.22	19.765	0.66	0.0066	121	0.66
106.91	19.829	0.98	0.0098	212	0.98
156.74	19.906	1.36	0.0136	312	1.36
208.78	19.973	1.69	0.0169	417	1.69
259.98	20.040	2.02	0.0202	521	2.02
303.90	20.105	2.34	0.0234	611	2.34
339.51	20.176	2.68	0.0268	685	2.68
367.06	20.242	3	0.03	743	3
388.99	20.309	3.32	0.0332	790	3.32
405.81	20.379	3.65	0.0365	827	3.65
418.15	20.447	3.97	0.0397	855	3.97
428.32	20.522	4.32	0.0432	879	4.32
436.70	20.586	4.62	0.0462	899	4.62
443.90	20.658	4.95	0.0495	917	4.95
448.58	20.732	5.29	0.0529	930	5.29
452.69	20.809	5.64	0.0564	942	5.64

455.90	20.882	5.97	0.0597	952	5.97
459.99	20.957	6.31	0.0631	964	6.31
461.79	21.027	6.62	0.0662	971	6.62
463.89	21.104	6.96	0.0696	979	6.96
466.07	21.177	7.28	0.0728	987	7.28
467.72	21.252	7.61	0.0761	994	7.61
469.34	21.328	7.94	0.0794	1001	7.94
470.81	21.410	8.29	0.0829	1008	8.29
471.49	21.485	8.61	0.0861	1013	8.61
472.10	21.563	8.94	0.0894	1018	8.94
473.22	21.639	9.26	0.0926	1024	9.26
474.72	21.718	9.59	0.0959	1031	9.59
475.23	21.800	9.93	0.0993	1036	9.93
477.56	21.882	10.27	0.1027	1045	10.27
476.75	21.961	10.59	0.1059	1047	10.59
477.27	22.042	10.92	0.1092	1052	10.92
478.00	22.134	11.29	0.1129	1058	11.29
478.12	22.212	11.6	0.116	1062	11.6
479.99	22.292	11.92	0.1192	1070	11.92
479.47	22.379	12.26	0.1226	1073	12.26
480.28	22.466	12.6	0.126	1079	12.6
480.41	22.564	12.98	0.1298	1084	12.98
481.47	22.639	13.27	0.1327	1090	13.27
481.89	22.723	13.59	0.1359	1095	13.59
482.29	22.808	13.91	0.1391	1100	13.91
484.39	22.895	14.24	0.1424	1109	14.24
482.90	22.986	14.58	0.1458	1110	14.58
482.82	23.073	14.9	0.149	1114	14.9
483.06	23.165	15.24	0.1524	1119	15.24

Reinforcement case, 1.5% of fiber _ Sample No.2					
Stress kPa	Corrected Area A' cm^2	strain %	strain ΔL/L	load reading	Displacement reading, L mm
0.00	19.635	0	0	0	0
2.04	19.637	0.01	0.0001	4	0.01
3.56	19.639	0.02	0.0002	7	0.02
7.63	19.649	0.07	0.0007	15	0.07
12.71	19.664	0.15	0.0015	25	0.15
18.80	19.680	0.23	0.0023	37	0.23
36.49	19.730	0.48	0.0048	72	0.48
80.69	19.829	0.98	0.0098	160	0.98
132.50	19.924	1.45	0.0145	264	1.45
189.28	20.023	1.94	0.0194	379	1.94
243.42	20.130	2.46	0.0246	490	2.46
290.08	20.236	2.97	0.0297	587	2.97
327.07	20.332	3.43	0.0343	665	3.43
353.72	20.440	3.94	0.0394	723	3.94
373.74	20.549	4.45	0.0445	768	4.45
390.22	20.655	4.94	0.0494	806	4.94
403.62	20.762	5.43	0.0543	838	5.43
414.93	20.871	5.92	0.0592	866	5.92
425.79	20.973	6.38	0.0638	893	6.38
435.36	21.086	6.88	0.0688	918	6.88
443.93	21.197	7.37	0.0737	941	7.37
451.33	21.315	7.88	0.0788	962	7.88
457.79	21.429	8.37	0.0837	981	8.37
464.17	21.544	8.86	0.0886	1000	8.86
469.42	21.665	9.37	0.0937	1017	9.37
474.22	21.783	9.86	0.0986	1033	9.86
479.60	21.914	10.4	0.104	1051	10.4

482.59	22.027	10.86	0.1086	1063	10.86
487.22	22.146	11.34	0.1134	1079	11.34
488.23	22.264	11.81	0.1181	1087	11.81
490.76	22.394	12.32	0.1232	1099	12.32
491.67	22.515	12.79	0.1279	1107	12.79
494.11	22.647	13.3	0.133	1119	13.3
493.02	22.778	13.8	0.138	1123	13.8
493.69	22.909	14.29	0.1429	1131	14.29
477.33	23.003	14.64	0.1464	1098	14.64

Reinforcement case, 1.5% of fiber _ Sample No.3					
Stress kPa	Corrected Area A' cm^2	strain %	strain ΔL/L	load reading	Displacement reading, L mm
0.00	19.635	0	0	0	0
3.56	19.637	0.01	0.0001	7	0.01
5.60	19.643	0.04	0.0004	11	0.04
10.17	19.657	0.11	0.0011	20	0.11
18.29	19.680	0.23	0.0023	36	0.23
36.02	19.714	0.4	0.004	71	0.4
64.75	19.769	0.68	0.0068	128	0.68
111.28	19.859	1.13	0.0113	221	1.13
162.96	19.944	1.55	0.0155	325	1.55
217.67	20.030	1.97	0.0197	436	1.97
267.40	20.120	2.41	0.0241	538	2.41
309.73	20.211	2.85	0.0285	626	2.85
342.91	20.297	3.26	0.0326	696	3.26
367.88	20.387	3.69	0.0369	750	3.69
386.70	20.481	4.13	0.0413	792	4.13
401.54	20.571	4.55	0.0455	826	4.55
413.24	20.666	4.99	0.0499	854	4.99

423.49	20.756	5.4	0.054	879	5.4
433.18	20.846	5.81	0.0581	903	5.81
440.74	20.942	6.24	0.0624	923	6.24
447.22	21.041	6.68	0.0668	941	6.68
453.17	21.140	7.12	0.0712	958	7.12
458.59	21.239	7.55	0.0755	974	7.55
463.13	21.333	7.96	0.0796	988	7.96
467.39	21.438	8.41	0.0841	1002	8.41
471.28	21.537	8.83	0.0883	1015	8.83
474.96	21.644	9.28	0.0928	1028	9.28
477.42	21.742	9.69	0.0969	1038	9.69
481.09	21.846	10.12	0.1012	1051	10.12
481.64	21.946	10.53	0.1053	1057	10.53
483.81	22.054	10.97	0.1097	1067	10.97
484.74	22.156	11.38	0.1138	1074	11.38
486.82	22.267	11.82	0.1182	1084	11.82
486.24	22.376	12.25	0.1225	1088	12.25
487.86	22.486	12.68	0.1268	1097	12.68
487.29	22.574	13.02	0.1302	1100	13.02
491.91	22.626	13.22	0.1322	1113	13.22
494.80	22.676	13.41	0.1341	1122	13.41
496.41	22.723	13.59	0.1359	1128	13.59
495.83	22.770	13.77	0.1377	1129	13.77
495.87	22.768	13.76	0.1376	1129	13.76
488.84	22.850	14.07	0.1407	1117	14.07
484.55	22.887	14.21	0.1421	1109	14.21

9. UU triaxial test

Axial strain %	UU triaxial strength kPa PP=0.5%	UU triaxial strength kPa PP=1%	UU triaxial strength kPa PP=1.5%
0	0	0	0
0.25	130.5691414	216.7447747	201.0764778
0.5	195.8537121	289.8634939	292.4748767
0.75	274.1951969	368.2049787	373.4277444
1	339.4797676	449.1578464	454.3806121
1.25	404.7643383	524.8879484	537.9448626
1.5	464.8261434	600.6180504	629.3432615
1.75	535.3334797	678.9595353	712.907512
2	592.7839019	746.8554888	791.2489969
2.25	647.6229413	812.1400595	861.7563332
2.5	699.8505979	869.5904817	940.0978181
2.75	741.6327231	911.372607	997.5482403
3	780.8034656	950.5433494	1054.998662
3.25	814.7514423	987.102709	1107.226319
3.5	840.8652706	1018.439303	1146.397061
3.75	864.3677161	1039.330366	1188.179187
4	880.036013	1057.610045	1224.738546
4.25	890.4815443	1068.055577	1261.297906
4.5	898.3156928	1070.666959	1290.023117
4.75	900.9270756	1065.444194	1313.525562
5	900.9270756	1065.444194	1331.805242
5.25	900.9270756	1065.444194	1347.473539
5.5	900.9270756	1062.832811	1363.141836
5.75	900.9270756	1062.832811	1368.364602
6	-	1062.832811	1381.421516
6.25	-	1062.832811	1386.644282
6.5	-	-	1394.47843

6.75	-	-	1394.47843
7	-	-	1399.701196
7.25	-	-	1399.701196
7.5	-	-	1407.535344
7.75	-	-	1407.535344

10. UU triaxial test under (F-T) cycles

Axial strain %	UU triaxial strength kPa, PP=0.5%		
	3 cycles	6 cycles	10 cycles
0	0	0	0
0.25	49.61627373	101.8439303	60.06180504
0.5	99.23254746	148.8488212	96.62116463
0.75	138.4032899	185.4081808	127.9577586
1	172.3512666	227.190306	161.9057353
1.25	201.0764778	263.7496656	188.0195636
1.5	235.0244545	300.3090252	219.3561575
1.75	268.9724313	334.257002	248.0813687
2	302.920408	370.8163616	274.1951969
2.25	331.6456192	407.3757212	300.3090252
2.5	360.3708303	443.9350808	326.4228535
2.75	389.0960414	477.8830575	347.3139161
3	415.2098696	509.2196515	373.4277444
3.25	438.7123151	532.7220969	394.318807
3.5	472.6602919	556.2245424	417.8212525
3.75	496.1627373	577.115605	438.7123151
3.75	519.6651828	595.3952848	454.3806121
4	548.3903939	608.4521989	472.6602919
4.25	569.2814565	621.5091131	485.717206
4.5	587.5611363	634.5660272	498.7741201
4.75	608.4521989	647.6229413	517.0537999
5	626.7318787	655.4570898	530.1107141

5.25	645.0115585	668.514004	540.5562454
5.5	660.6798555	676.3481524	551.0017767
5.75	681.5709181	686.7936838	558.8359252
6	702.4619807	697.2392151	566.6700737
6.25	710.2961292	702.4619807	571.8928393
6.5	731.1871918	707.6847464	577.115605
6.75	739.0213403	710.2961292	582.3383706
7	746.8554888	710.2961292	587.5611363
7.25	754.6896373	710.2961292	587.5611363
7.5	759.9124029	710.2961292	592.7839019
7.75	767.7465514	718.1302777	595.3952848
8	770.3579342	720.7416605	598.0066676
8.25	778.1920827	725.9644262	598.0066676
8.5	778.1920827	725.9644262	600.6180504
8.75	783.4148484	725.9644262	600.6180504
9	788.637614	725.9644262	600.6180504
9.25	793.8603797	-	600.6180504
9.5	793.8603797	-	600.6180504
9.75	793.8603797	-	600.6180504
10	-	-	-

Axial strain %	UU triaxial strength kPa, PP=1%		
	3 cycles	6 cycles	10 cycles
0	0	0	0
0.25	54.83903939	94.00978181	75.73010201
0.5	107.0666959	154.0715868	125.3463757
0.75	156.6829697	211.5220091	167.128501
1	198.4650949	258.5269	211.5220091
1.25	240.2472202	310.7545565	253.3041343
1.5	282.0293454	389.0960414	289.8634939
1.75	326.4228535	412.5984868	331.6456192

2	368.2049787	464.8261434	365.5935959
2.25	417.8212525	522.2765656	404.7643383
2.5	454.3806121	566.6700737	443.9350808
2.75	496.1627373	621.5091131	488.3285888
3	530.1107141	665.9026211	530.1107141
3.25	569.2814565	707.6847464	566.6700737
3.5	600.6180504	741.6327231	598.0066676
3.75	629.3432615	772.9693171	621.5091131
3.75	652.845707	801.6945282	650.2343242
4	681.5709181	825.1969736	671.1253868
4.25	702.4619807	846.0880363	689.4050666
4.5	720.7416605	869.5904817	707.6847464
4.75	744.244106	882.6473959	723.3530433
5	762.5237858	890.4815443	741.6327231
5.25	780.8034656	903.5384585	759.9124029
5.5	801.6945282	908.7612241	767.7465514
5.75	817.3628252	913.9839898	780.8034656
6	833.0311221	919.2067554	796.4717625
6.25	846.0880363	924.4295211	801.6945282
6.5	864.3677161	927.0409039	812.1400595
6.75	874.8132474	932.2636696	822.5855908
7	885.2587787	932.2636696	825.1969736
7.25	895.70431	932.2636696	830.4197393
7.5	906.1498413	932.2636696	835.6425049
7.75	919.2067554	937.4864352	840.8652706
8	929.6522868	937.4864352	846.0880363
8.25	940.0978181	932.2636696	851.3108019
8.5	947.9319665	929.6522868	853.9221847
8.75	955.766115	924.4295211	859.1449504
9	966.2116463	924.4295211	864.3677161
9.25	974.0457948	-	866.9790989

Axial strain %	9.5	981.8799433	-	866.9790989
	9.75	-	-	866.9790989
	10	-	-	-

Axial strain %	UU triaxial strength kPa, PP=1.5%		
	3 cycles	6 cycles	10 cycles
0	0	0	0
0.25	73.11871918	138.4032899	91.39839898
0.5	143.6260555	214.1333919	148.8488212
0.75	211.5220091	279.4179626	201.0764778
1	268.9724313	339.4797676	255.9155171
1.25	323.8114707	394.318807	297.6976424
1.5	381.2618929	433.4895494	342.0911505
1.75	441.3236979	480.4944403	396.9301899
2	496.1627373	522.2765656	441.3236979
2.25	564.0586908	558.8359252	485.717206
2.5	613.6749646	590.1725191	537.9448626
2.75	671.1253868	621.5091131	582.3383706
3	715.5188949	652.845707	621.5091131
3.25	767.7465514	689.4050666	665.9026211
3.5	812.1400595	718.1302777	707.6847464
3.75	848.6994191	741.6327231	736.4099575
3.75	882.6473959	767.7465514	757.3010201
4	919.2067554	796.4717625	791.2489969
4.25	947.9319665	817.3628252	812.1400595
4.5	974.0457948	840.8652706	846.0880363
4.75	1005.382389	864.3677161	851.3108019
5	1028.884834	890.4815443	866.9790989
5.25	1054.998662	908.7612241	880.036013
5.5	1081.112491	932.2636696	895.70431
5.75	1104.614936	950.5433494	911.372607

6	1125.505999	968.8230292	919.2067554
6.25	1141.174296	987.102709	929.6522868
6.5	1167.288124	1010.605154	945.3205837
6.75	1180.345038	1028.884834	953.1547322
7	1196.013335	1036.718983	960.9888807
7.25	1209.070249	1052.38728	971.434412
7.5	1222.127163	1060.221428	984.4913261
7.75	1240.406843	1083.723874	992.3254746
8	1256.07514	1088.946639	1002.771006
8.25	1269.132054	1096.780788	1010.605154
8.5	1279.577586	1107.226319	1018.439303
8.75	1290.023117	1120.283233	1028.884834
9	1305.691414	1128.117382	1041.941748
9.25	1316.136945	1138.562913	1047.164514
9.5	1326.582477	1151.619827	1057.610045
9.75	1326.582477	1164.676741	1060.221428
10	1326.582477	1169.899507	1065.444194
10.25	1326.582477	1180.345038	1073.278342
10.5	1326.582477	1193.401952	1078.501108
10.75	1326.582477	1201.236101	1081.112491
11	-	1201.236101	1081.112491
11.25	-	1211.681632	1083.723874
11.5	-	1219.515781	1083.723874
11.75	-	1235.184078	1088.946639
12	-	1243.018226	1088.946639
12.25	-	1256.07514	1091.558022
12.5	-	1266.520672	1094.169405
12.75	-	1274.35482	1094.169405
13	-	1279.577586	1096.780788
13.25	-	1284.800351	1102.003553
13.5	-	1290.023117	1102.003553

13.75	-	1292.6345	1109.837702
14	-	-	1109.837702
14.25	-	-	1109.837702

11. Free swelling test

Time (min)	Swell Strain $\delta H/H\%$ PP=0.5%	Swell Strain $\delta H/H\%$ PP=1%	Swell Strain $\delta H/H\%$ PP=1.5%
0	0	0	0
0.25	0.035	0.055	0.025
1	0.055	0.075	0.03
4	0.09	0.1	0.05
9	0.105	0.11	0.075
16	0.15	0.14	0.095
25	0.2	0.2	0.205
36	0.26	0.255	0.325
49	0.305	0.295	0.395
64	0.35	0.325	0.445
81	0.4	0.39	0.545
100	0.455	0.45	0.625
121	0.515	0.505	0.705
169	0.72	0.665	0.795
196	0.865	0.825	0.88
225	0.99	0.97	0.945
1200	1.405	1.205	1.205
1440	1.405	1.205	1.205
1600	1.405	1.205	1.205

12. Oedometer/consolidation test

Reinforcement case. Applied vertical stress is 80 kPa				
Sqrt (time)	Time (min)	Axial Strain $\delta H/H\%$ PP=0.5%	Axial Strain $\delta H/H\%$	Axial Strain $\delta H/H\%$

			PP=1%	PP=1.5%
0	0	0	0	0
0.5	0.25	0.25	0.3	0.3
1	1	0.35	0.4	0.41
2	4	0.355	0.405	0.455
3	9	0.375	0.42	0.5
4	16	0.395	0.44	0.54
5	25	0.4	0.45	0.55
6	36	0.405	0.465	0.555
7	49	0.435	0.485	0.59
8	64	0.445	0.495	0.595
9	81	0.455	0.515	0.6
10	100	0.48	0.535	0.615
11	121	0.495	0.55	0.635
13	169	0.5	0.555	0.645
14	196	0.51	0.56	0.655
15	225	0.515	0.565	0.675
34.64	1200	0.53	0.575	0.74
38	1440	0.54	0.585	0.755

Reinforcement case. Applied vertical stress is 160 kPa				
Sqrt (time)	Time (min)	Axial Strain $\delta H/H\%$ PP=0.5%	Axial Strain $\delta H/H\%$ PP=1%	Axial Strain $\delta H/H\%$ PP=1.5%
0	0	0	0	0
0.5	0.25	0.56	0.665	0.945
1	1	0.61	0.695	1
2	4	0.66	0.705	1.1
3	9	0.72	0.745	1.185
4	16	0.755	0.785	1.23
5	25	0.78	0.81	1.29

6	36	0.82	0.83	1.35
7	49	0.84	0.855	1.39
8	64	0.865	0.875	1.425
9	81	0.9	0.9	1.455
10	100	0.925	0.92	1.5
11	121	0.965	0.955	1.585
13	169	1	0.98	1.625
14	196	1.035	1.01	1.665
15	225	1.095	1.05	1.705
34.64	1200	1.195	1.205	1.775
38	1440	1.215	1.24	1.795

Reinforcement case. Applied vertical stress is 320 kPa				
Sqrt (time)	Time (min)	Axial Strain $\delta H/H\%$ PP=0.5%	Axial Strain $\delta H/H\%$ PP=1%	Axial Strain $\delta H/H\%$ PP=1.5%
0	0	0	0	0
0.5	0.25	1.245	1.43	2.1
1	1	1.42	1.525	2.33
2	4	1.495	1.585	2.435
3	9	1.545	1.63	2.525
4	16	1.62	1.725	2.65
5	25	1.65	1.75	2.715
6	36	1.695	1.775	2.75
7	49	1.735	1.8	2.79
8	64	1.75	1.81	2.81
9	81	1.765	1.82	2.835
10	100	1.775	1.83	2.85
11	121	1.795	1.86	2.89
13	169	1.82	1.88	2.905
14	196	1.845	1.905	2.945

15	225	1.895	1.925	2.965
34.64	1200	1.995	2.03	3.045
38	1440	2.005	2.055	3.055

The calculated void ratio for each vertical applied load is in the tables below:

Reinforcement case. Void ratio changes under the applied vertical stress is 80 kPa				
Sqrt (time)	Time (min)	Axial Strain $\delta H/H\%$ PP=0.5%	Axial Strain $\delta H/H\%$ PP=1%	Axial Strain $\delta H/H\%$ PP=1.5%
0	0	0.7197	0.7197	0.7197
0.5	0.25	0.6768	0.6682	0.6682
1	1	0.6596	0.6510	0.6492
2	4	0.6587	0.6501	0.6415
3	9	0.6553	0.6475	0.6338
4	16	0.6518	0.6441	0.6269
5	25	0.6510	0.6424	0.6252
6	36	0.6501	0.6398	0.6243
7	49	0.6449	0.6363	0.6183
8	64	0.6432	0.6346	0.6174
9	81	0.6415	0.6312	0.6166
10	100	0.6372	0.6277	0.6140
11	121	0.6346	0.6252	0.6105
13	169	0.6338	0.6243	0.6088
14	196	0.6320	0.6234	0.6071
15	225	0.6312	0.6226	0.6037
34.64	1200	0.6286	0.6209	0.5925
38	1440	0.6269	0.6191	0.5899

Reinforcement case. Void ratio changes under the applied vertical stress is 160 kPa				
Sqrt (time)	Time (min)	Axial Strain δH/H% PP=0.5%	Axial Strain δH/H% PP=1%	Axial Strain δH/H% PP=1.5%
0	0	0.7197	0.7197	0.7197
0.5	0.25	0.6234	0.6054	0.5572
1	1	0.6148	0.6002	0.5478
2	4	0.6062	0.5985	0.5306
3	9	0.5959	0.5916	0.5160
4	16	0.5899	0.5847	0.5082
5	25	0.5856	0.5804	0.4979
6	36	0.5787	0.5770	0.4876
7	49	0.5753	0.5727	0.4807
8	64	0.5710	0.5693	0.4747
9	81	0.5650	0.5650	0.4695
10	100	0.5607	0.5615	0.4618
11	121	0.5538	0.5555	0.4472
13	169	0.5478	0.5512	0.4403
14	196	0.5418	0.5461	0.4334
15	225	0.5314	0.5392	0.4265
34.64	1200	0.5142	0.5125	0.4145
38	1440	0.5108	0.5065	0.4111

Reinforcement case. Void ratio changes under the applied vertical stress is 320 kPa				
Sqrt (time)	Time (min)	Axial Strain δH/H% PP=0.5%	Axial Strain δH/H% PP=1%	Axial Strain δH/H% PP=1.5%
0	0	0.7197	0.7197	0.7197
0.5	0.25	0.5056	0.4738	0.3586
1	1	0.4755	0.4575	0.3190
2	4	0.4626	0.4472	0.3010

3	9	0.4540	0.4394	0.2855
4	16	0.4411	0.4231	0.2640
5	25	0.4360	0.4188	0.2528
6	36	0.4282	0.4145	0.2468
7	49	0.4214	0.4102	0.2399
8	64	0.4188	0.4085	0.2365
9	81	0.4162	0.4068	0.2322
10	100	0.4145	0.4050	0.2296
11	121	0.4111	0.3999	0.2227
13	169	0.4068	0.3964	0.2202
14	196	0.4025	0.3921	0.2133
15	225	0.3939	0.3887	0.2098
34.64	1200	0.3767	0.3706	0.1961
38	1440	0.3749	0.3663	0.1944

APPX 3: Drying tests' readings

time	Water content (w%)					
min	PP=0%	PP=0.5%	PP=1%	PP=1.5%	Cement	Lime
0	57.86	62.10	62.52	62.80	62.68	60.36
30	56.58	60.01	60.69	61.14	61.07	57.32
60	56.12	59.17	60.02	60.59	60.46	56.68
90	55.69	58.52	59.43	60.04	59.85	56.02
120	55.03	57.87	58.84	59.49	59.15	55.27
150	54.53	57.31	58.23	58.85	58.54	54.79
180	54.05	56.89	57.80	58.40	58.12	54.43
210	53.63	56.43	57.25	57.80	57.67	54.07
240	53.31	56.21	57.08	57.66	57.29	53.91
1440	39.76	41.17	43.88	45.69	43.62	38.74
1470	39.00	40.46	43.21	45.05	42.86	38.02
1500	38.96	40.17	43.00	44.89	42.32	37.65
1530	38.63	39.86	42.74	44.66	42.02	37.21
1560	37.94	39.53	42.29	44.13	41.53	36.82
1590	37.58	39.15	41.90	43.74	41.06	36.44
1620	37.09	38.91	41.47	43.17	40.70	36.18
1650	36.43	38.29	40.90	42.64	40.21	35.52
1680	35.48	37.25	40.01	41.84	39.30	34.72
2880	13.19	16.94	22.51	26.22	19.33	14.11
2910	12.07	16.26	21.69	25.30	18.39	13.74
2940	11.84	15.67	21.12	24.76	18.11	13.55
2970	11.71	15.11	20.52	24.12	17.66	13.31
3000	11.36	14.87	20.14	23.66	17.21	13.22
3030	11.13	14.43	19.60	23.05	16.78	12.91
3060	10.78	14.21	19.41	22.87	16.22	12.64
3090	10.32	14.12	19.22	22.62	15.98	12.43
3120	9.89	13.67	18.66	21.99	15.37	12.06

4320	5.47	6.43	9.81	12.06	8.13	7.67
4410	4.35	5.61	8.88	11.06	7.15	7.00
4470	3.89	5.25	8.45	10.59	6.70	6.52
4560	3.49	4.12	7.21	9.26	5.39	5.70
2880	13.19	16.94	22.51	26.22	19.33	14.11
2910	12.07	16.26	21.69	25.30	18.39	13.74
2940	11.84	15.67	21.12	24.76	18.11	13.55
2970	11.71	15.11	20.52	24.12	17.66	13.31
3000	11.36	14.87	20.14	23.66	17.21	13.22

****

RESUME

Name Surname   : Talal TALEB
Place and Date of Birth   : 01/01/1986
Foreign Languages   : English/Turkish/Arabic
Work Experience   : Engineering consultant and projects manager in
agence d'aide a la cooperation tecnigeu et au development.
Contact (e-mail)   : eng.talaltaleb@hotmail.com

Publications

Taleb T. and Unsever Y.S. (2021), "Effect of Polypropylene Fibers on Physical and Strength Properties of Local Clayey Soil", In *Proceedings of 14th International Congress on Advances in Civil Engineering*, pp: 611–618. https://avesis.uludag.edu.tr/yayin/93540931-94fe-4c51-8b99-7a39455c819a/effect-of-polypropylene-fibers-on-physical-and-strength-properties-of-local-clayey-soil

Taleb T. and Unsever Y.S. (2022), "Study on Strength and Swell Behavioral Change and Properties of the Clay–Fiber Mixtures", *Sustainability*, vol 14 (6767). DOI: https://doi.org/10.3390/su14116767.

Taleb T. and Unsever Y.S. (2022), "Evaluation of high plasticity clay stabilization methods for resisting the environmental changes", *Geomechanics and Engineering*, volume 30, number 5, pages 461-469. DOI: https://doi.org/10.12989/gae.2022.30.5.461.